Environmental
Studies
Revolving
Funds

056

Wind Speeds from Underwater Acoustic Measurements during the Canadian Atlantic Storms Program

Canada

December 1986

The Environmental Studies Revolving Funds are financed from special levies on the oil and gas industry and administered by the Canada Oil and Gas Lands Administration for the Minister of Energy, Mines and Resources, and by the Northern Affairs Program for the Minister of Indian Affairs and Northern Development.

Environmental Studies Revolving Funds
Report No. 056
December, 1986

WIND SPEEDS FROM UNDERWATER ACOUSTIC MEASUREMENTS DURING THE CANADIAN ATLANTIC STORMS PROGRAM

D. D. Lemon

Arctic Sciences Ltd.
1986 Mills Road, R.R.2
Sidney, B.C.
V8L 3S1

Scientific Advisor: C. Anderson

The correction citation for this report is:

Lemon, D.D. 1986. Wind speeds from underwater acoustic measurements, during the Canadian Atlantic Storms Program. Environmental Studies Revolving Funds Report No. 056. Ottawa. 104 p.

Published under the auspices of the
Environmental Studies Revolving Funds
ISBN-0-920783-55-4

TABLE OF CONTENTS

	Page
LIST OF FIGURES	iv
LIST OF TABLES	viii
ACKNOWLEDGEMENTS	ix
SUMMARY	x
RESUME	x
1.0 INTRODUCTION	1
2.0 INSTRUMENTATION AND METHODS	2
2.1 INSTRUMENT DEPLOYMENT AND RECOVERY	2
2.2 INSTRUMENT DESCRIPTION	2
2.3 CALIBRATION	9
3.0 DATA REDUCTION AND ANALYSIS	13
3.1 TAPE TRANSLATION, DESPIKING AND CALCULATION OF NOISE SPECTRUM LEVELS	13
3.2 CALCULATION OF WIND-SPEED RECORD	44
3.3 COMPARISON WITH SURFACE-BUOY WIND SPEEDS	97
4.0 CONCLUSIONS	103
5.0 REFERENCES	104

LIST OF FIGURES

	Page
Figure 1: Location of CASP stations at which WOTAN instruments were deployed.	3
Figure 2: WOTAN stand-alone mooring system.	4
Figure 3: WOTAN attached to standard current-meter mooring.	5
Figure 4: Block diagram of three-channel WOTAN instruments.	7
Figure 5: Sample instrument calibration curves.	10
Figure 6: Raw data plot from station 1.	14
Figure 7: Despiked data from station 1.	18
Figure 8: Despiked data from station 2.	22
Figure 9: Despiked data from station 5.	26
Figure 10: Despiked data from station 12.	32
Figure 11: Despiked data from station 13.	38
Figure 12: Final section of raw data record from station 2, showing recovery of the instrument.	45

Page

Figure 13: Spectral plot of apparent noise contamination at station 2. 46

Figure 14: Time series of noise spectrum levels at station 1. 47

Figure 15: Time series of noise spectrum levels at station 2. 51

Figure 16: Time series of noise spectrum levels at station 5. 55

Figure 17: Time series of noise spectrum levels at station 12. 61

Figure 18: Time series of noise spectrum levels at station 13. 67

Figure 19: Noise spectrum levels at 8.0, 14.5 and 25.0 kHz plotted against the noise spectrum level at 4.3 kHz for 2 stations in Queen Charlotte Sound. 74

Figure 20: Wind speed at CASP station 1, computed from the 4.3-kHz signal only. 75

Figure 21: Wind speed at CASP station 2, computed from the 4.3-kHz signal only. 76

Figure 22: Wind speed at CASP station 5, computed from: (a) the wide-band 4.3-kHz signal only; (b) the narrow-band 4.3-kHz signal only. 77

Figure 23: Wind speed at CASP station 12, computed from: (a) the wide-band 4.3-kHz signal only; (b) the narrow-band 4.3-kHz signal only. 79

Figure 24: Wind speed at CASP station 13, computed from: (a) the wide-band 4.3-kHz signal only; (b) the narrow-band 4.3-kHz signal only. 81

Page

Figure 25: Definition of line W and zone A used in computing wind speed. 86

Figure 26: Wind speed at station 1 computed from the 4.3-kHz and 8.0-kHz signals, using the relationship derived from the Queen Charlotte Sound measurements. 88

Figure 27: Wind speed at station 2 computed from the 4.3-kHz and 8.0-kHz signals, using the relationship derived from the Queen Charlotte Sound measurements. 89

Figure 28: Wind speed at station 5 computed from the narrow-band 4.3-kHz and 8.0-kHz signals, using the relationship derived from the Queen Charlotte Sound measurements. 90

Figure 29: Wind speed at station 12 computed from the narrow-band 4.3-kHz and 8.0-kHz signals, using the relationship derived from the Queen Charlotte Sound measurements. 91

Figure 30: Wind speed at station 13 computed from the narrow-band 4.3-kHz and 8.0-kHz signals, using the relationship derived from the Queen Charlotte Sound measurements. 92

Figure 31: Noise spectrum level at 8.0-kHz vs noise spectrum level at 4.3-kHz at station 1 for the period February 8-28, 1986. 93

Figure 32: Noise spectrum level at 8.0 kHz vs noise spectrum level at 4.3 kHz at station 5 for the period February 8-28, 1986. 94

Page

Figure 33: Noise spectrum level at 8.0 kHz vs noise spectrum level at 4.3 kHz at station 12 for the period February 8-28, 1986. 95

Figure 34: Noise spectrum level at 8.0 kHz vs noise spectrum level at 4.3 kHz at station 13 for the period February 8-28, 1986. 96

Figure 35: Wind speed at station 1 computed from the 4.3-kHz and 8.0-kHz signals, using the relationship defined specifically for this station. 98

Figure 36: Wind speed at station 5 computed from the narrow-band 4.3-kHz and 8.0-kHz signals, using the relationship defined specifically for this station. 99

Figure 37: Wind speed at station 12 computed from the narrow-band 4.3-kHz and 8.0-kHz signals, using the relationship defined specifically for this station. 100

Figure 38: Wind speed at station 13 computed from the narrow-band 4.3-kHz and 8.0-kHz signals, using the relationship defined specifically for this station. 101

Figure 39: Wind speed from surface buoy at CASP station 2. 102

LIST OF TABLES

		Page
Table 1:	Locations and depths of WOTAN moorings.	2
Table 2:	Timing data for WOTAN deployments and recoveries.	6
Table 3:	Centre frequency assignments by data channel number for each WOTAN instrument.	7
Table 4:	Scaling factor, full-scale value and dynamic range as a function of duty cycle for Sea Data Model 661.	8
Table 5:	Calibration constants for WOTAN instruments used in the CASP experiment.	12
Table 6:	Values for the wind-speed constants a and b at 4.3-kHz frequency from three locations.	83

ACKNOWLEDGEMENTS

Funding for this project was provided by the Environmental Studies Revolving Funds. Two of the WOTAN instruments were provided by Dr. D.M. Farmer of the Institute of Ocean Sciences, Sidney, B.C. The author wishes to thank the officers and crew of CSS Dawson for their assistance in deploying the instruments. He also wishes to acknowledge the support and advice received from Drs. C. Anderson and F. Dobson of the Bedford Institute of Oceanography, and Dr. D.M. Farmer, Dr. S. Waddell and Mr. S. Vagle of the Institute of Ocean Sciences. Within Arctic Sciences Ltd., the calibration and preparation of the instruments was skillfully performed by G. Pleriot; G. Wilton designed and installed the moorings; G. Dudddrige processed the data; while S. Norton, N. Andrew and D. Stover produced the report.

SUMMARY

Five WOTAN (Wind Observation Through Ambient Noise) sensors were deployed as part of the wind measurement program in the Canadian Atlantic Storms Program (CASP); three from November 1985 to April 1986, and two from December 1985 to March 1986. The purpose was to test the WOTAN's potential for providing wind-speed measurements at mesoscale spacing. The deployment was highly successful, achieving a recovery rate for useful data of better than 90%. Contamination from an unknown noise source was found in the latter half of the record from station 2. This report deals with the calibration of the instruments, the collection and basic processing of the acoustic data, and the estimation of wind speed from those data. Time series of wind speeds calculated from the WOTAN measurements are presented, using two different algorithms, for four of the five stations.

RÉSUMÉ

Cinq capteurs OVBF (obervation du vent à travers le bruit de fond) ont été déployés en même temps que le programme de mesure du vent, dans la cadre du Programme canadien sur les tempêtes de l'Atlantique (PCTA). Trois l'ont été de novembre 1985 à avril 1986 et deux de décembre 1985 à mars 1986. L'objectif était de déterminer si ces capteurs seraient capables de fournir des mesures sur la vitesse du vent d'une échelle moyenne. Le déploiement fut un grand succès, réalisant un taux de récupération pour les données utilisables de plus de 90%. De la pollution en provenance de bruits inconnus fut constatée dans la dernière moitié de l'enregistrement de la station 2. Ce rapport traite de l'étalonnage des instruments, de cueillete de données acoustiques et de leur traitement primaire ansi que de l'estimation de la vitesse du vent à partir de ces données. Des séries chronologiques des vitesse éoliennes calculées à partir des mesures fournies par ces capteurs sont présentées en se servant de deux algorithmes différents pour quatre des cinq stations.

1.0 INTRODUCTION

Five underwater ambient noise sensors, known as WOTANs (Wind Observation Through Ambient Noise), were deployed as part of the wind measurement program in the Canadian Atlantic Storms Program (CASP). The purpose was to test their potential for providing wind-speed measurements at mesoscale spacing. Marine wind measurements formed an essential part of the program to understand storm generation and intensification processes off the Atlantic coast of Canada. The WOTAN's inclusion in the project was made possible by funding from the Environmental Studies Revolving Funds (ESRF).

WOTAN instruments measure wind speed over the sea by exploiting the fact that the ambient noise field in the ocean at frequencies between 2 kHz and 30 kHz is dominated by sound produced by the action of the wind on the sea surface (Knudsen et al. 1948). A well-established empirical relationship has been found to exist between the surface wind speed and the intensity of the ambient noise field, thus allowing underwater measurements of the sound field to be converted to surface wind speeds. During the last decade, oceanographers have made increasing use of the technique to make wind-speed measurements at sea (Shaw et al. 1978; Evans and Watts 1981; Kerman et al. 1983; Lemon et al. 1984; Farmer and Lemon 1984).

Although wind-generated noise is the dominant source of oceanic ambient noise in the 2-30 kHz range, it is by no means the only one. Shipping, rainfall, sea creatures and on- and offshore industry all contribute as well, and, under the right circumstances, can dominate the wind-generated noise. Identification of periods in the noise record where these other sources dominate is, of course, necessary to produce reliable wind-speed records. Noise from these various sources exhibits differing spectral characteristics and this fact can be exploited to help in identifying the source of any particular section of the noise record. Wind-generated noise decreases with frequency at a rate of 17 dB/decade, until wind speeds greater than about 12 ms^{-1} occur, after which the decrease becomes more rapid at frequencies above 8 kHz (Farmer and Lemon 1984). Noise arising from shipping and industrial activity is usually concentrated at lower frequencies, producing a redder spectrum than wind-generated noise when it occurs at frequencies high enough to be observed in the wind-generated band. The spectrum of rain-generated noise is the subject of active research at the moment, and appears to be more complex than had been previously thought (Franz 1959; Wenz 1962). Current work (Jasco 1985; Nystuen 1986) shows that rain-generated noise has a spectral peak at about 15 kHz, the shape of which may be wind-speed dependent.

The CASP acoustic data set, particularly when examined in conjunction with precipitation data from shore stations and meteorological radars, may well shed further light on the characteristics of the rain-generated noise spectrum. Such work is beyond the scope of this report which deals only with the collection and basic processing of the acoustic data, and the estimation of wind speed from those data.

2.0 INSTRUMENTATION AND METHODS

2.1 INSTRUMENT DEPLOYMENT AND RECOVERY

The five WOTAN instruments were deployed at CASP stations 1, 2, 5, 12 and 13, located as shown in Figure 1. The instruments at stations 1, 2, 12 and 13 were deployed using a stand-alone mooring design (Figure 2). The instrument at station 5 was incorporated in a standard current meter mooring (Figure 3). In both cases, the WOTANs were effectively bottom-mounted. Arctic Sciences' personnel deployed the instruments at stations 5, 12 and 13 from CSS Dawson between November 26 and 29 1985 as part of the regular CASP deployment cruises, and deployed the WOTANs at stations 1 and 2 on December 11 1985 using a vessel chartered from Dominion Divers Ltd. Table 1 lists the position and station depths for each instrument. Table 2 summarizes the timing information (clock start and stop, times of first and last readings and times of deployment and recovery) for each instrument.

Table 1: Locations and depths of WOTAN moorings.

Station	Unit	Latitude	Longitude	Depth (m)
1	01	44°32.65'N	63°03.94'W	63
2	02	44°27.58'N	62°58.25'W	93
5	11	43°57.21'N	62°44.30'W	225
12	09	42°57.90'N	62°11.32'W	165
13	12	44°30.16'N	61°42.10'W	165

2.2 INSTRUMENT DESCRIPTION

The WOTAN instruments were built by the Sea Data Corporation of Newton, Mass. and are officially known as Model 661 Subsurface Wind Recorders. A detailed description of their construction and operation may be found in Hill (1984). Briefly, each unit consists of a broadband, omnidirectional hydrophone, a preamplifier, and up to 13 bandpass filters arranged in parallel, each followed by an RMS-to-DC converter and integrating analog-to-digital (A/D) converter. The output of the A/D converters and the on-board clock is logged to a high-density, four-track cassette recorder. Figure 4 shows a block diagram of a three-channel unit.

The first instruments built were three-channel units operated with a standard set of frequencies chosen from the values 4.3 kHz, 8.0 kHz, 14.5 kHz and 25.0 kHz. (This set of frequencies has persisted for historical reasons -- they were chosen for the prototype instruments to avoid the operating frequencies of various other acoustic devices operating in the original experiment, and have been used ever since to preserve compatibility with the older data.) The instruments used in the present experiment were equipped with six or seven channels to provide greater spectral resolution. The

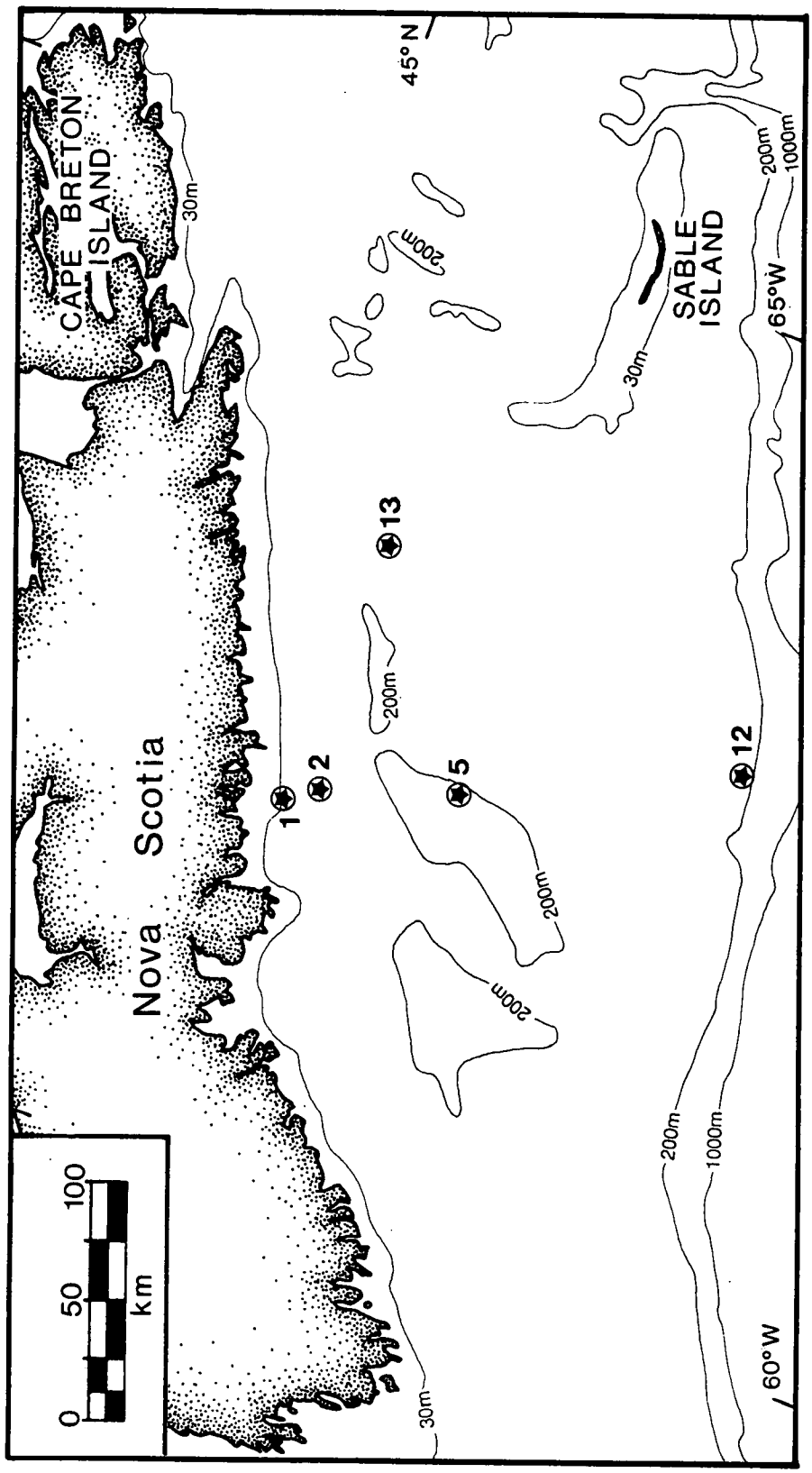

Figure 1: Location of CASP stations at which WOTAN instruments were deployed.

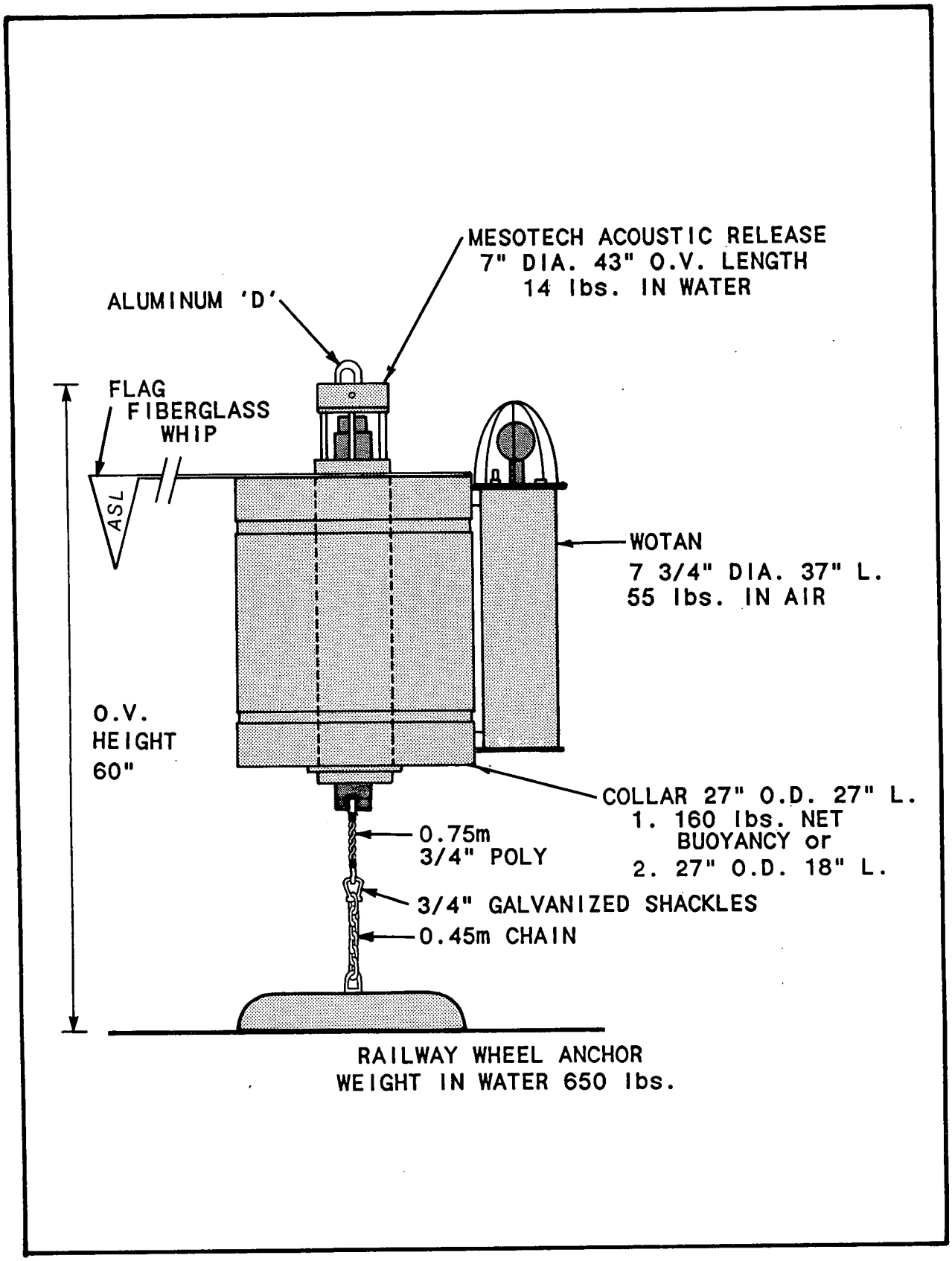

Figure 2: WOTAN stand-alone mooring system.

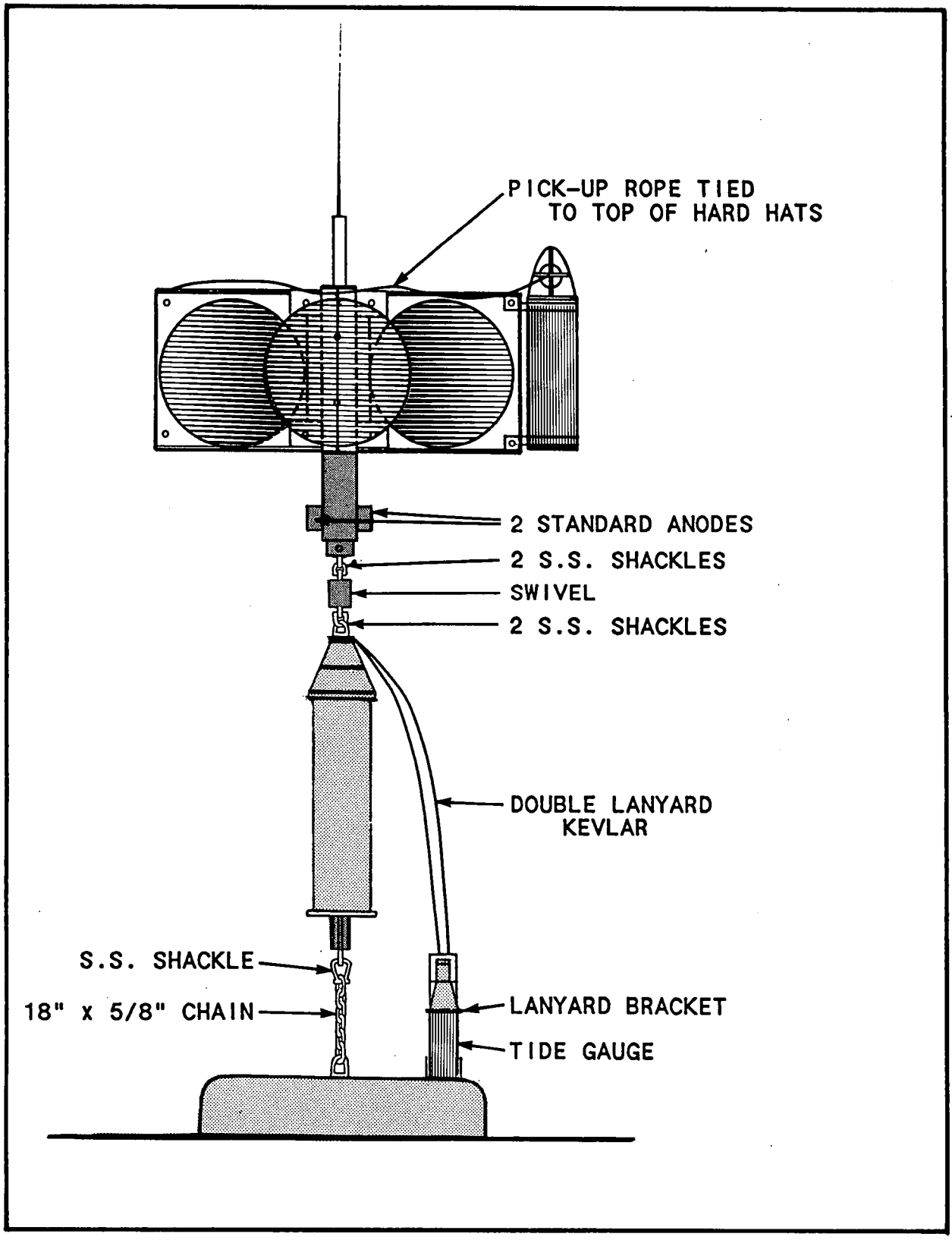

Figure 3: WOTAN attached to standard current-meter mooring.

Table 2: Timing data for WOTAN deployments and recoveries.[a]

Station	Clock Start	First Reading	In Water	On Bottom	Released	Out of Water	Last Reading
1	00:08:25 11 Dec 1985	00:15:00 11 Dec 1985	12:28:30 11 Dec 1985	12:30:00 11 Dec 1985	Not Recorded	12:35:00 13 Mar 1986	10:07:21 14 Mar 1986
2	00:08:25 11 Dec 1985	00:14:58 11 Dec 1985	14:09:00 11 Dec 1985	14:15:00 11 Dec 1985	13:31:00 13 Mar 1986	Not Recorded	10:07:32 14 Mar 1986
5	16:23:16 22 Nov 1985	16:30:00 22 Nov 1985	Not Recorded	18:25:00 26 Nov 1985	08:16:00 05 Apr 1985	08:25:00 05 Apr 1986	11:30:33 10 Apr 1986
12	16:23:26 22 Nov 1985	16:30:00 22 Nov 1985	09:14:00 27 Nov 1985	09:30:00 27 Nov 1985	14:08:31 09 Apr 1986	14:17:00 09 Apr 1986	14:37:42 09 Apr 1986
13	16:23:26 22 Nov 1985	16:30:00 22 Nov 1985	20:22:00 29 Nov 1985	20:27:00 29 Nov 1985	13:52:00 06 Apr 1986	14:00:00 06 Apr 1986	14:45:17 06 Apr 1986

[a] All times are Atlantic Standard Time.

improved spectral resolution was desired in particular for rain noise, with the hope of improving the separation procedure for noise arising from different sources. The centre frequencies of the filters with which each instrument was equipped are listed in Table 3.

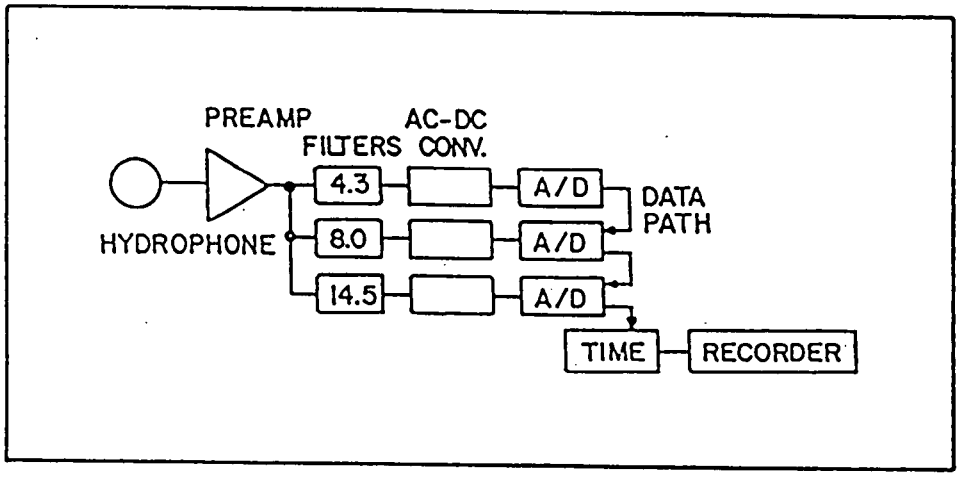

Figure 4: Block diagram of 3-channel WOTAN instruments (after Hill, 1984)

Table 3: Centre frequency assignments by data channel number for each WOTAN instrument

Station	Unit	Data Channel[a] (kHz)						
		1	2	3	4	5	6	7
1	01	8.0	12.5	14.5	16.8	25.0	4.3(W)	--
2	02	8.0	12.5	14.5	16.8	25.0	4.3(W)	--
5	11	4.3	8.0	12.5	14.5	16.8	25.0	4.3(W)
12	09	4.3	8.0	12.5	14.5	16.8	25.0	4.3(W)
13	12	4.3	8.0	12.5	14.5	16.8	25.0	4.3(W)

[a] The data channel numbers refer to the order in which the data are recorded on the tape by the multiplexer.)

Increasing the number of frequency channels required a change to the bandpass filters to reduce their bandwidth. They originally were two-pole active filters; the present filters are four-pole active devices. The channels labelled 4.3W in Table 3 had the older two-pole filters. They were incorporated with the preamplifier cards and have, therefore, been retained in all of the instruments. The seven-channel units incorporate an additional, four-pole 4.3-kHz filter. The change to four-pole filters greatly increased the power consumption of the instrument, which required a change to cycled operation for longer deployments. The instruments were originally designed to record continuous averages of the ambient noise signal. Samples could be recorded at rates varying from 2 to 128 samples per hour. Between recording cycles, the bandpassed noise intensity signals were continuously accumulated by the integrating A/D converters and were then divided by a number proportional to the length of the measurement period, so that a true average intensity (mean square amplitude) was recorded for each channel. Because of the increased power consumption of the instruments, this mode of operation was no longer possible for longer deployments. The instruments were, therefore, changed to cycled operation; power may be applied to the measurement circuitry for all, one-quarter or one-eighth of the sampling period. The active time occurs at the end of the period. Of the active time (during cycled operation) 3.5556% of the sampling interval is used for a warm-up period, so that the actual measurement duty cycles are 100%, 21.444% and 8.9444%. No corresponding adjustment is made to the scaling factor used to compute the averages, so that the full-scale value and dynamic range of the instrument depends on the duty-cycle setting. At the one-quarter and one-eighth settings, the recorded values must be scaled up by the reciprocal of the measurement cycle fraction to produce true averages which may be compared with each other or with the data from continuous sampling. Table 4 summarizes these parameters.

Table 4: Scaling factor, full-scale value and dynamic range as a function of duty cycle for Sea Data model 661

Nominal Duty Cycle (%)	Measurement Duty Cycle (%)	Scaling Factor	Full-Scale Value	Dynamic Range (bits)
100.0	100.000	1.000	57600	15.8
25.0	21.444	4.663	12352	13.6
12.5	8.9444	11.180	5152	12.3

All five WOTANs were set to sample eight times per hour, with a nominal 12.5% duty cycle. The clock starting times in Table 2 were chosen so that one out of every eight sampling intervals ended on the hour.

2.3 CALIBRATION

Calculation of surface wind speeds from ambient noise data requires two separate calibration steps: first, the ambient noise intensity data recorded by the instrument must be converted to noise spectrum levels (the standard units are dB re 1 μ Pa/Hz); second, noise spectrum levels must then be converted to surface wind speeds. This section is concerned with the first step, the conversion of the raw data to noise spectrum levels.

The procedure is as follows. Measured levels of electronic white noise are injected into the preamplifiers of the instrument, and the output of each channel is recorded. When corrections are made for the bandwidth of the source and the voltmeter used to measure it, the instrument outputs are then calibrated in terms of RMS voltages at the input of the preamplifier. With the addition of the calibration data for the hydrophone, the instrument output is calibrated for ambient noise spectrum levels. The calibration data (instrument counts vs RMS noise voltage injected) were plotted to check for linearity (Figure 5 provides an example). A least-squares fit of counts to RMS input voltage was than made over the linear portion of the curve to give the following relationship:

$$N = m \cdot v_{in} + N_1 \qquad (1)$$

where:

N is the number of counts recorded (100% duty cycle is assumed),

v_{in} is the measured RMS noise voltage input to the preamplifier,

m is the slope of the least-squares line, and

N_1 is the intercept of the least-squares line (ideally, N_1 should be zero).

Let BW be the bandwidth of the filter in the channel, let GBW be the bandwidth of the white-noise generator, and let P be the spectrum level of the white-noise voltage it generates.

Then $v_{in} = \sqrt{K \cdot P \cdot GBW}$, where K is a factor that corrects for the ratio between the noise generator bandwidth and the bandwidth of the voltmeter used to measure v_{in} (Motchenbacher and Fitchen 1973). For the measurements to be reported here, K = 0.850. Then

$$N = m(K \cdot GBW)^{1/2} P^{1/2} + N_1 \qquad (2)$$

If the injected noise is white, then $m = \beta\sqrt{BW}$, where BW is the bandwidth of the filter in the channel being calibrated and β is the gain. If we assume that BW is narrow enough that the ocean ambient noise is effectively white within that band, then, with the hydrophone submerged

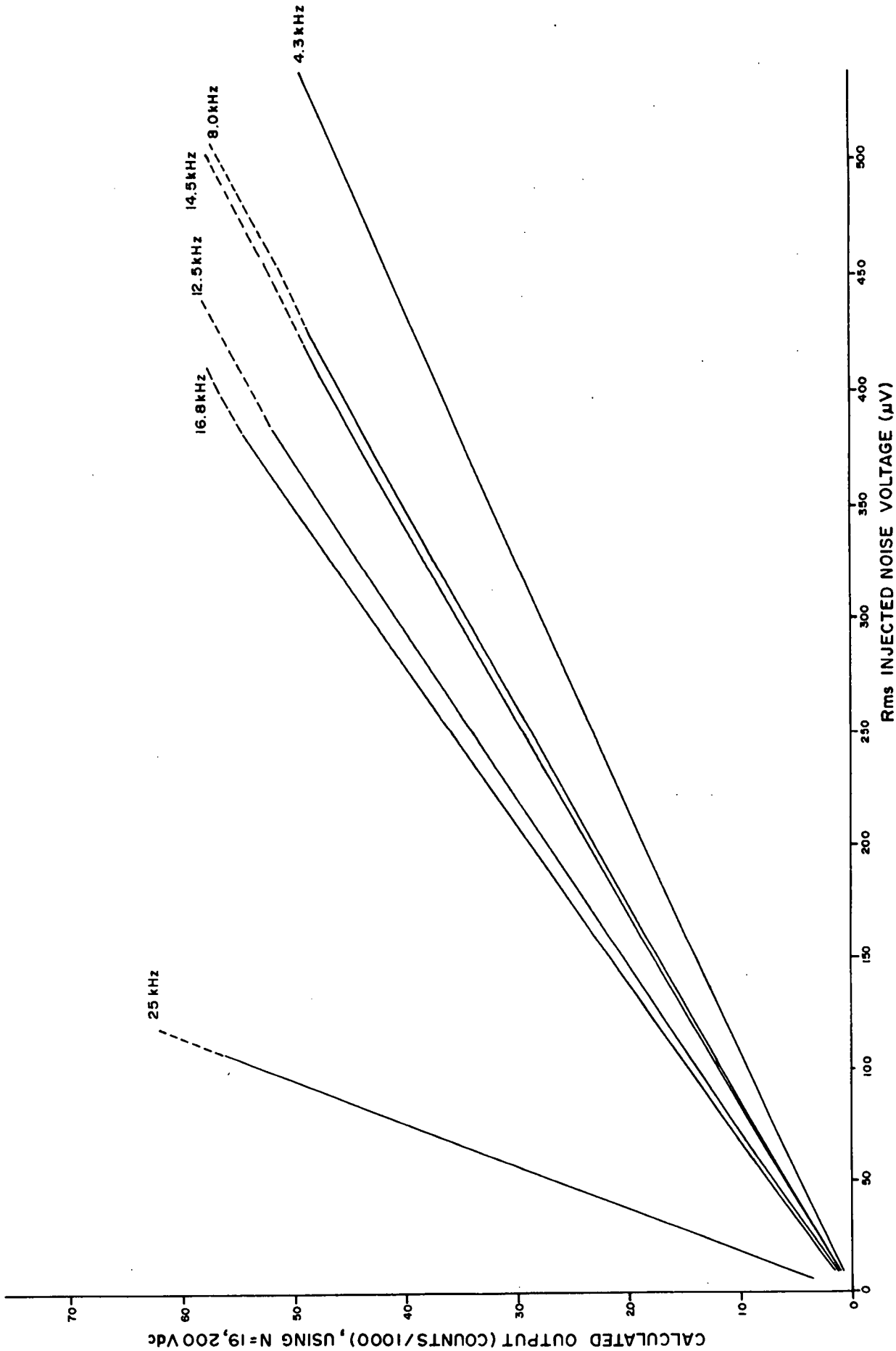

Figure 5: Sample instrument calibration curves.

$$N = m(K \cdot GBW)^{1/2}\ 10^{NSL/20}\ 10^{b/20} + N_1 \qquad (3)$$

where NSL is the ambient noise spectrum level, in dB re 1 μ Pa/Hz and b is the hydrophone response in dB re 1 v/ μ Pa. Equation (3) is more conveniently written in the form

$$NSL = 20\ \log_{10}(N-N_1) - 20\ \log_{10}[m(K\ GBW)^{1/2}]-b$$

$$= 20\ \log_{10}(N-N_1)-B \qquad (4)$$

Equation (4) is the basic WOTAN calibration relation, giving the noise spectrum level in terms of the counts registered in each channel, with all the constants lumped together in B. Calibration measurements were made for the instruments at stations 1 and 2 before and after deployment, and for the other three instruments before deployment. N_1 and m were taken from the least-squares fits described above and b was taken from the hydrophone manufacturer's calibration data. The values of N_1 and B for each channel and instrument are listed in Table 5.

Table 5: Calibration constants for WOTAN instruments used in the CASP experiment.

Board No.	Data Channel	Frequency (kHz)	N_1		B (dB)	
	Station 1	Instrument 01[a]	(Transducer 115)			
Not Recorded	1	8.0	-19	(-5)[b]	19.6	(0.0)[b]
	2	12.5	52	(118)	21.2	(0.0)
	3	14.5	-84	(-4)	20.3	(0.1)
	4	16.8	-35	(170)	23.7	(0.2)
	5	25.0	-120	(-61)	29.8	(0.0)
	6	4.3(W)	-43	(128)	17.7	(0.0)
	Station 2	Instrument 02[a]	(Transducer 114)			
Not Recorded	1	8.0	50	(-59)[b]	19.7	(0.1)[b]
	2	12.5	26	(-113)	20.8	(0.2)
	3	14.5	-81	(-49)	22.0	(0.1)
	4	16.8	49	(-116)	23.4	(0.1)
	5	25.0	-45	(105)	30.3	(0.0)
	6	4.3(W)	10	(-96)	21.1	(0.2)
	Station 5	Instrument 11	(Transducer 154)			
4	1	4.3			-38	19.5
27	2	8.0			134	20.3
6	3	12.5			116	21.7
18	4	14.5			66	23.2
10	5	16.8			35	24.5
14	6	25.0			-37	30.3
104	7	4.3(W)			54	20.8
	Station 12	Instrument 09	(Transducer 152)			
26	1	4.3			-57	19.4
24	2	8.0			-9	20.4
5	3	12.5			-3	21.5
20	4	14.5			23	22.4
12	5	16.8			126	24.0
16	6	25.0			-251	29.1
105	7	4.3(W)			-59	20.9
	Station 13	Instrument 12[c]	(Transducer 156)			
28	1	4.3			28	19.0
23	2	8.0			-82	20.3
8	3	12.5			-13	21.8
19	4	14.5			46	22.8
11	5	16.8			58	24.3
15	6	25.0			15	29.6
102	7	4.3(W)			-40	20.6

[a] Values are averages of the before- and after-deployment calibration measurements.

[b] Differences between before- and after-deployment measurements.

[c] The calibrated hydrophone response for was not available from the manufacturer, who supplied average data from the production run which included that unit. Variation between units in the same run is quoted as $\leq$ 1 dB.

3.0 DATA REDUCTION AND ANALYSIS

3.1 TAPE TRANSLATION, DESPIKING AND CALCULATION OF NOISE SPECTRUM LEVELS

The instrument cassette tapes were translated at the Institute of Ocean Sciences, using a Sea Data Model 12 reader and a Hewlett-Packard computer system. All cassettes translated cleanly, with less than 0.05% parity errors in any of the tapes. The total number of records and the final clock reading were verified against each instrument's start and stop time and sampling interval. The time base accuracy for all five instruments was within the instrument manufacturer's specification (less than 1 minute error in 6 months): the WOTAN at station 1 gained 9 s in 3 months, station 2 lost 4 s in 3 months, station 5 lost 33 s in 4.5 months, station 12 lost 12 s in 4.5 months and station 13 lost 17 s in 4.5 months. After translation and conversion to standard nine-track tape format, the time channels were converted to GMT and the raw data records were plotted. A sample plot of the raw data from station 1 is shown in Figure 6.

As may be seen in Figure 6, the raw data contains a significant number of spikes. Some, such as the one that occurs on January 2, are not present in all channels and may be negative. These are almost certainly recording errors and not actual noise events. There are others, such as the one late on January 5 and the one on January 24, that occur in all channels and that show a systematic variation with frequency (providing they do not reach full scale, which is 5152 in this case), and are very likely short-lived noises. The sharp peaks seen on January 13 and 14, however, are of several hours' duration and are larger at higher frequencies, suggesting rainfall as a possible source.

The first step towards producing a wind-speed record is to remove the first two types of spikes from the record. This was done using a simple, threshold-despiking program which deleted spikes up to three samples in width. Deleted points were replaced by a linear interpolation between neighbouring valid points. The threshold was determined from visual inspection and was set at 850 for the 4.3-kHz (wide and narrow) and the 8.0-kHz channels and at 475 for all other channels. The first valid point (i.e., starting point for the despiking program) was chosen by inspection; after that point any group of up to three points which differed from the preceding value by more than the threshold was deleted and replaced by an interpolation. Figures 7 to 11 show the despiked data.

A particular problem is evident at station 2 (Figure 8). After January 14 there are no occasions on which the noise levels drop to near zero on any of the channels, in contrast to records from all the other instruments and to itself before January 14. Comparison with the record from station 1 (12 km distant) shows that before January 14, the records are nearly identical on all channels. After January 14, only the upper portions of the plots from station 2 appear similar to those from station 1, and those portions have been shifted upward. The data suggest that after January 14, the instrument at station 2 was subjected to a constant relatively high level of background noise. One possible explanation would be a fault in the instrument which generated

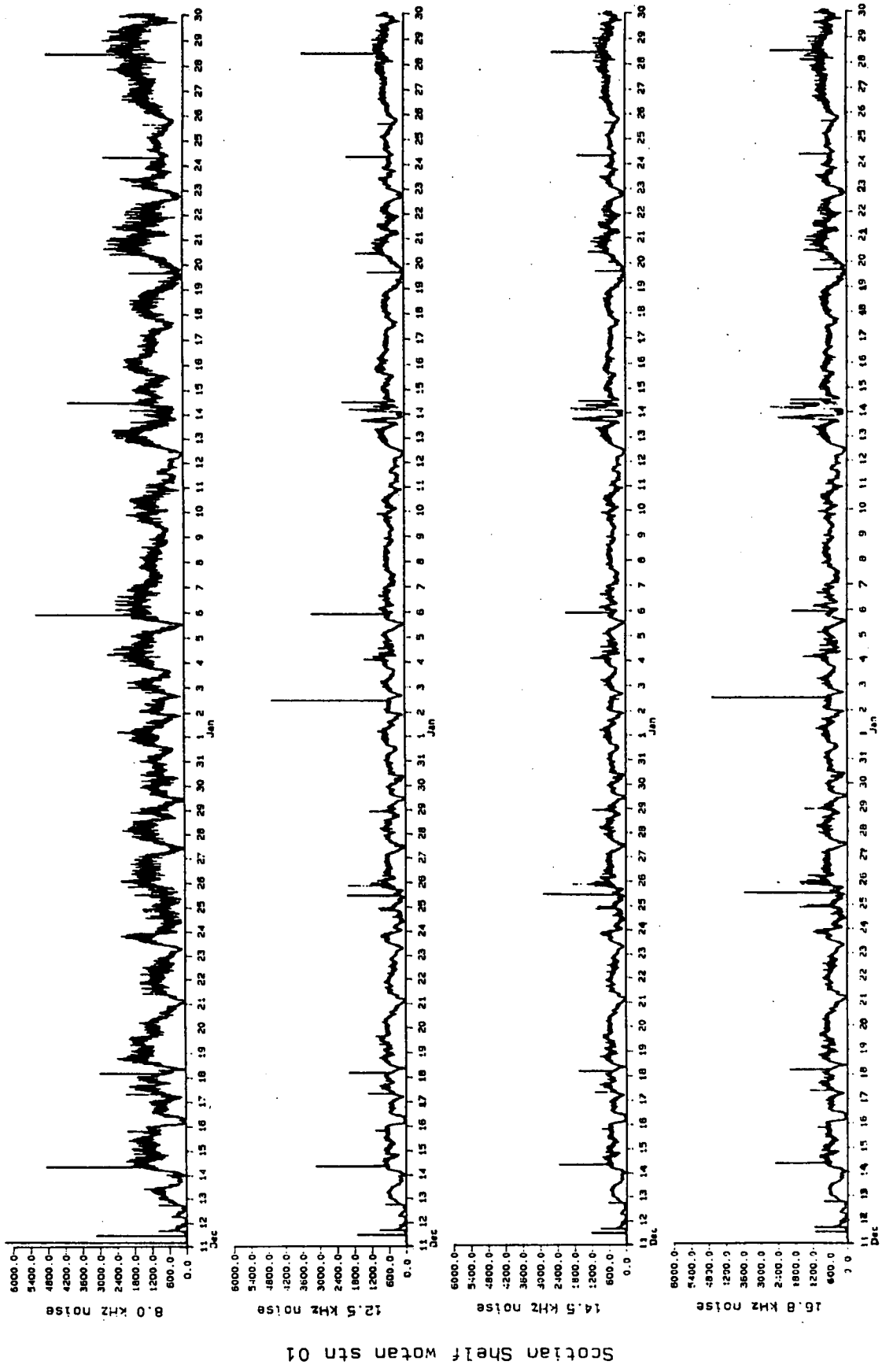

Figure 6 (part 1): Raw data plot from station 1.

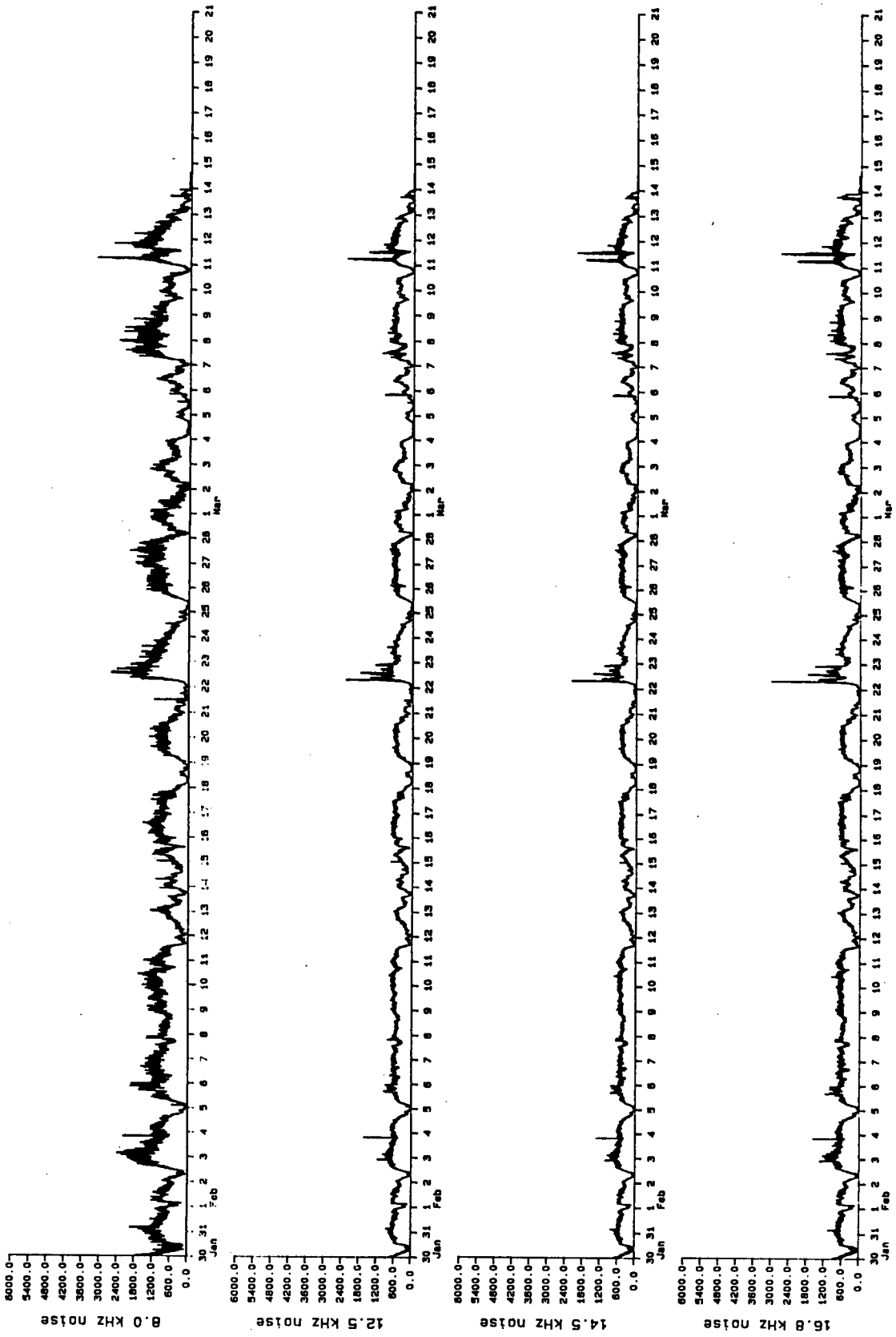

Figure 6 (part 2): Raw data plot from station 1.

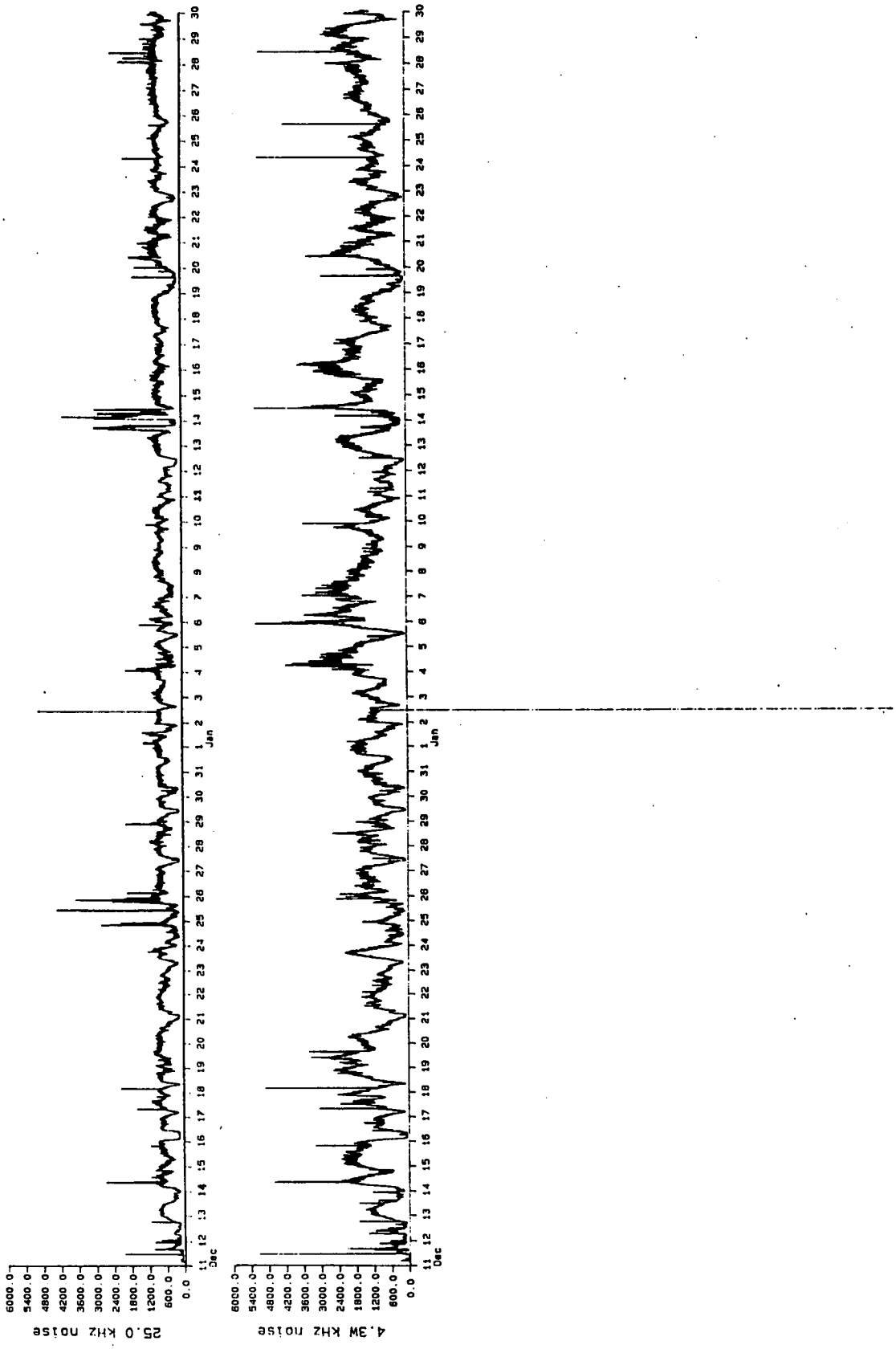

Figure 6 (part 3): Raw data plot from station 1.

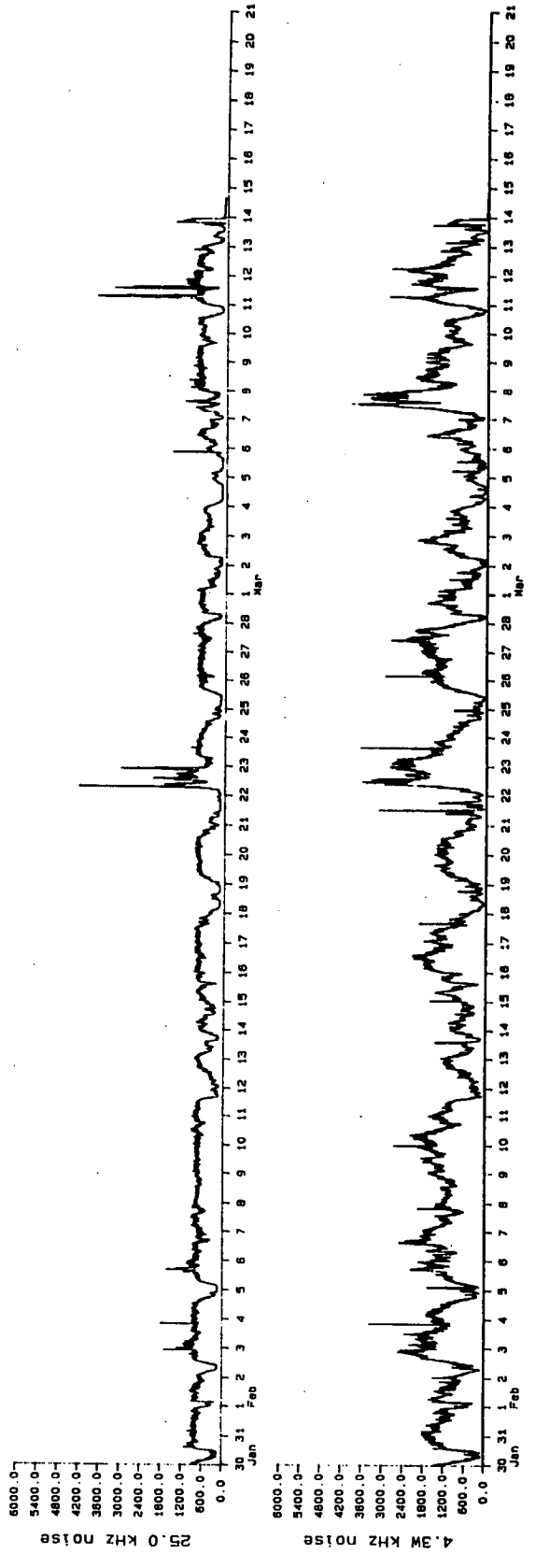

Figure 6 (part 4): Raw data plot from station 1.

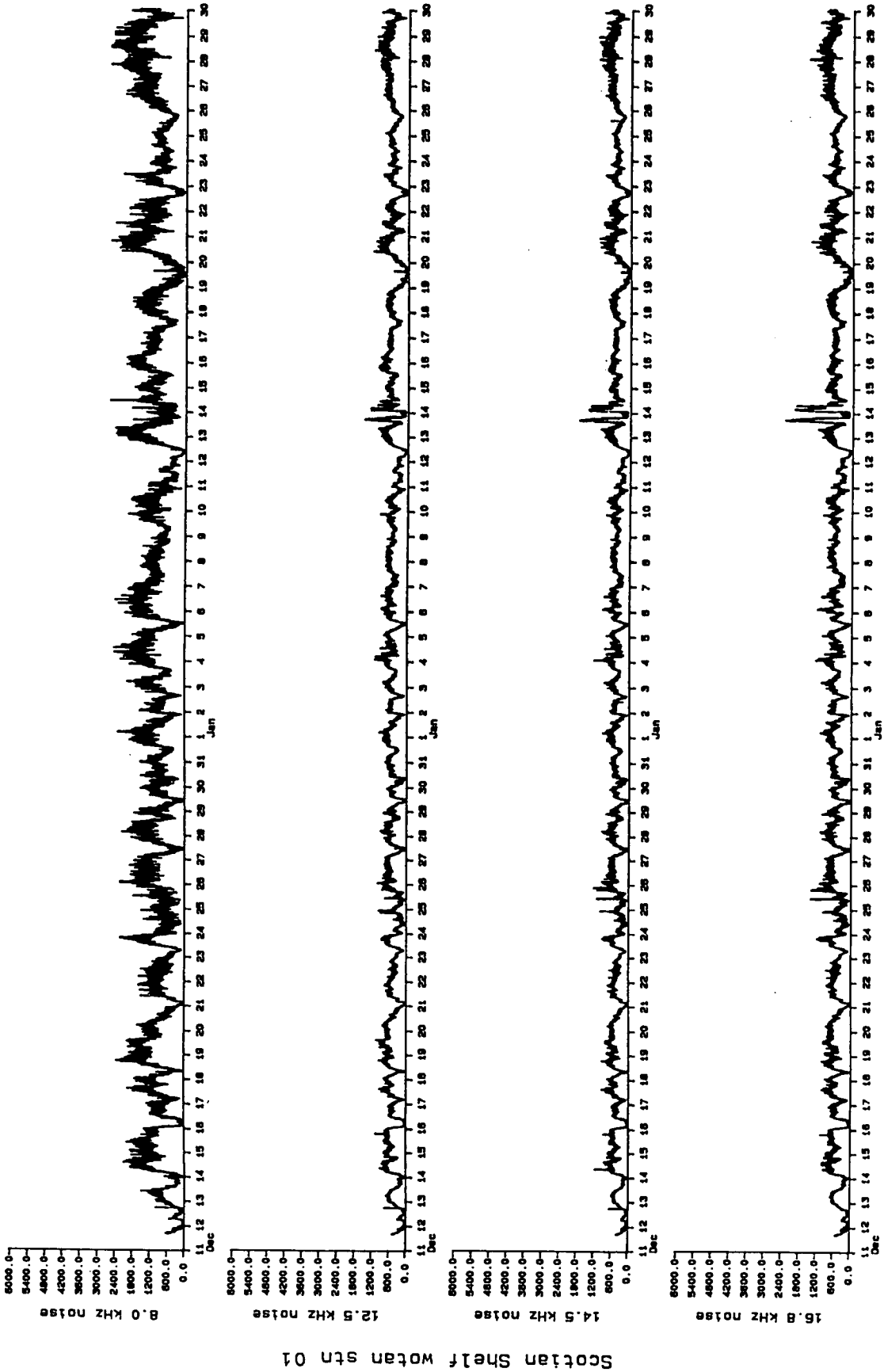

Figure 7 (part 1): Despiked data from station 1.

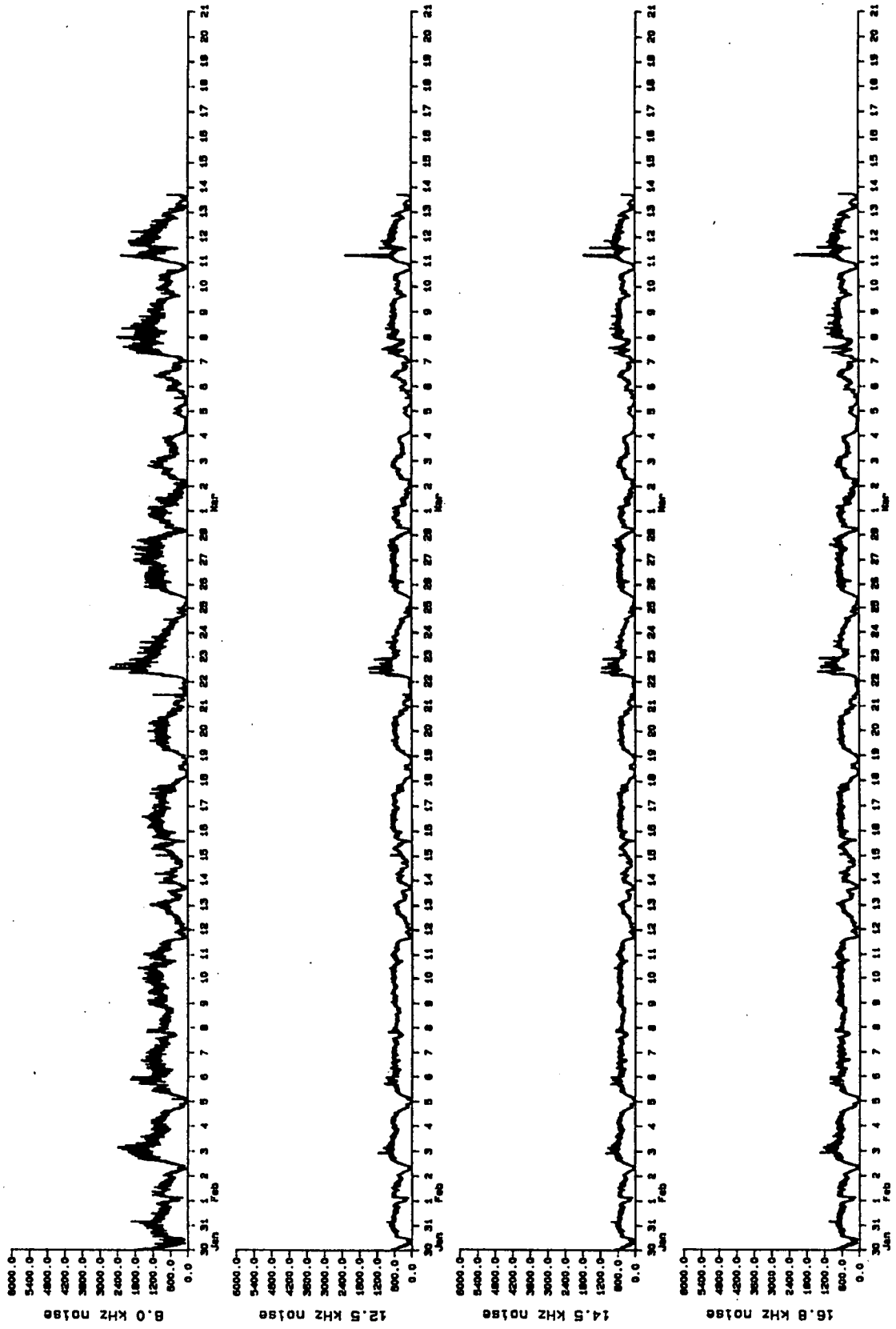

Figure 7 (part 2): Despiked data from station 1.

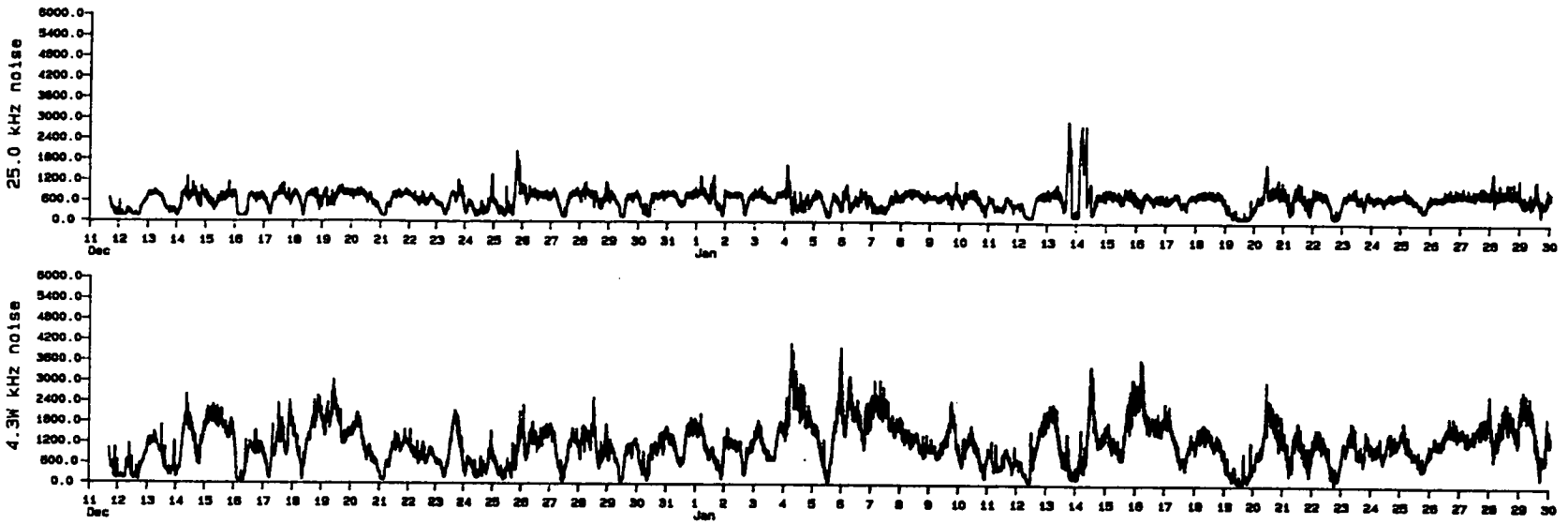

Figure 7 (part 3): Despiked data from station 1.

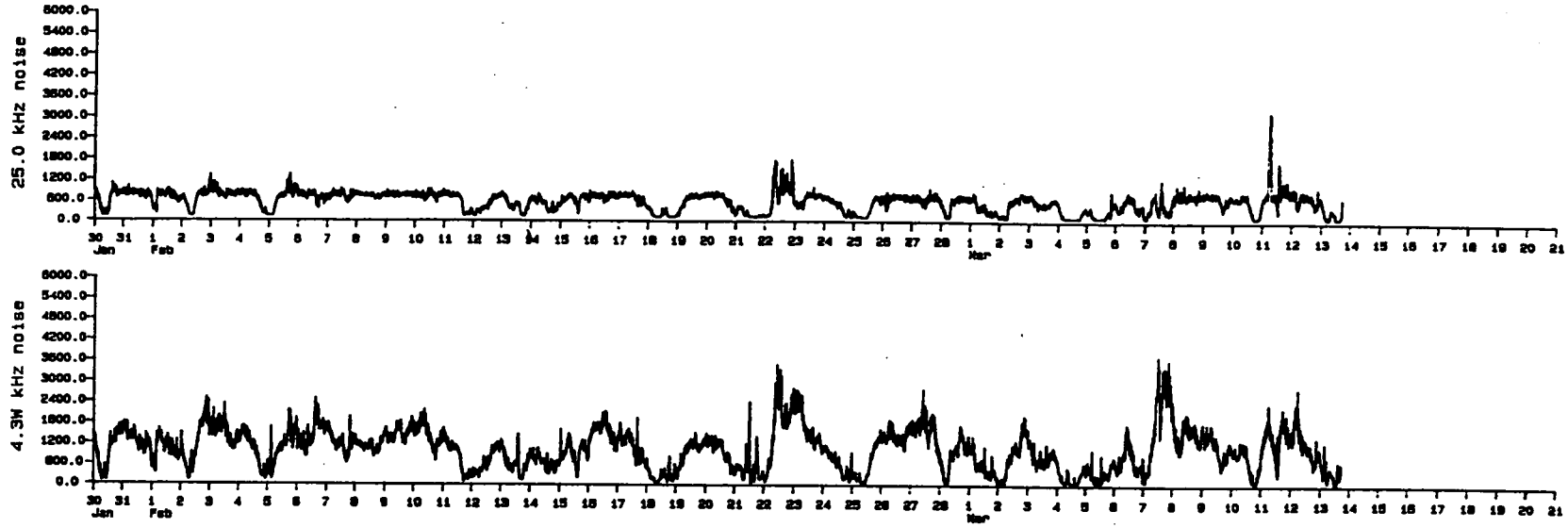

Figure 7 (part 4): Despiked data from station 1.

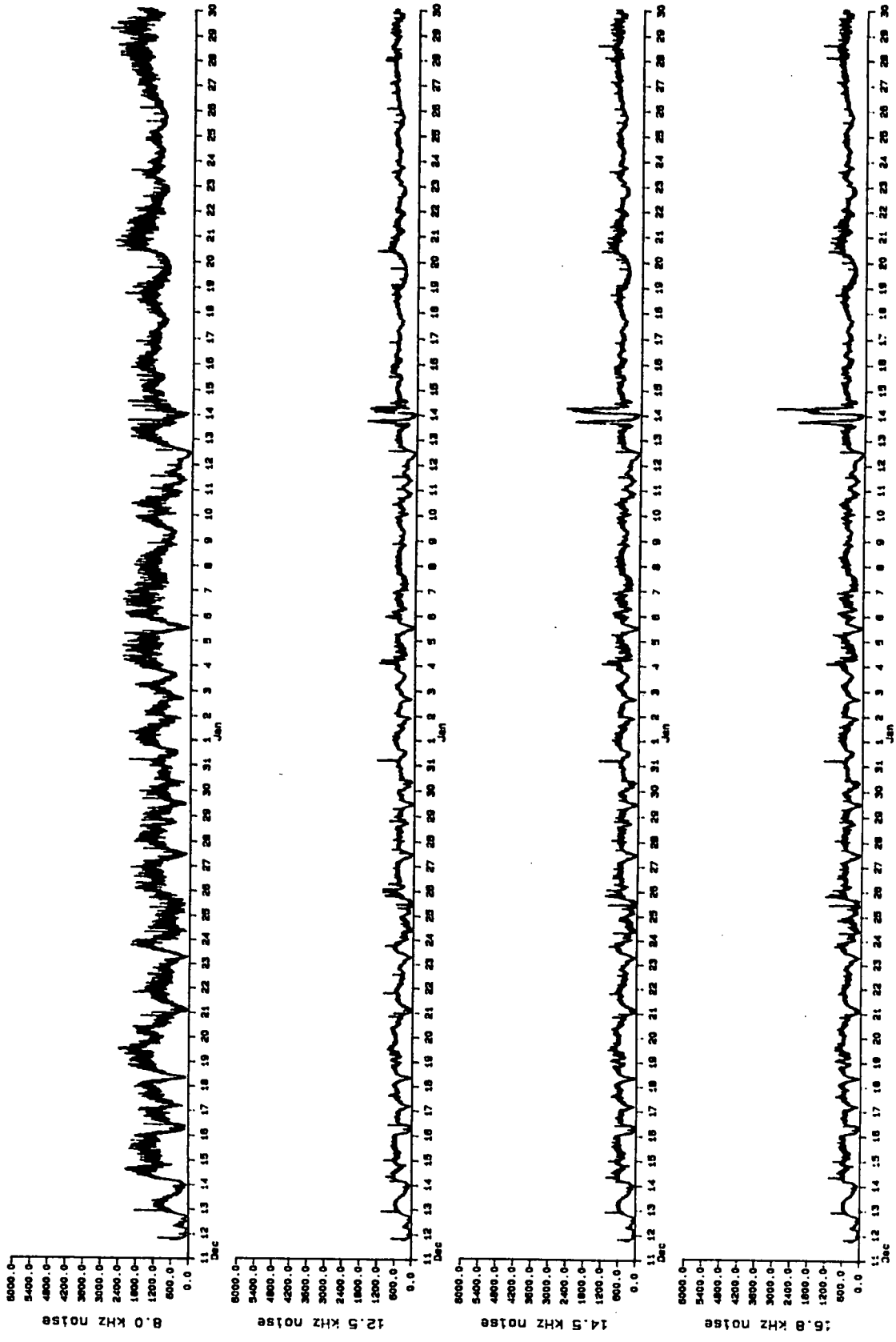

Figure 8 (part 1): Despiked data from station 2.

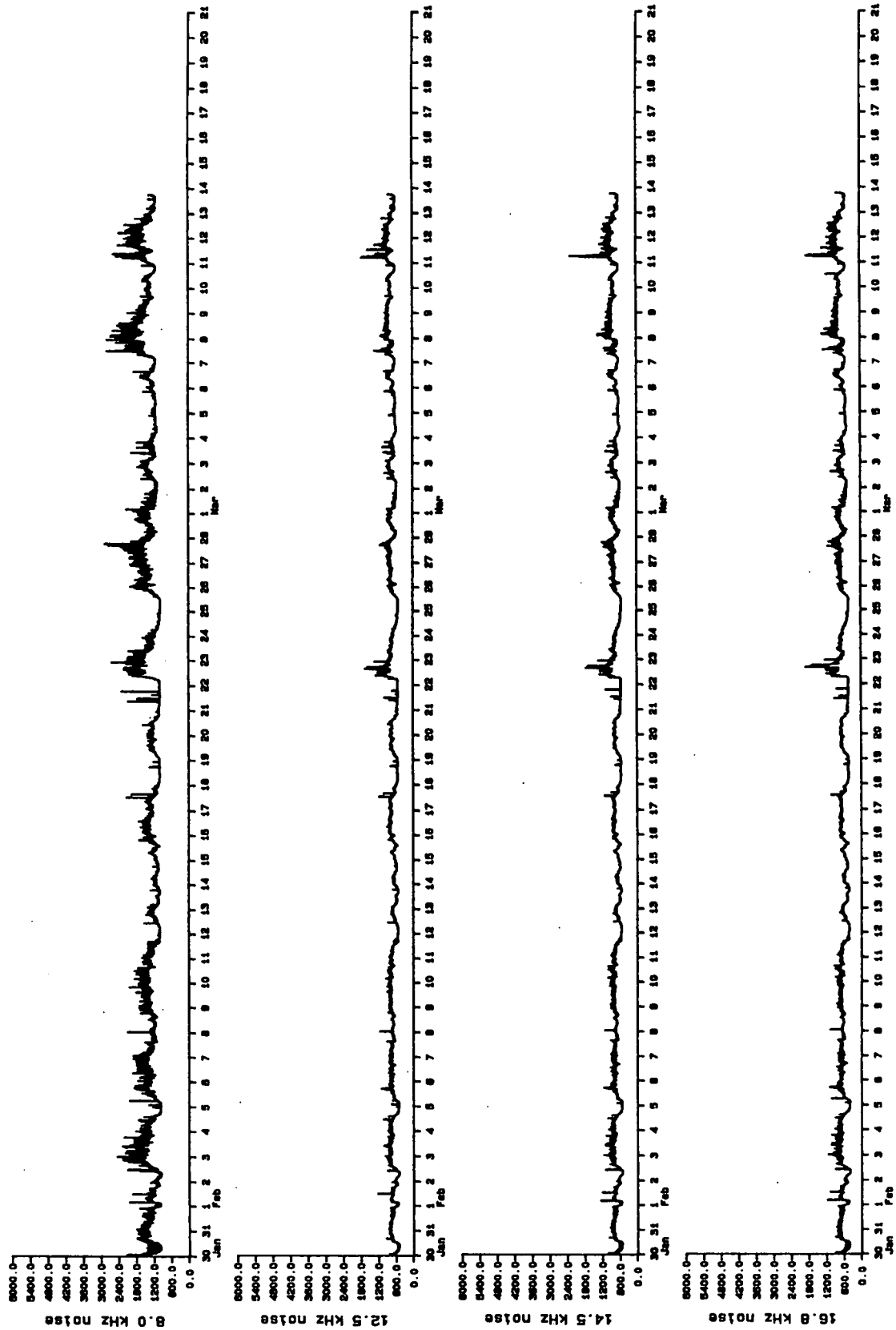

Figure 8 (part 2): Despiked data from station 2.

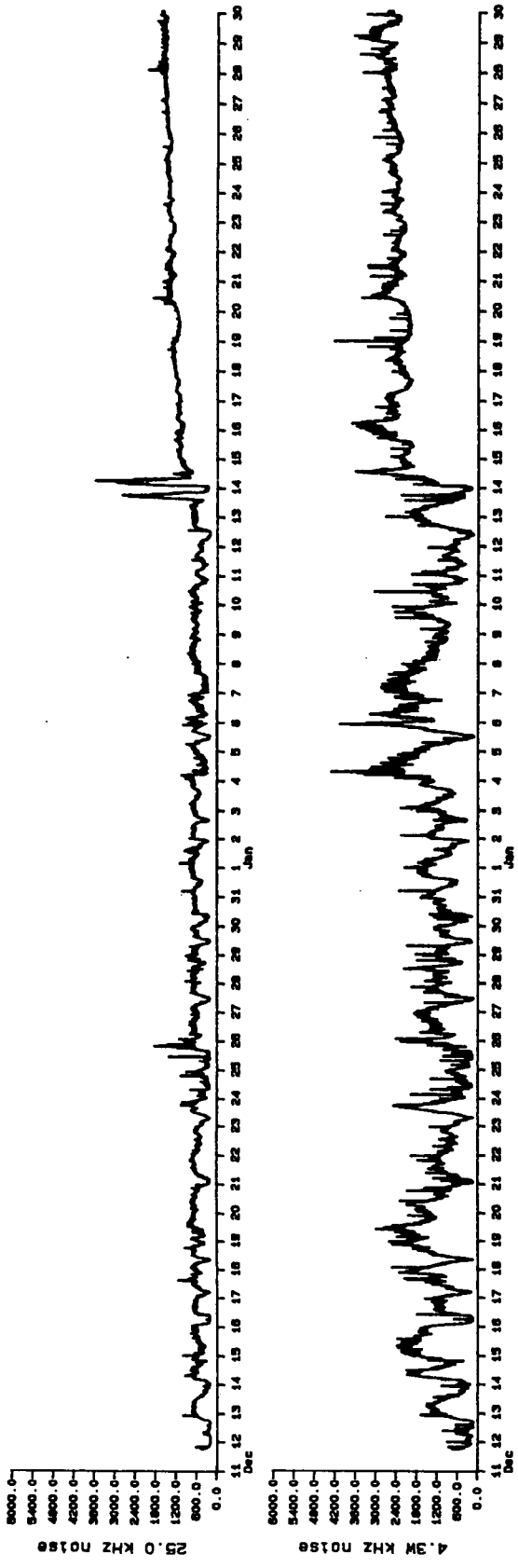

Figure 8 (part 3): Despiked data from station 2.

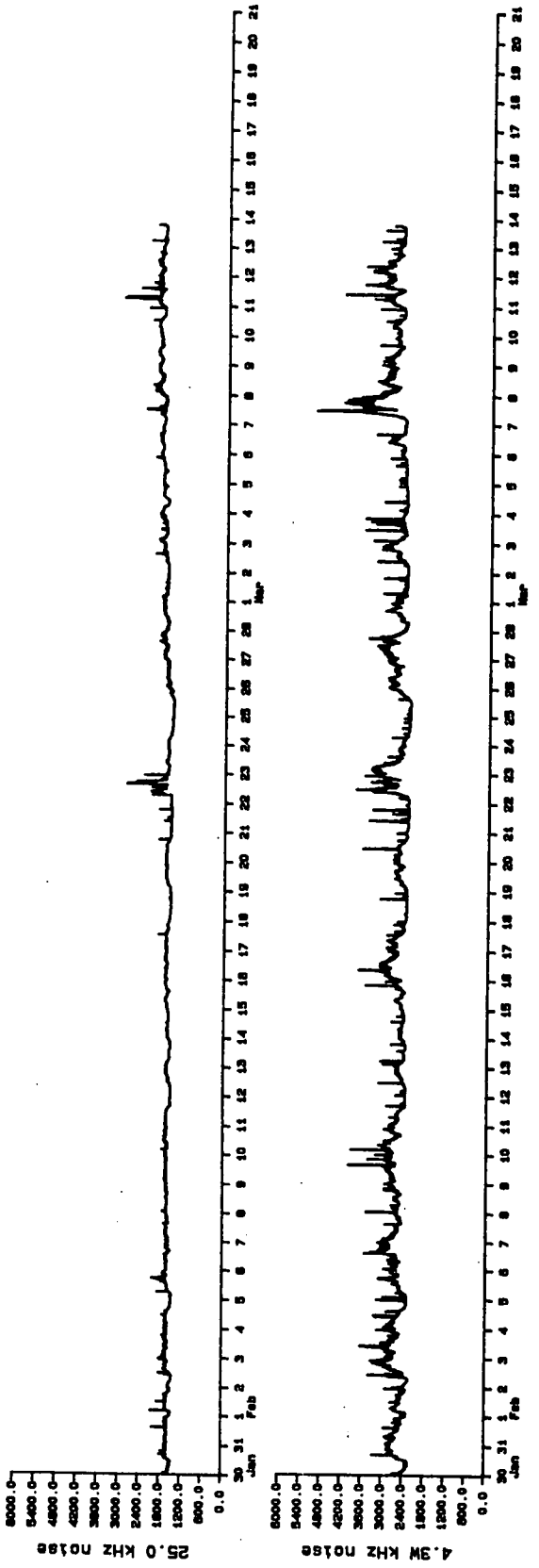

Figure 8 (part 4): Despiked data from station 2.

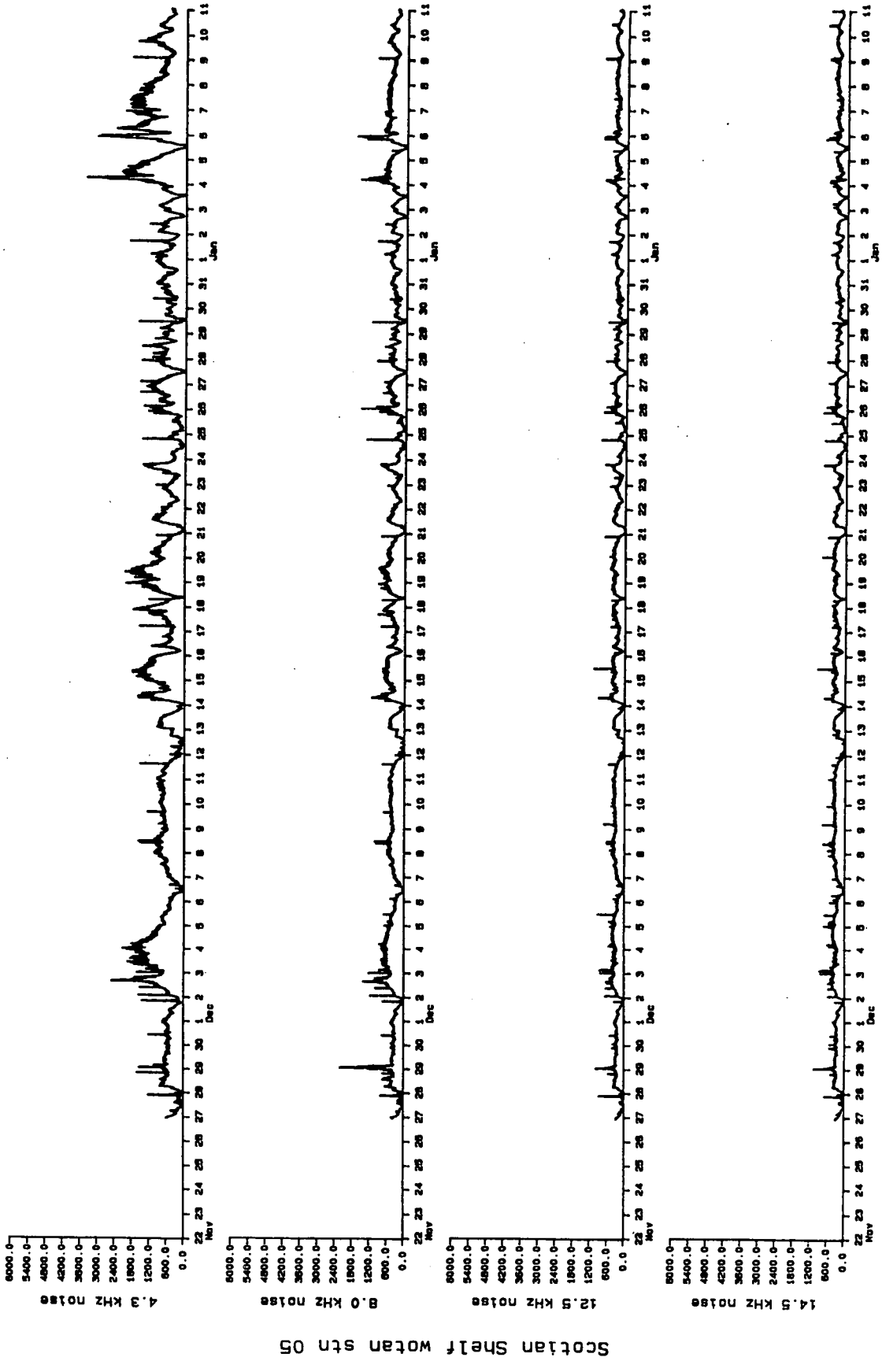

Figure 9 (part 1): Despiked data from station 5.

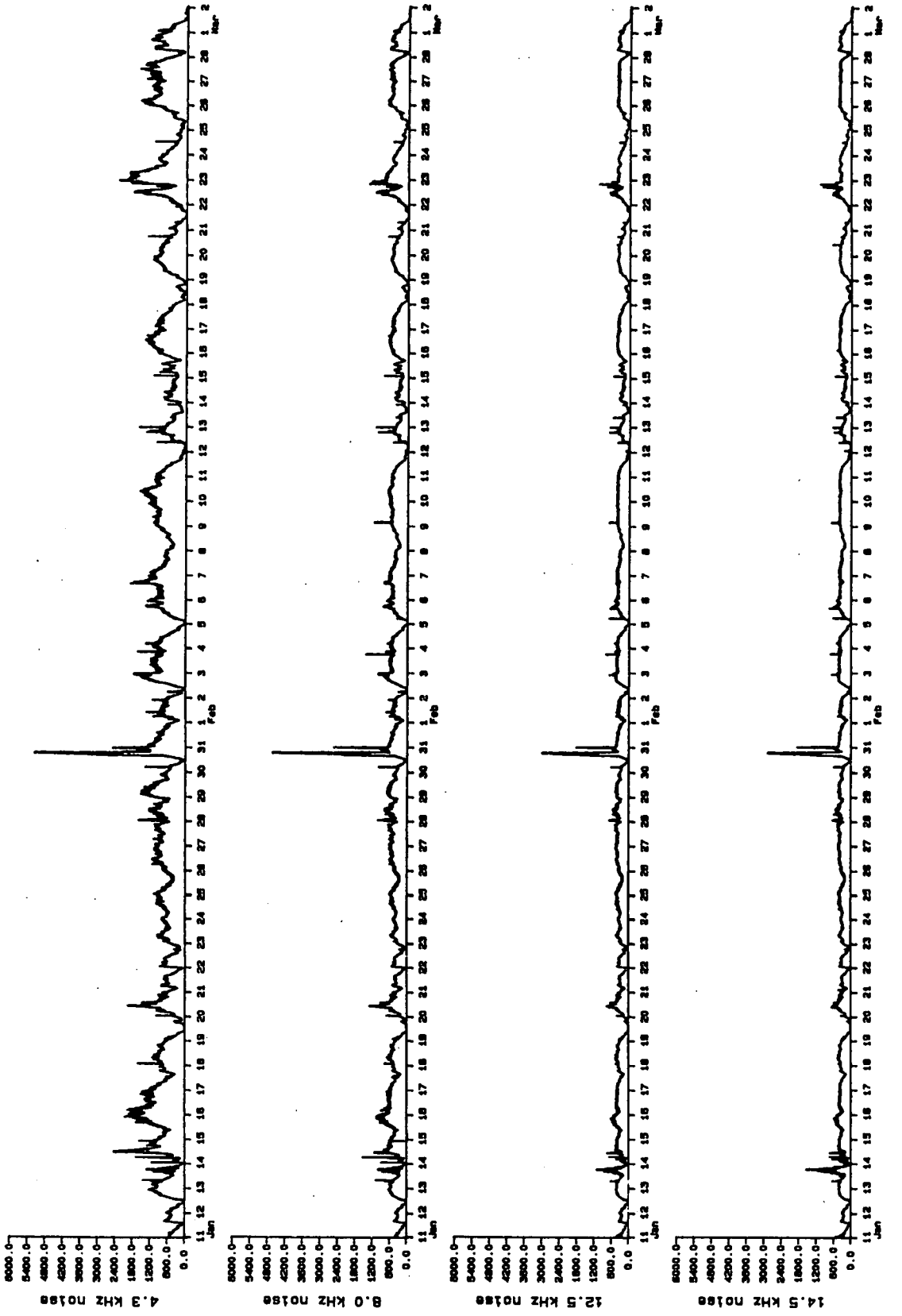

Figure 9 (part 2): Despiked data from station 5.

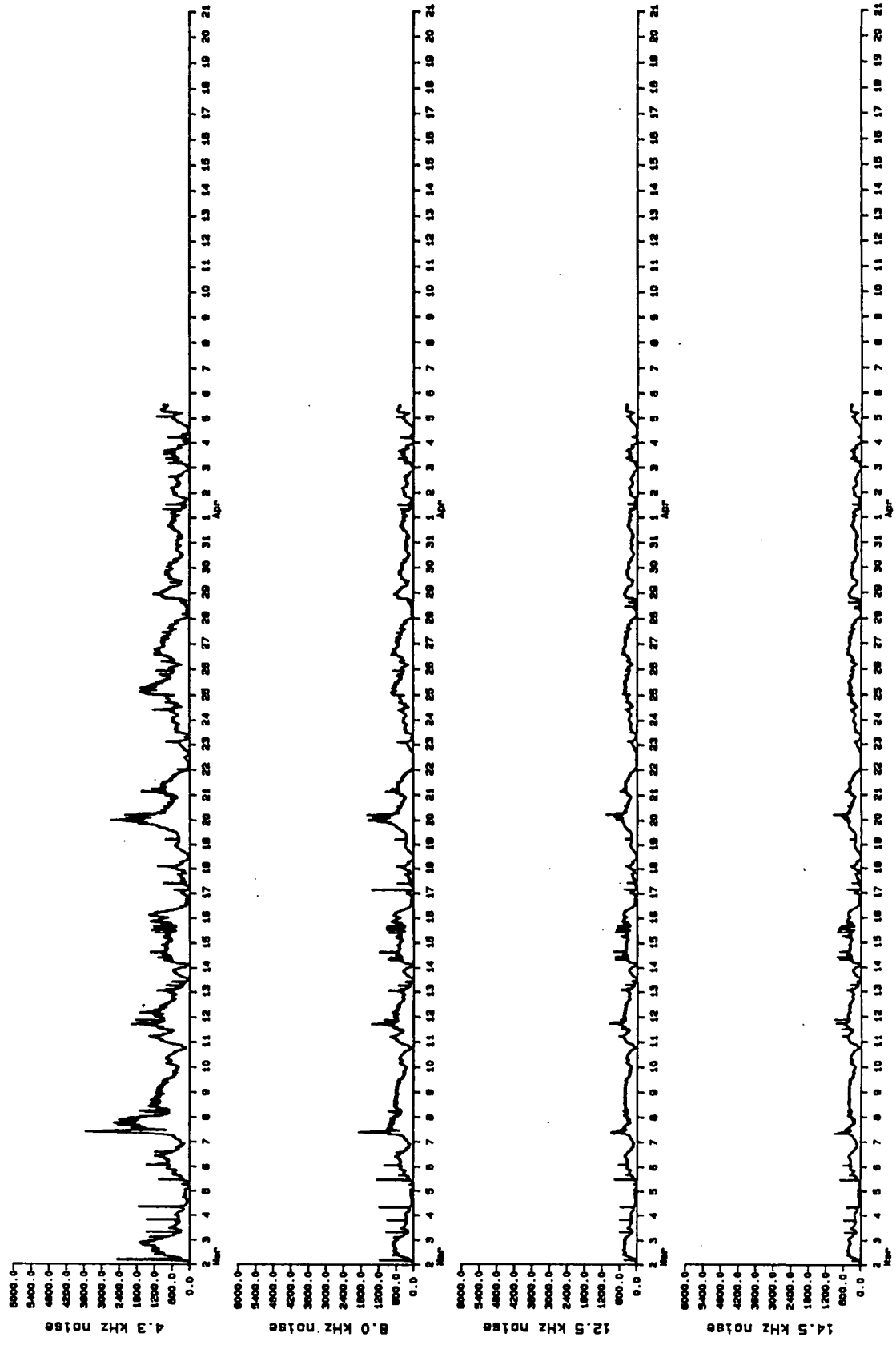

Figure 9 (part 3): Despiked data from station 5.

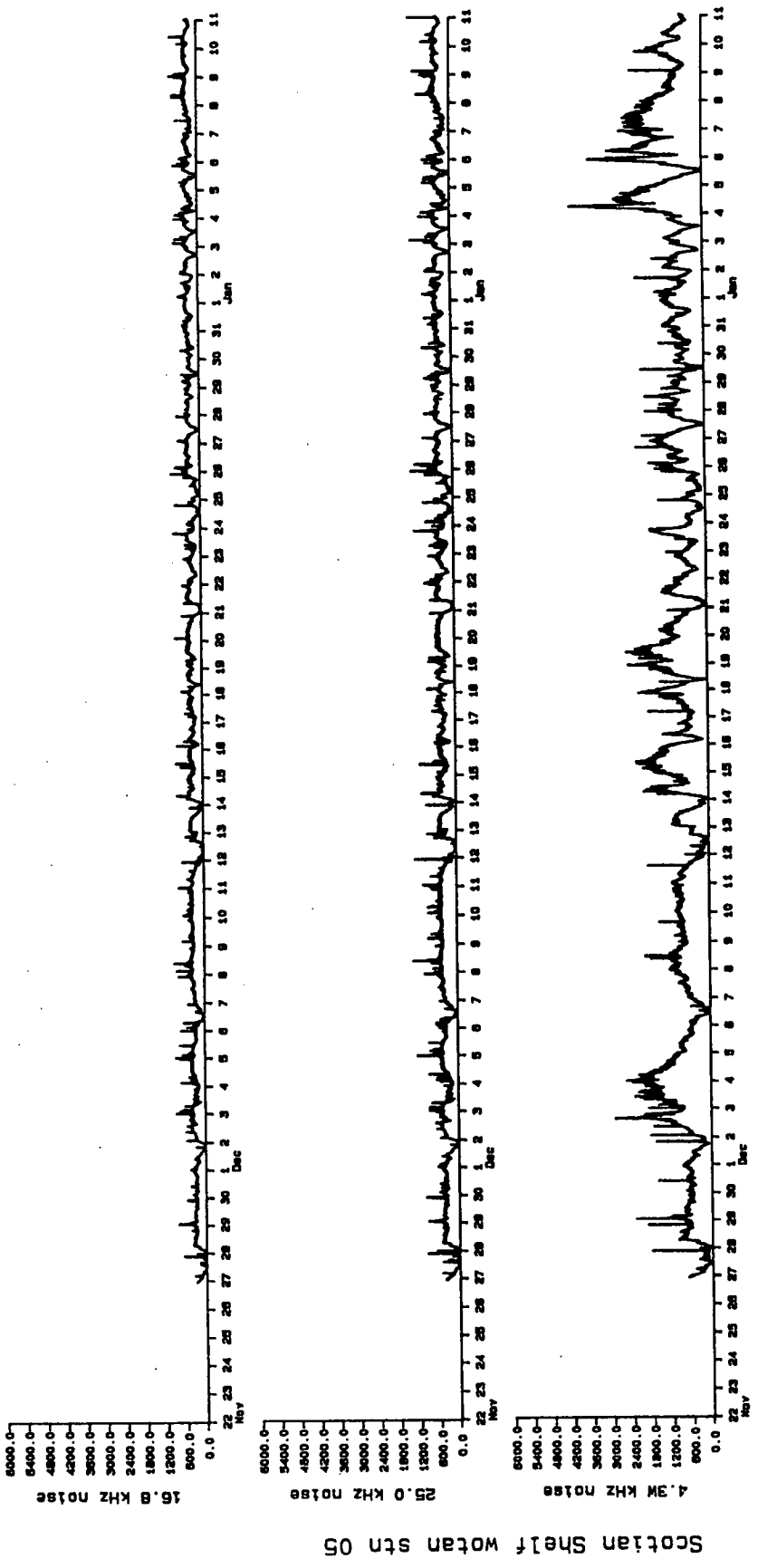

Figure 9 (part 4): Despiked data from station 5.

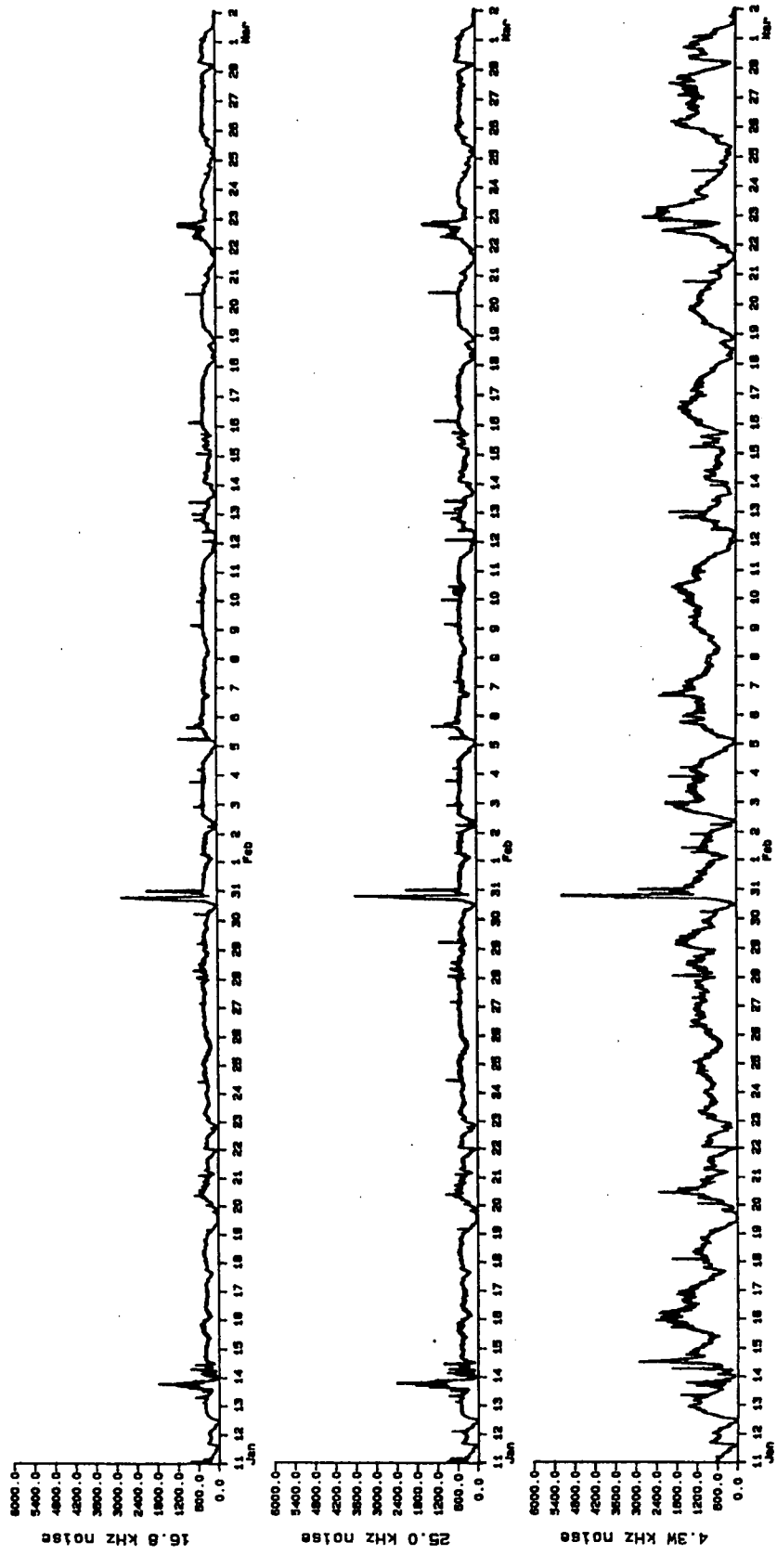

Figure 9 (part 5): Despiked data from station 5.

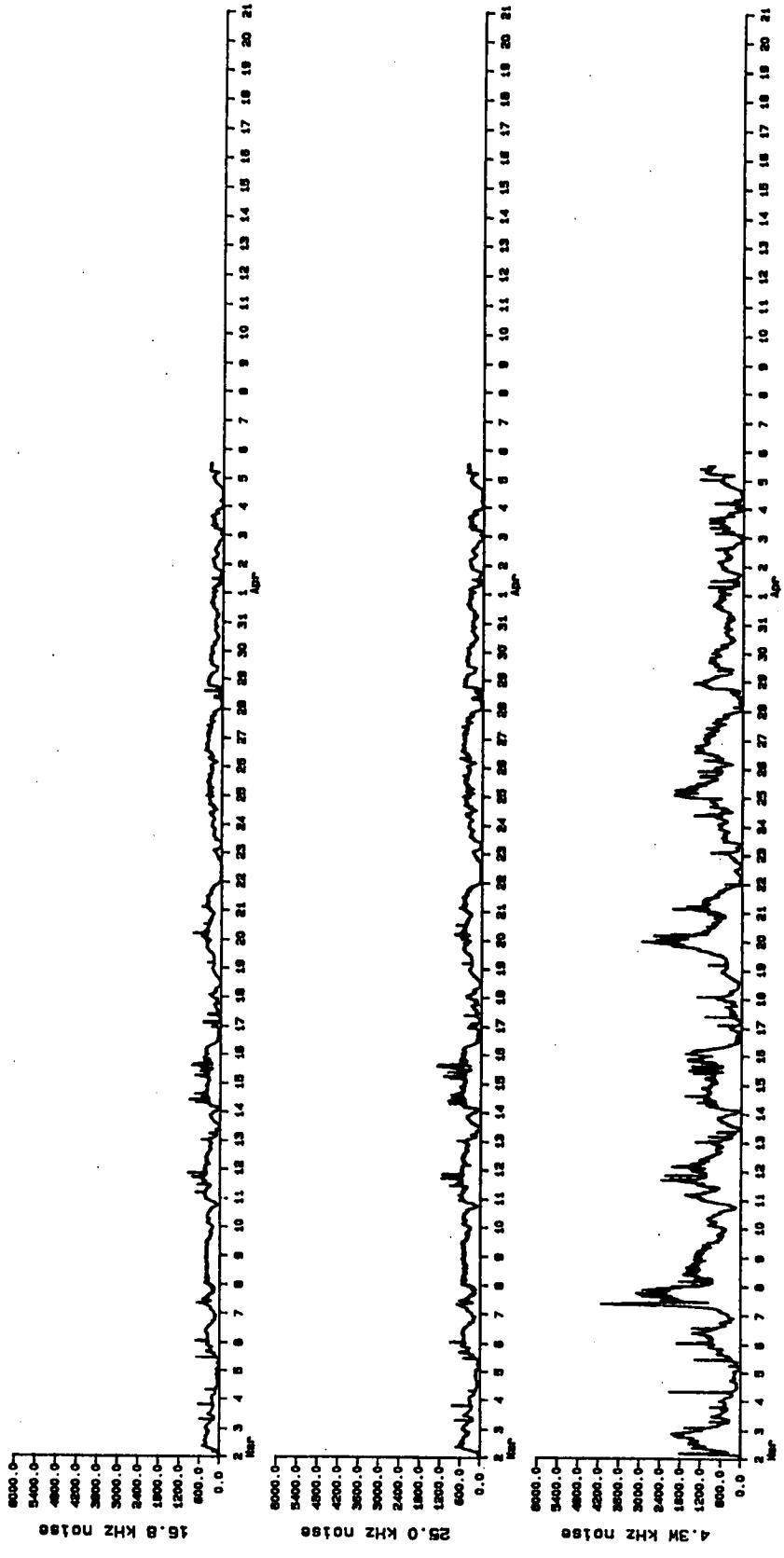

Figure 9 (part 6): Despiked data from station 5.

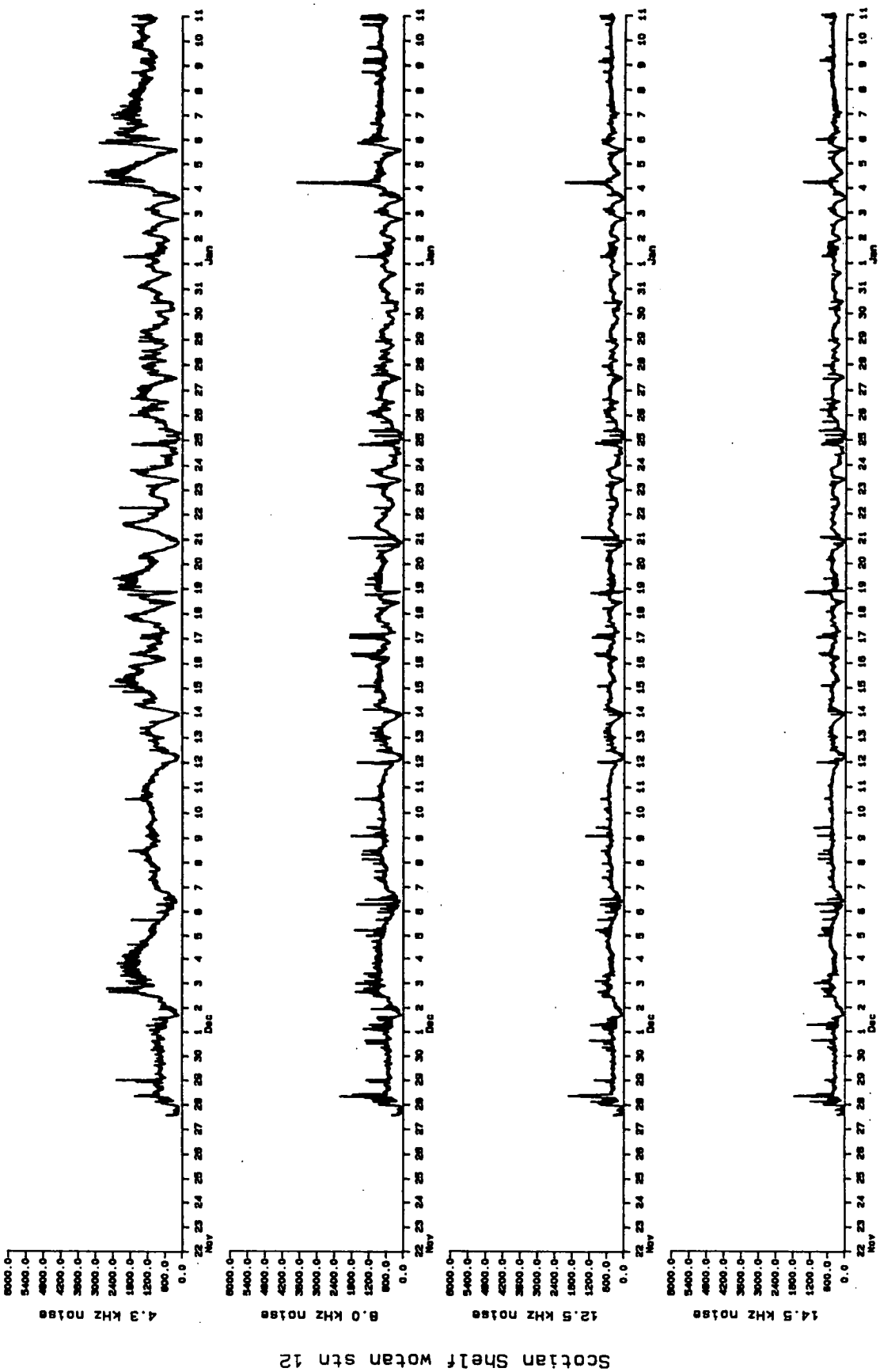

Figure 10 (part 1): Despiked data from station 12.

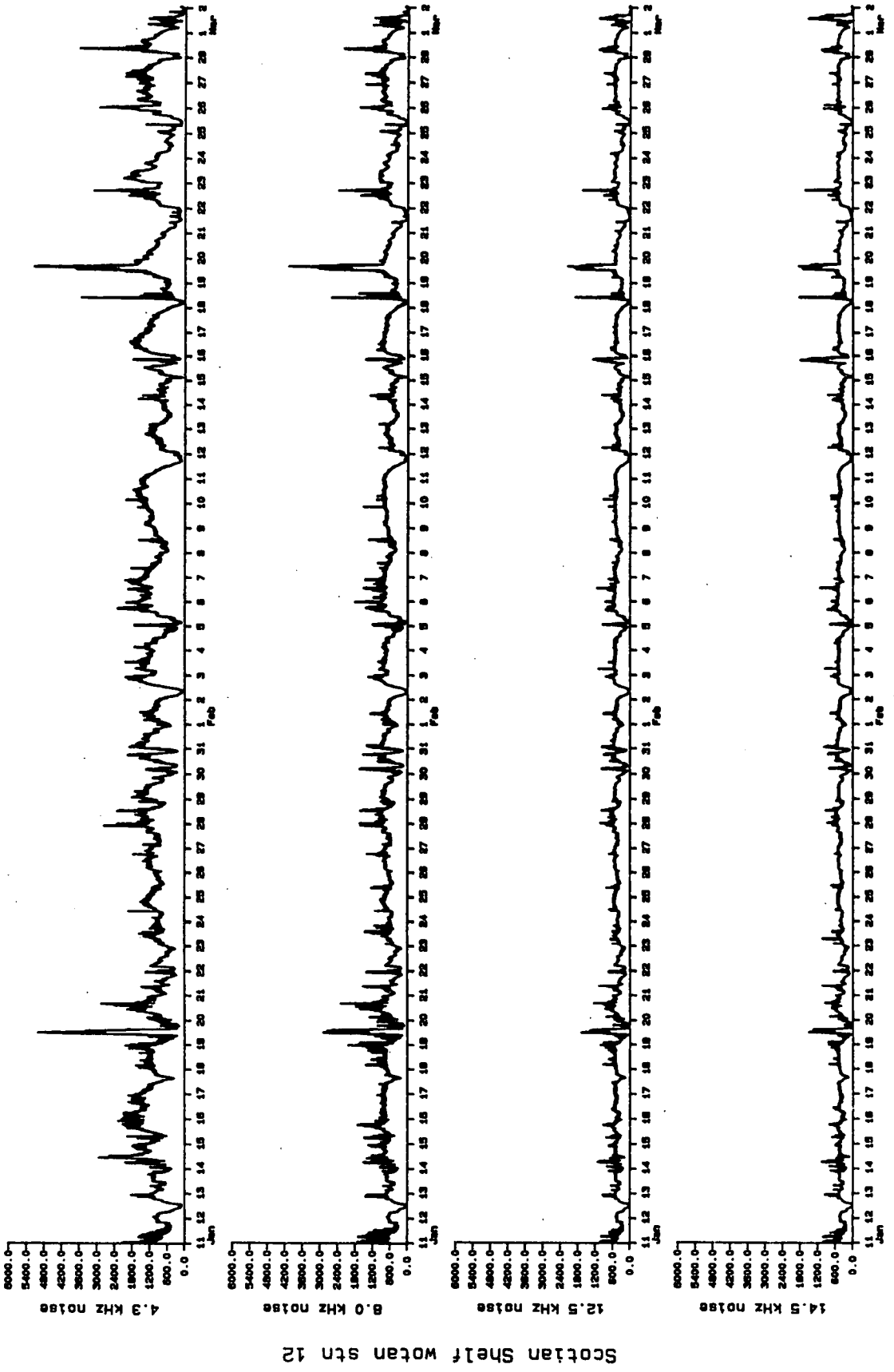

Figure 10 (part 2): Despiked data from station 12.

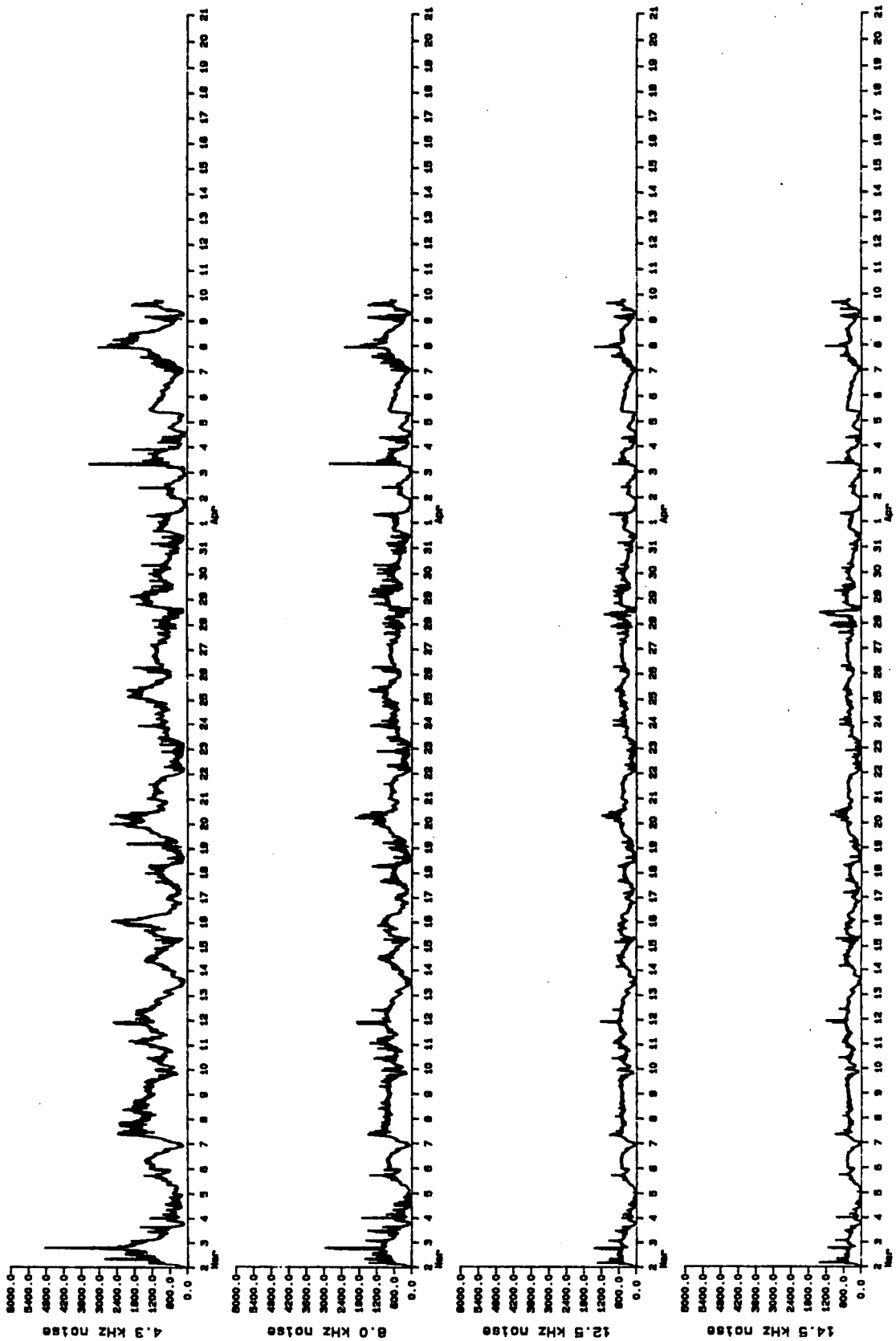

Figure 10 (part 3): Despiked data from station 12.

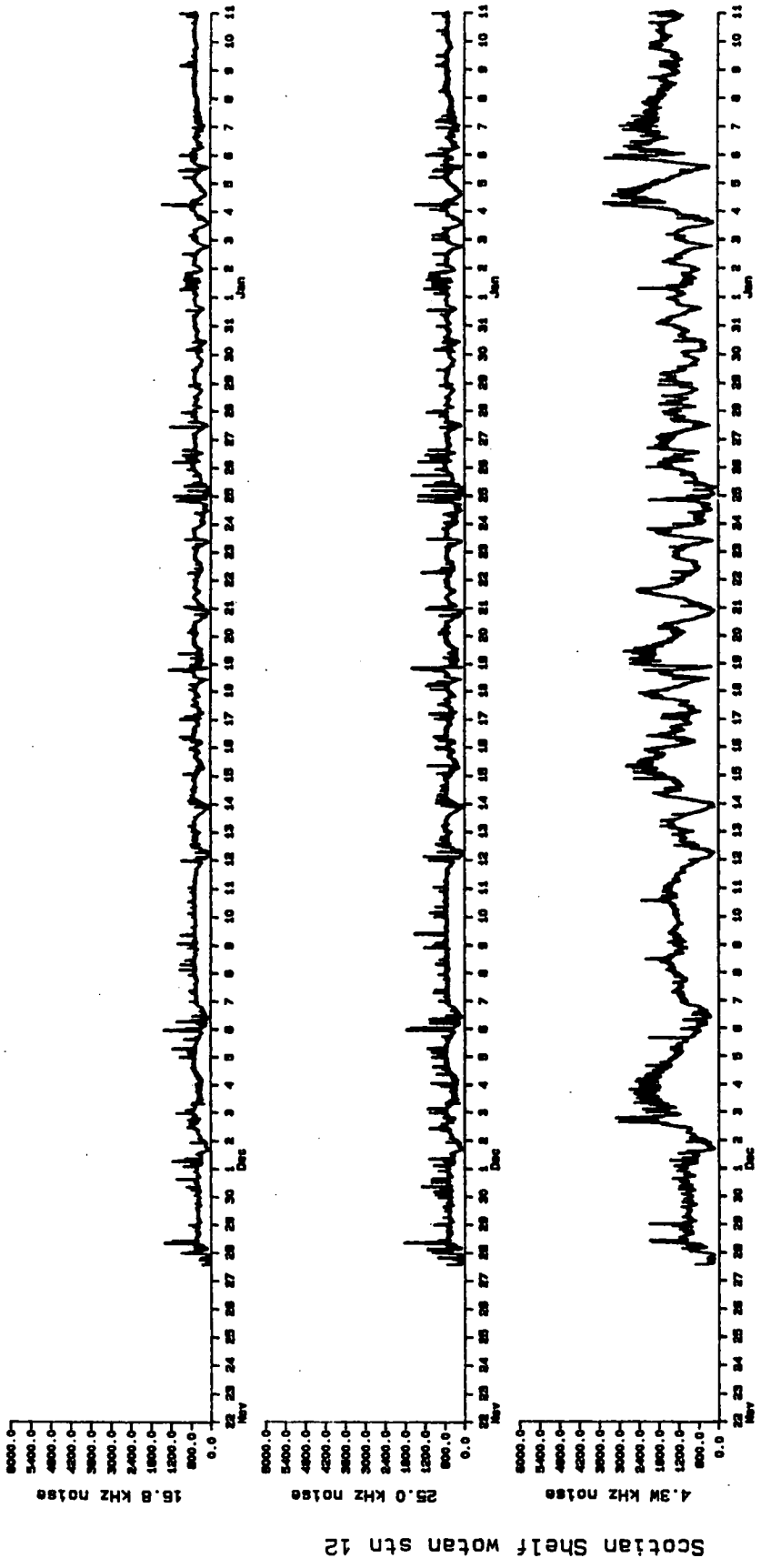

Figure 10 (part 4): Despiked data from station 12.

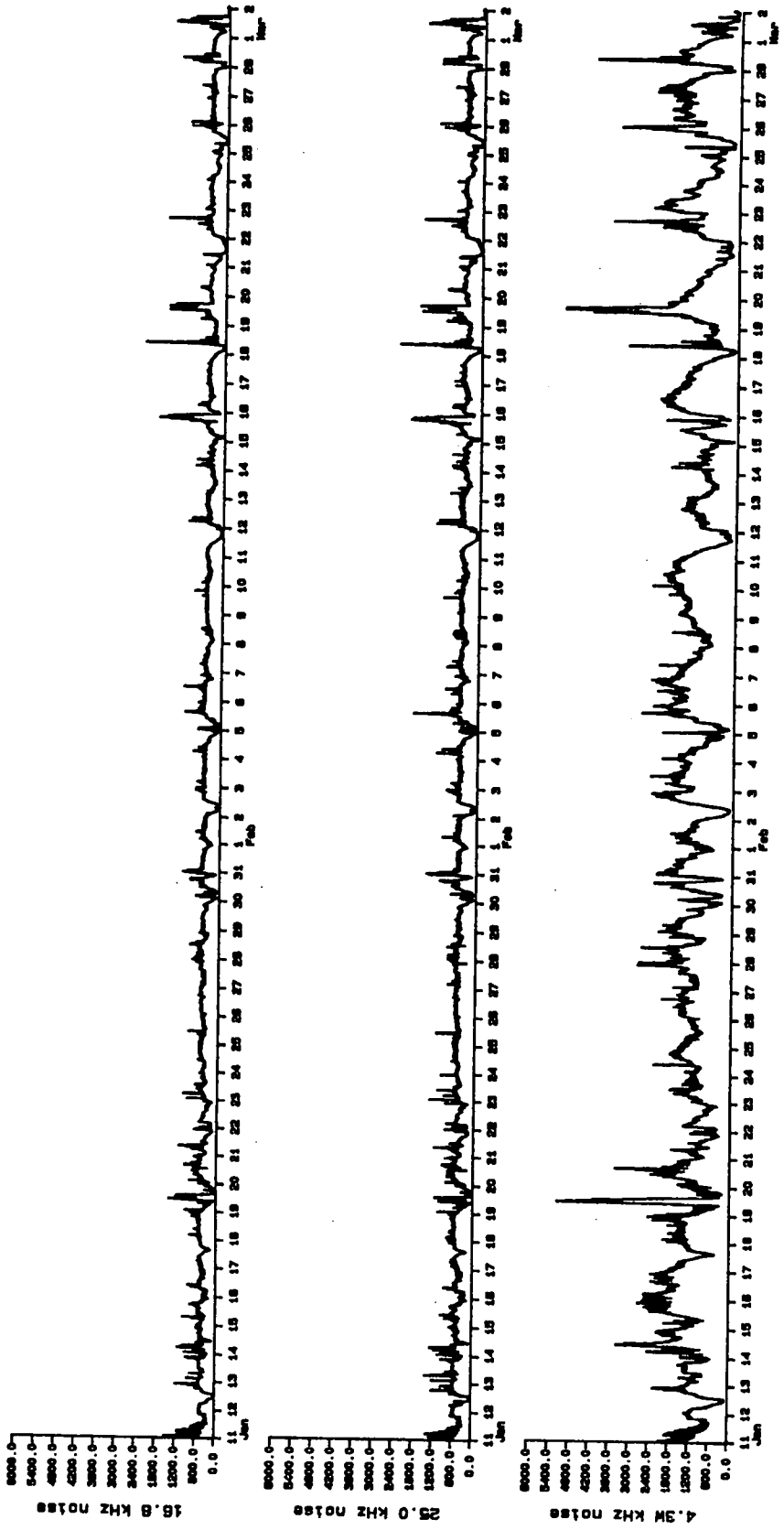

Figure 10 (part 5): Despiked data from station 12.

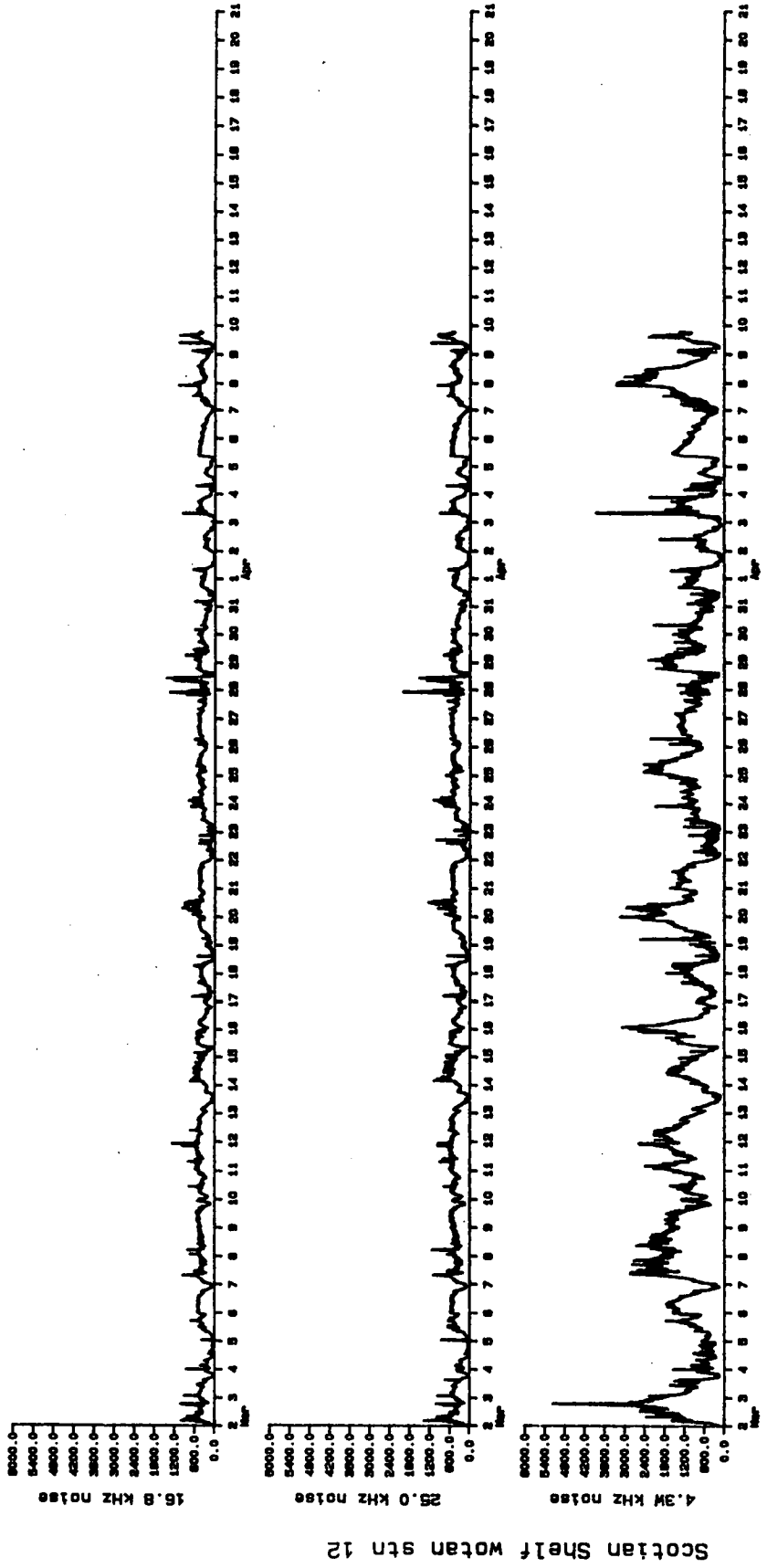

Figure 10 (part 6): Despiked data from station 12.

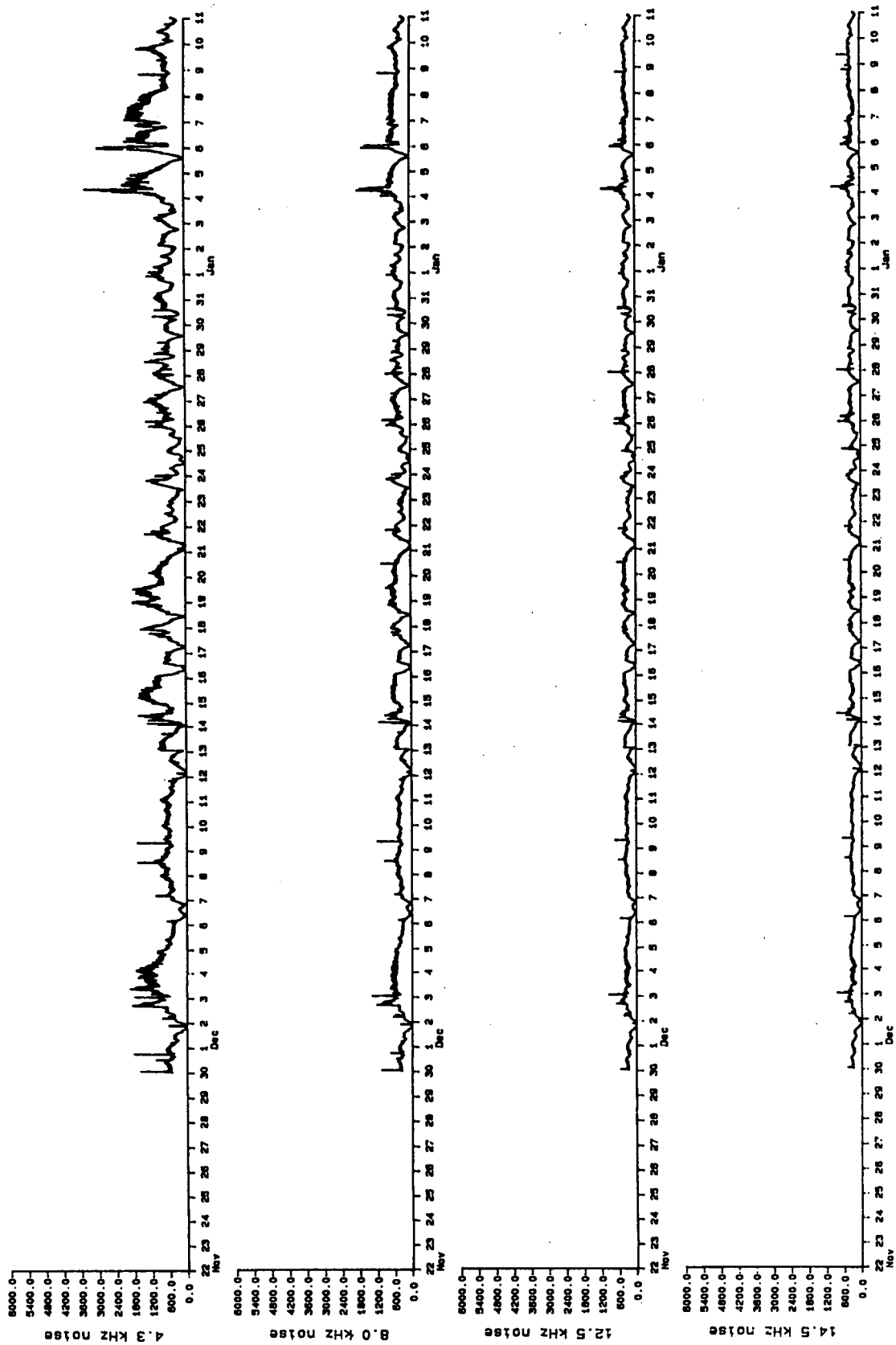

Figure 11 (part 1): Despiked data from station 13.

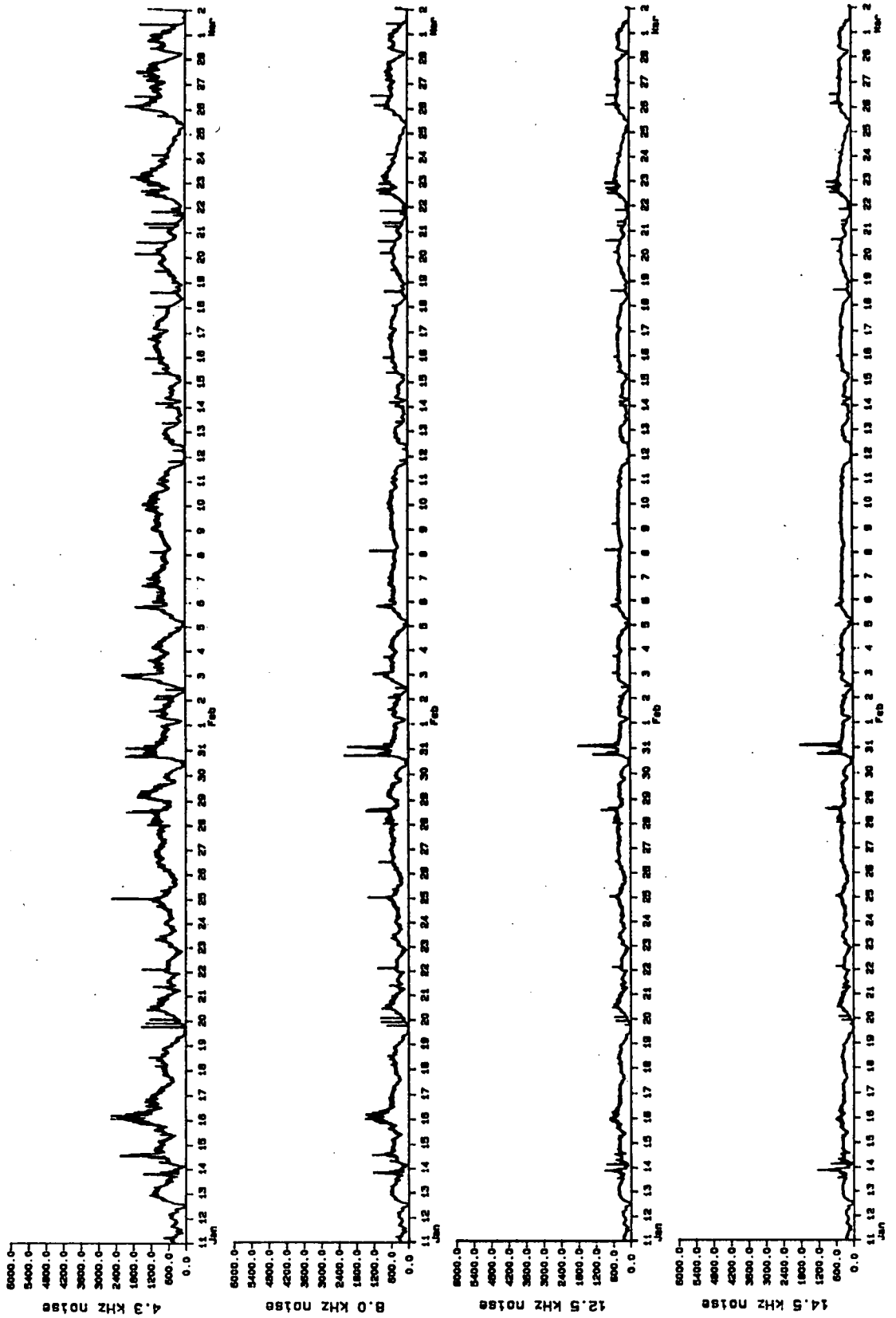

Figure 11 (part 2): Despiked data from station 13.

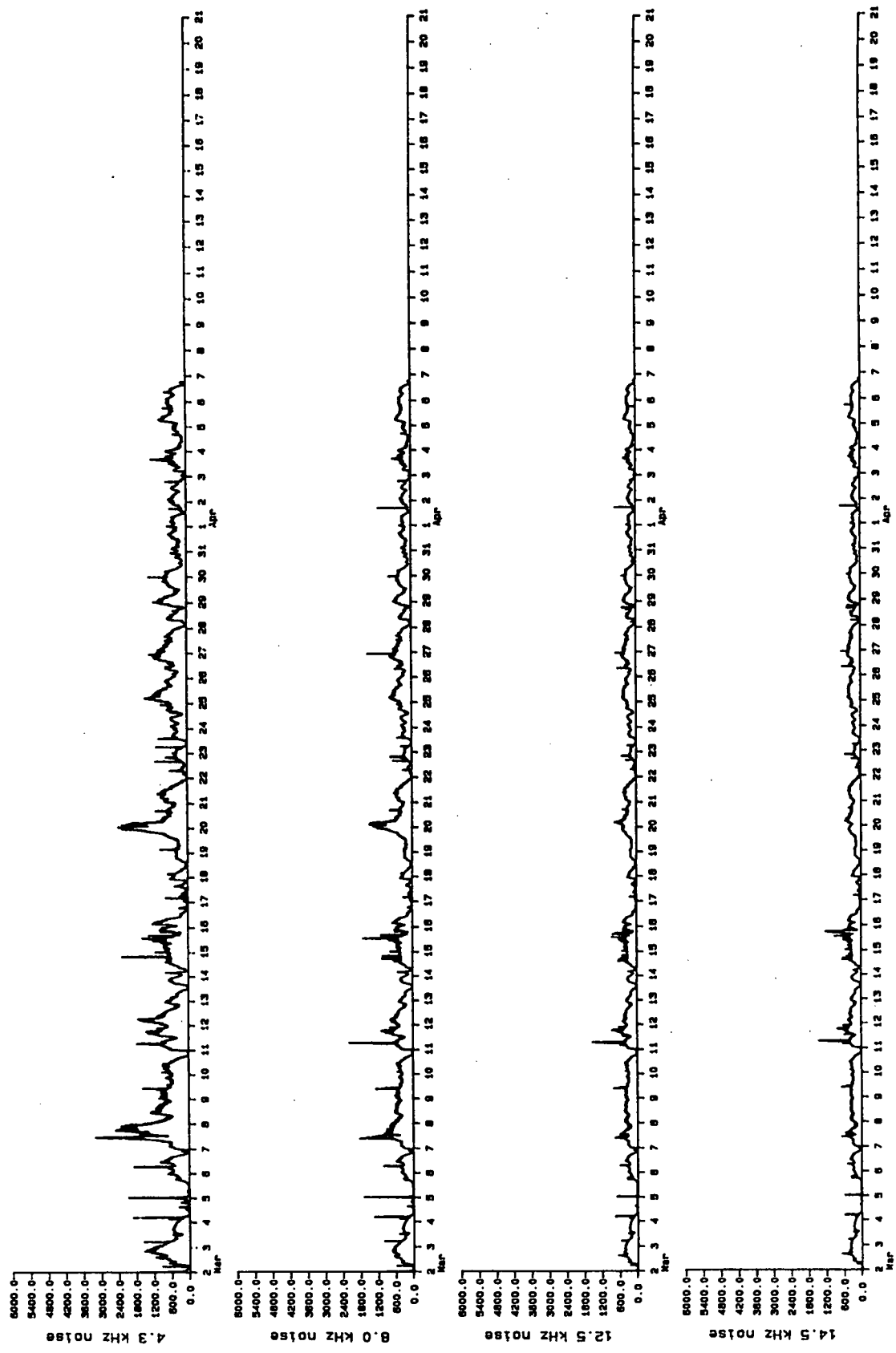

Figure 11 (part 3): Despiked data from station 13.

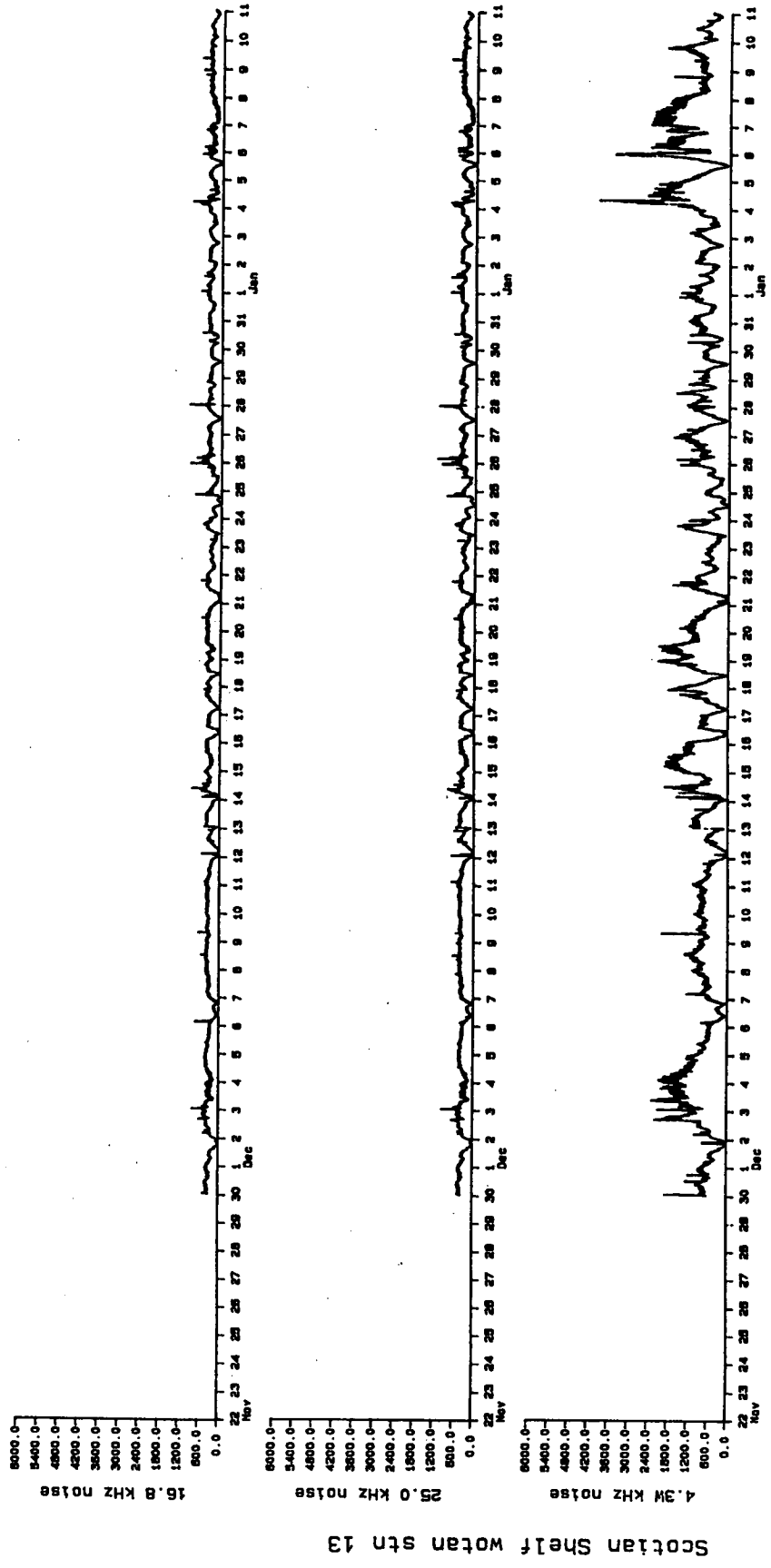

Figure 11 (part 4): Despiked data from station 13.

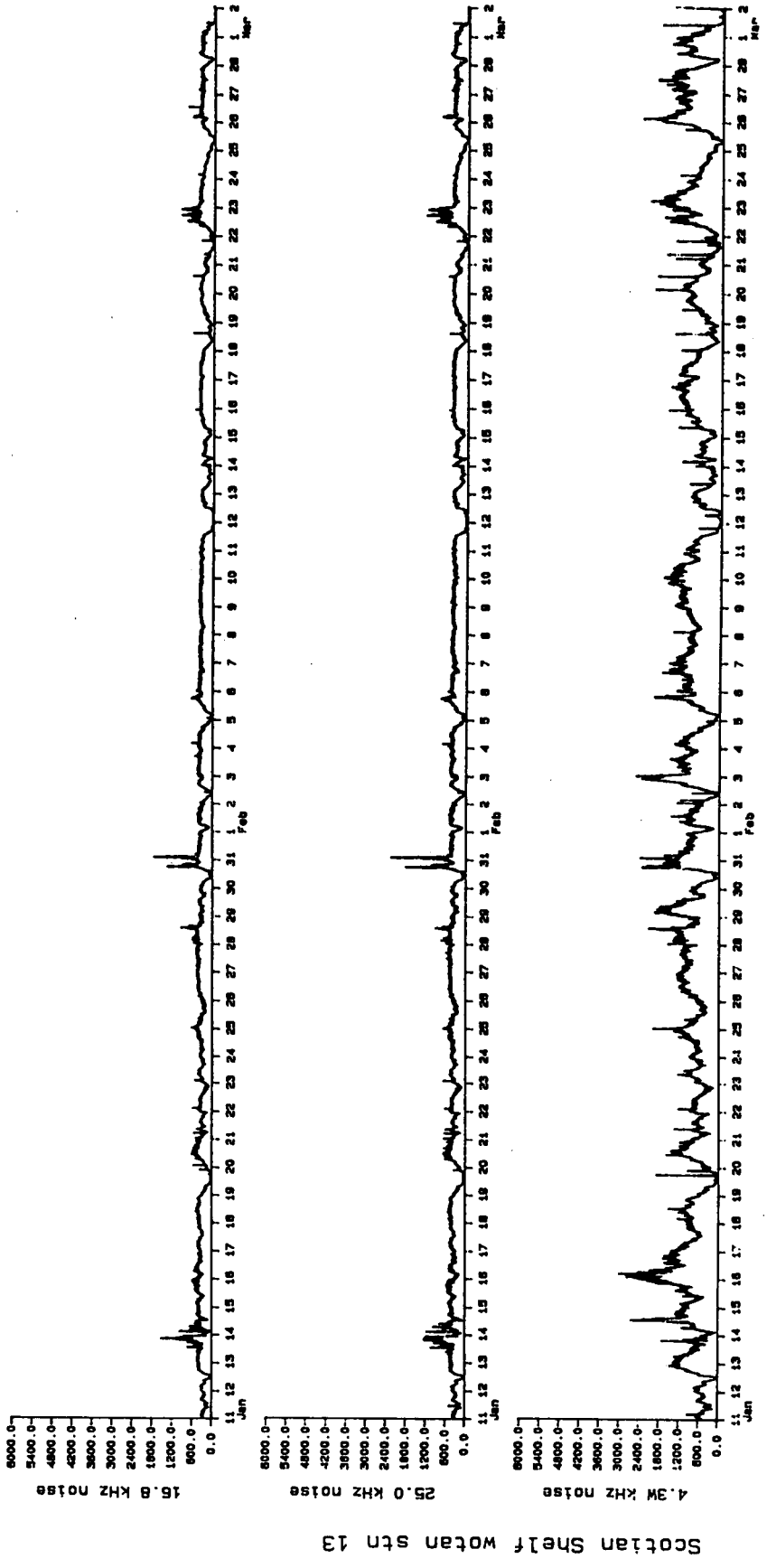

Figure 11 (part 5): Despiked data from station 13.

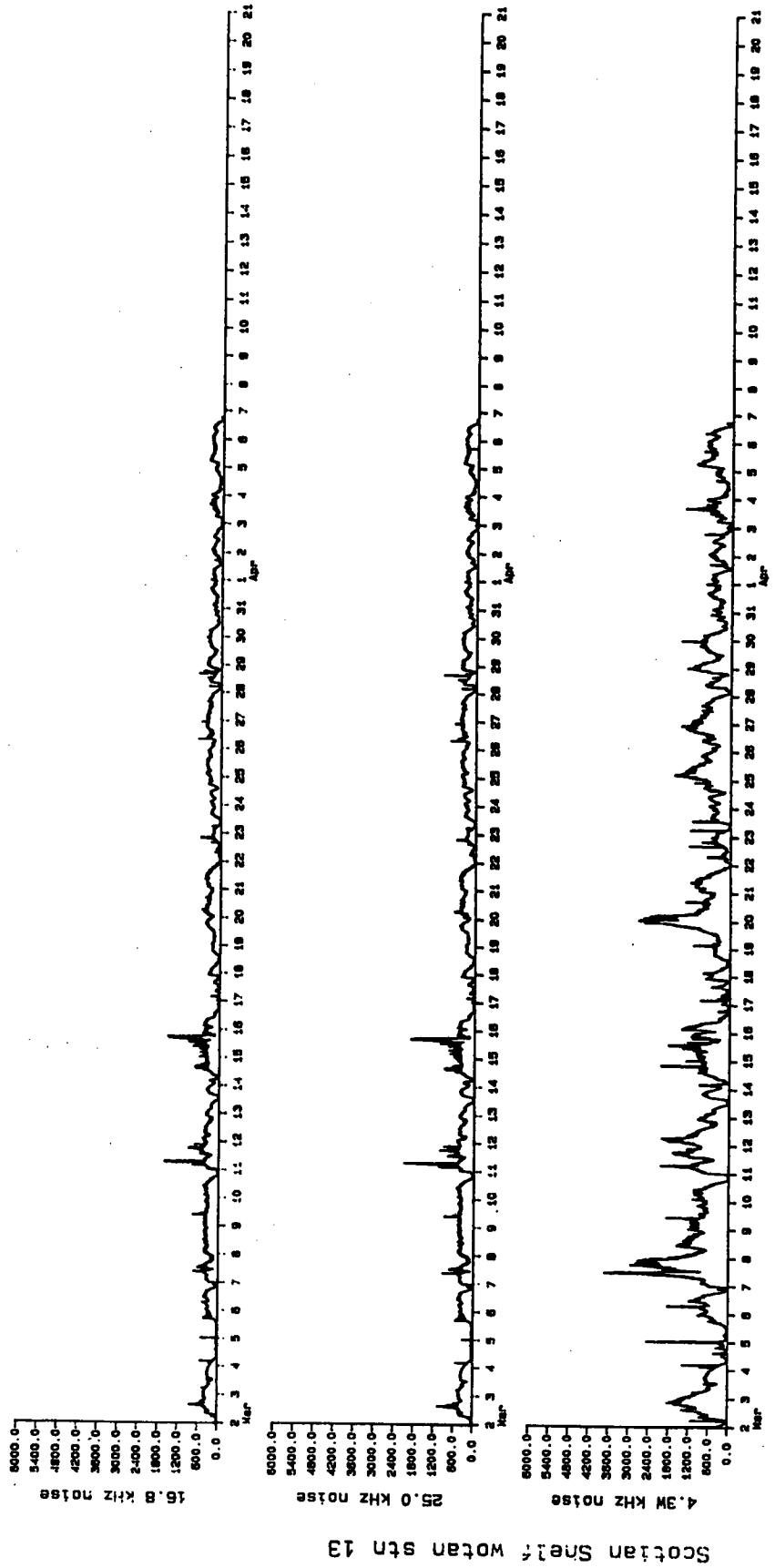

Figure 11 (part 6): Despiked data from station 13.

electronic noise, which is, however, not likely. Figure 12 shows the portion of the record from station 2 spanning the instrument's recovery. The noise level on all channels dropped to near zero as the instrument was removed from the water (1730 GMT March 13). This effect is seen on all instruments as the hydrophone couples much less efficiently to air than to water. The subsequent calibration of the unit from station 2 produced results virtually identical to those found in the pre-deployment calibration, with no indication of any increase in the internal noise level of the unit.

Two other possible causes for this noise come to mind; one internal, the other external to the instrument. Because the excess noise appeared on all channels, if it originated in the instrument the fault would have to have been in the preamplifier or hydrophone, as those are the only elements common to all the channels. The behaviour of the instrument when removed from the water and during the subsequent calibration appears to rule out the preamplifier. If the hydrophone was at fault, the effect must have required at least submergence and possibly the application of pressure to take place. It is possible that a pinhole leak in the transducer molding and the subsequent electrical path through seawater could produce noise.[1] This possibility unfortunately cannot be checked at present as the unit was redeployed in the Arctic immediately after recovery and will not return until October 1986. At that time, it could be examined to verify whether a transducer leak did occur. (It was fitted with a different preamplifier, thus eliminating that as a possible source.)

The remaining possibility is that an external noise source was continuously present at station 2 from January 14 until the WOTAN was recovered. Noise from shipping or offshore industrial activity does not seem likely because of the lack of any interruptions and the magnitude of the signal at high frequencies. There were several CASP moorings in the immediate vicinity, however, including a WAVEC directional surface-wave measurement buoy and a surface meteorological buoy. It is possible that one or more components of these moorings may have worked loose and begun to squeak or rattle. There is, however, no way to confirm this hypothesis.

Figure 13 shows a spectral plot of the level of noise contamination estimated from the mean minimum noise levels in the time series of Figure 8 (after January 14).

The despiked time series were converted to noise spectrum levels by application of the calibration equations listed in Table 5. Plots of the calibrated noise level data are shown in Figures 14–18.

3.2 CALCULATION OF WIND-SPEED RECORD

Computation of wind speed from the acoustic signal is complicated by two factors: noise from other sources (the chief one being rainfall) and the effects of bubbles generated near the surface on sound at frequencies of 8 kHz and above when the wind speed exceeds 8 $m \cdot s^{-1}$. Farmer and Lemon (1984) presented data which demonstrated that the bubbles attenuate the wind-generated noise. The effect increases with acoustic frequency and wind

---

[1] S. Waddell, 1986, Institute of Ocean Sciences, personal communication.

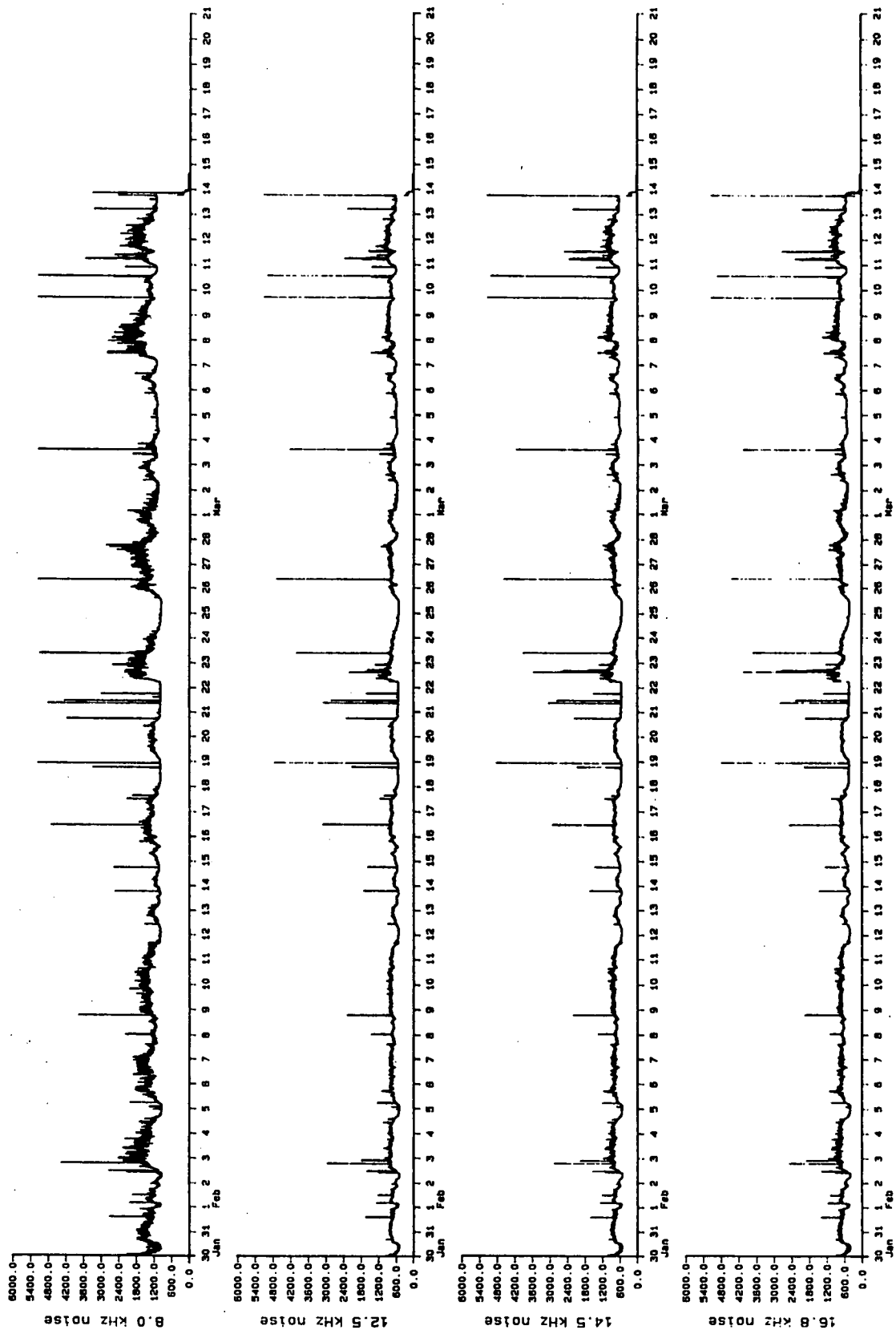

Figure 12: Final section of raw data record from station 2, showing recovery of the instrument.

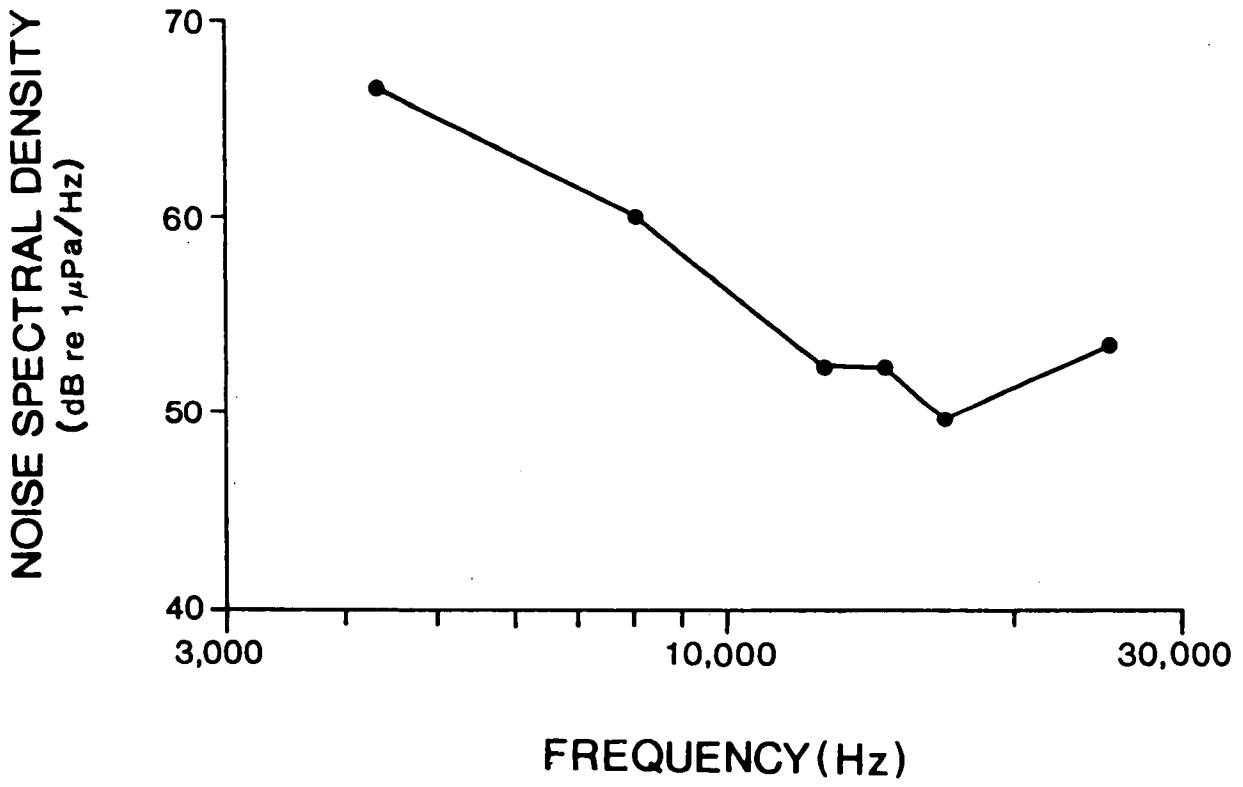

Figure 13: Spectral plot of apparent noise contamination at station 2.

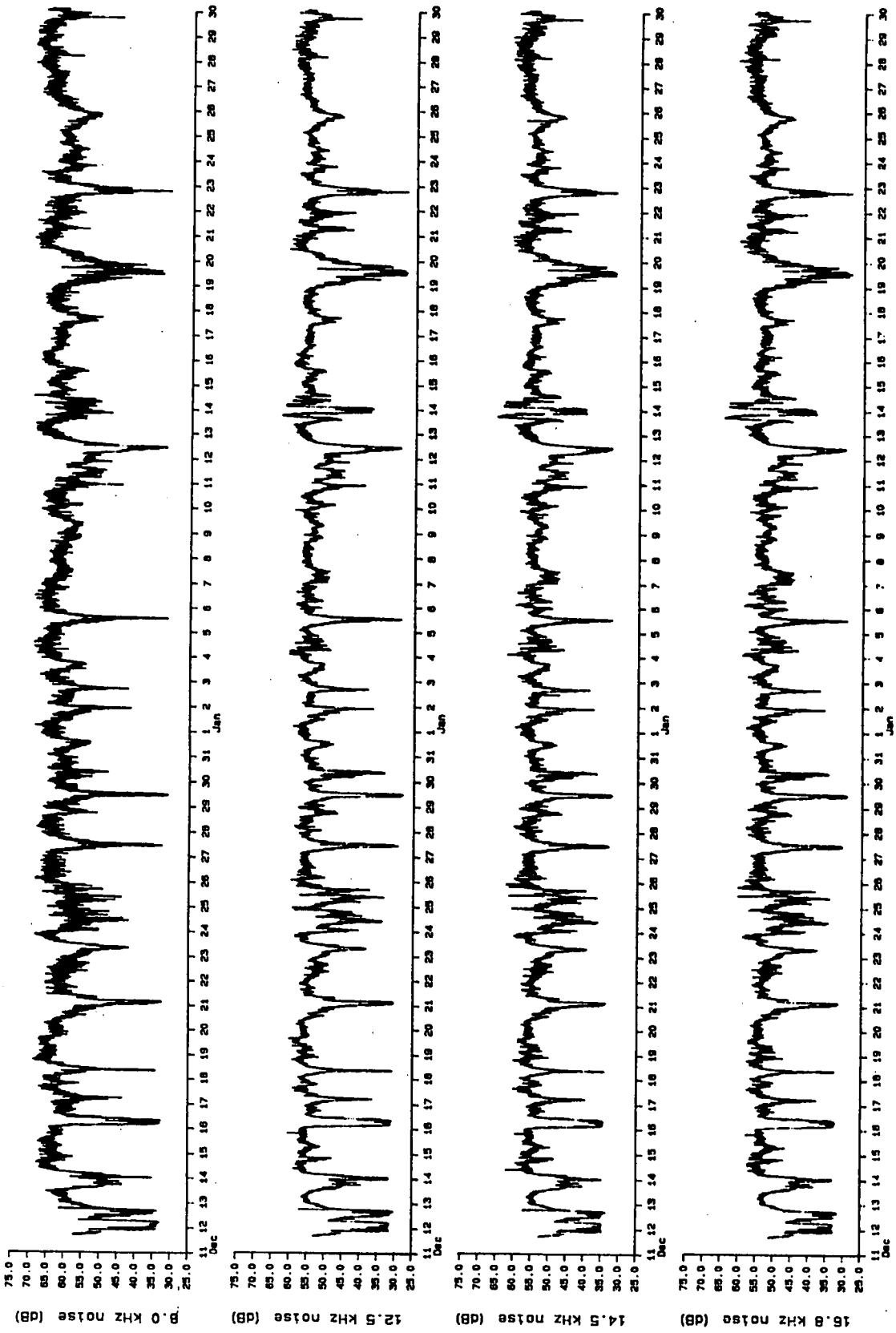

Figure 14 (part 1): Time series of noise spectrum levels at station 1.

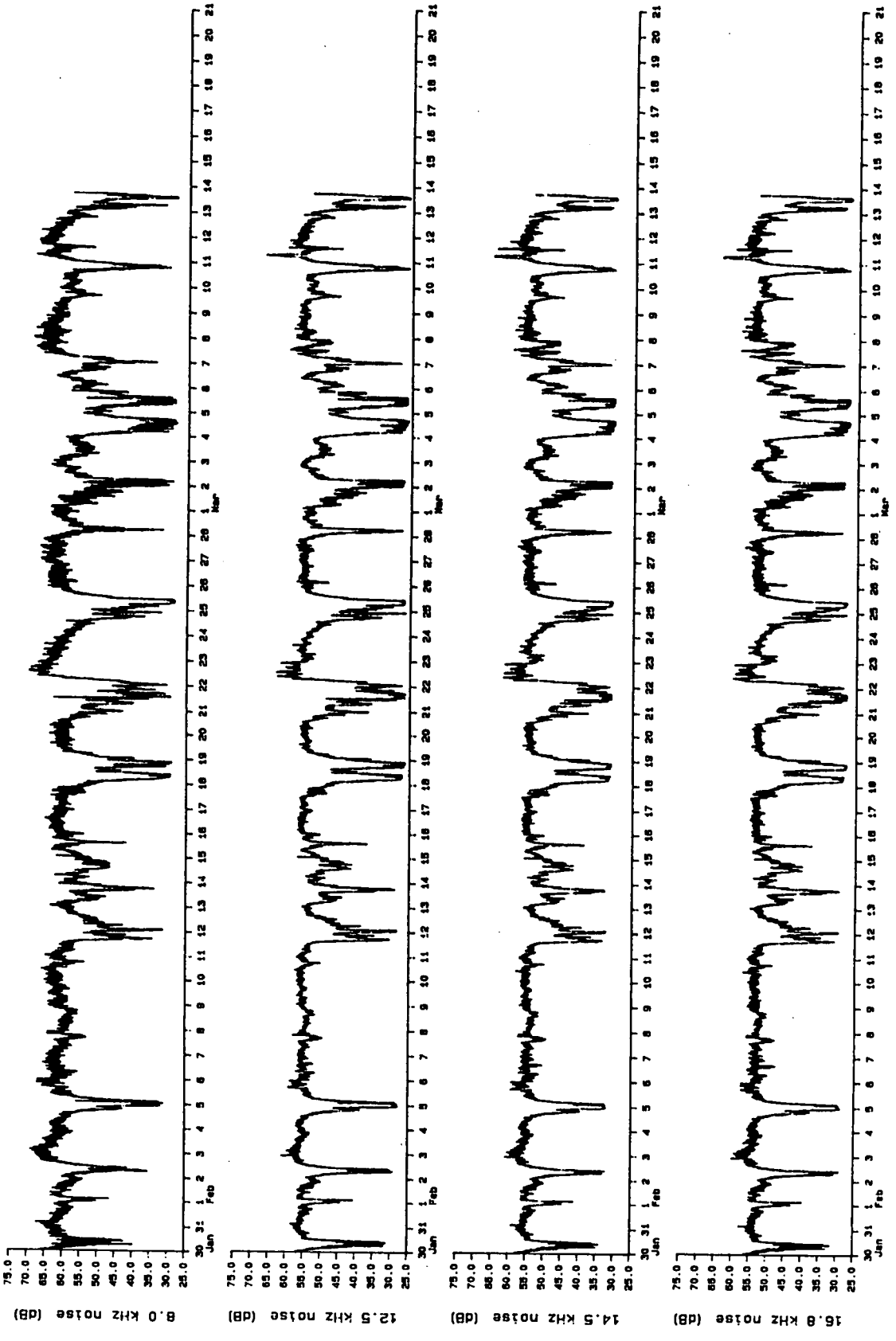

Figure 14 (part 2): Time series of noise spectrum levels at station 1.

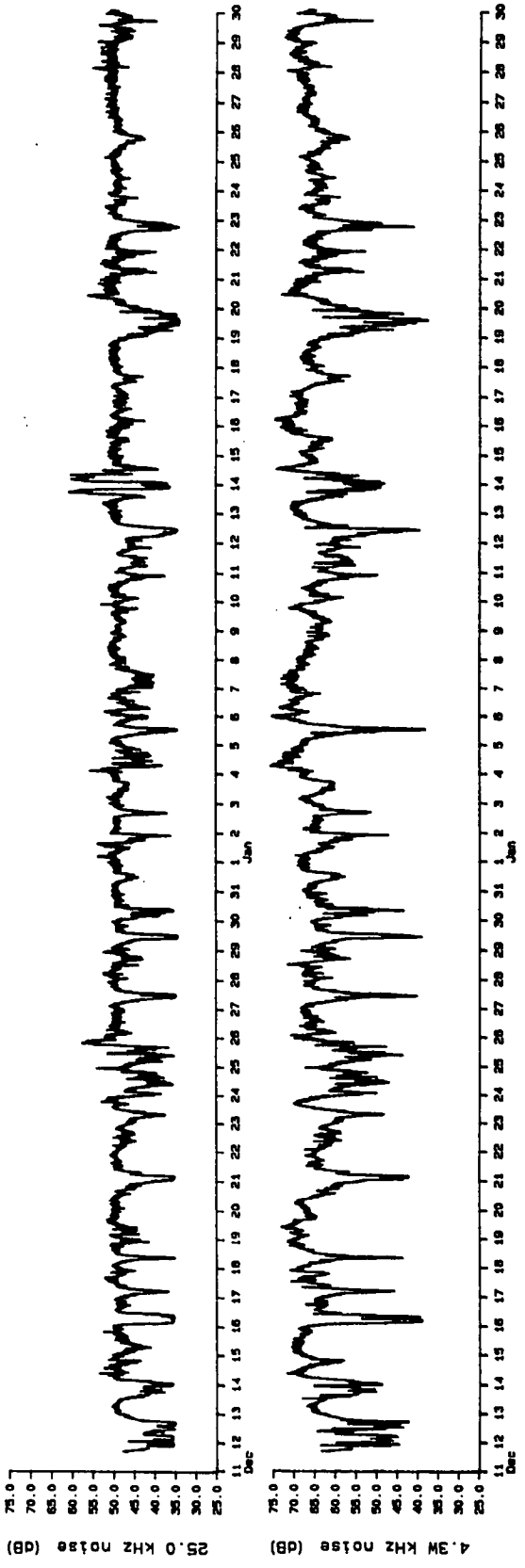

Figure 14 (part 3): Time series of noise spectrum levels at station 1.

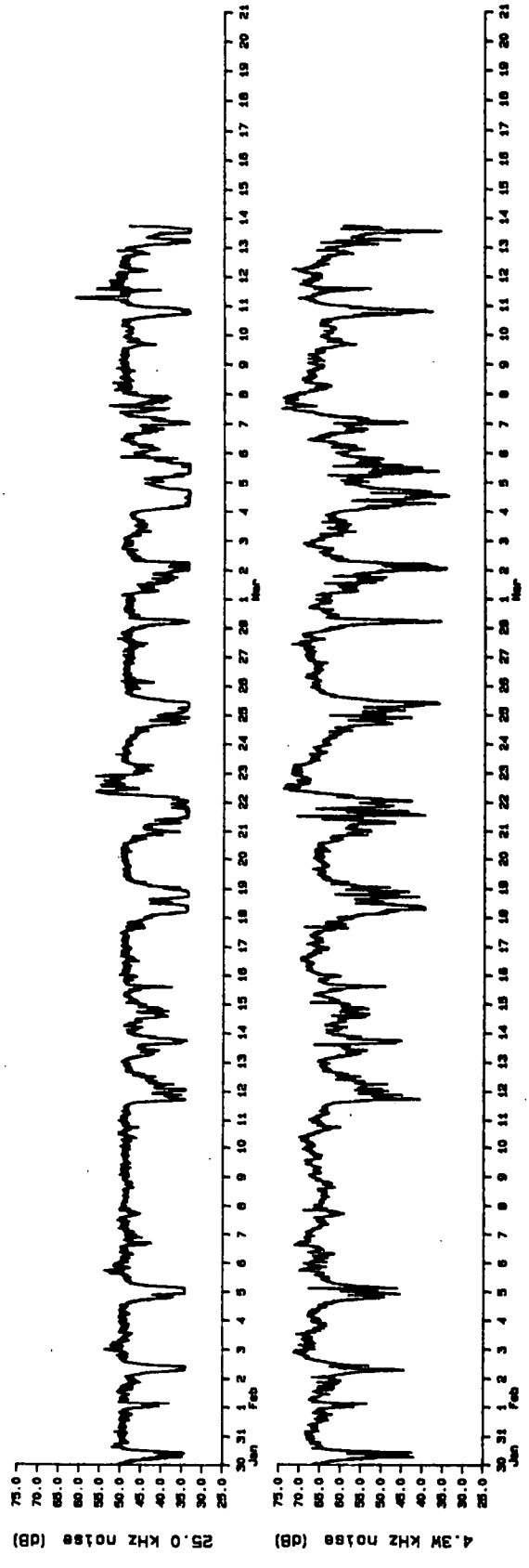

Figure 14 (part 4): Time series of noise spectrum levels at station 1.

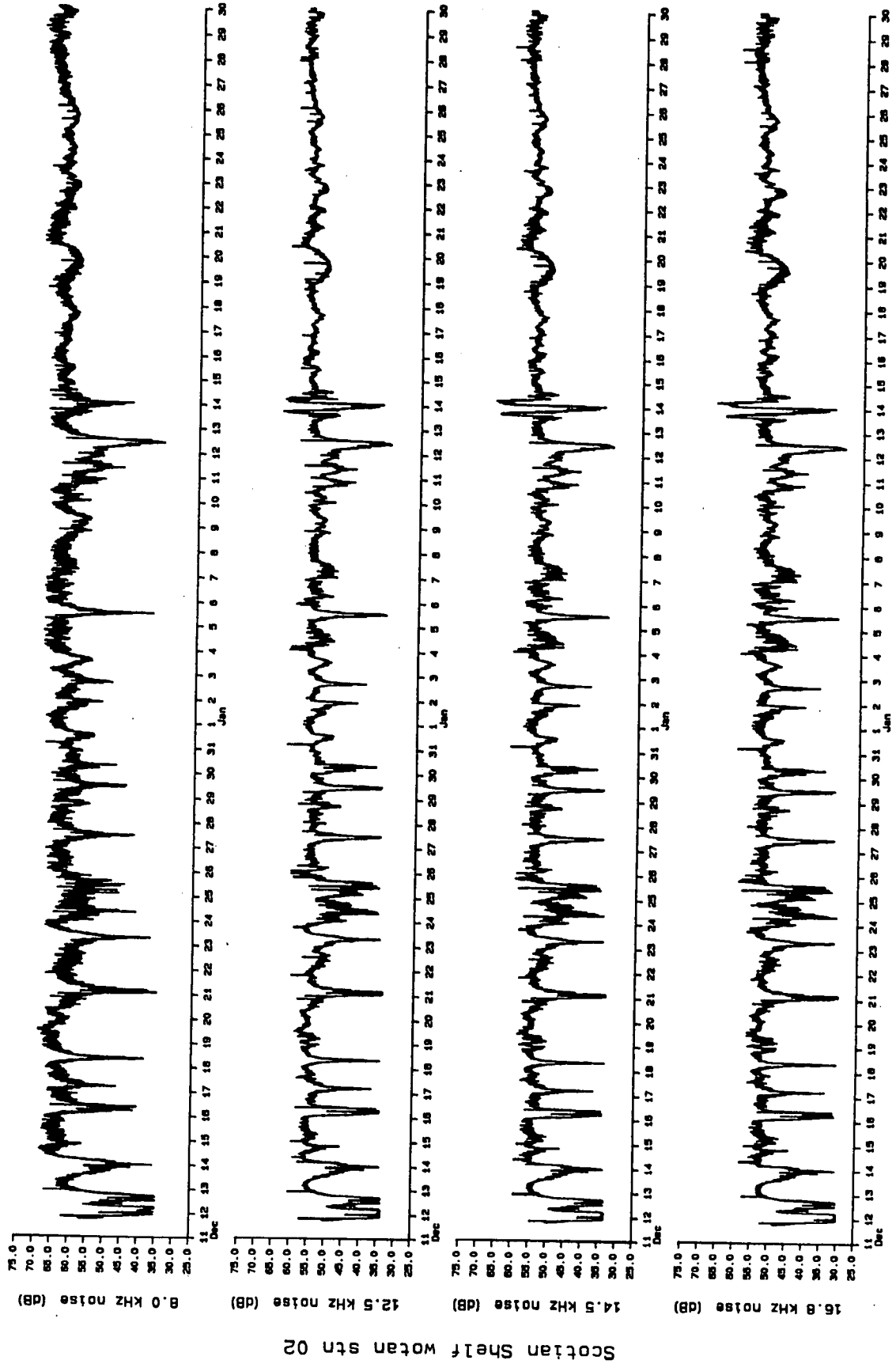

Figure 15 (part 1): Time series of noise spectrum levels at station 2.

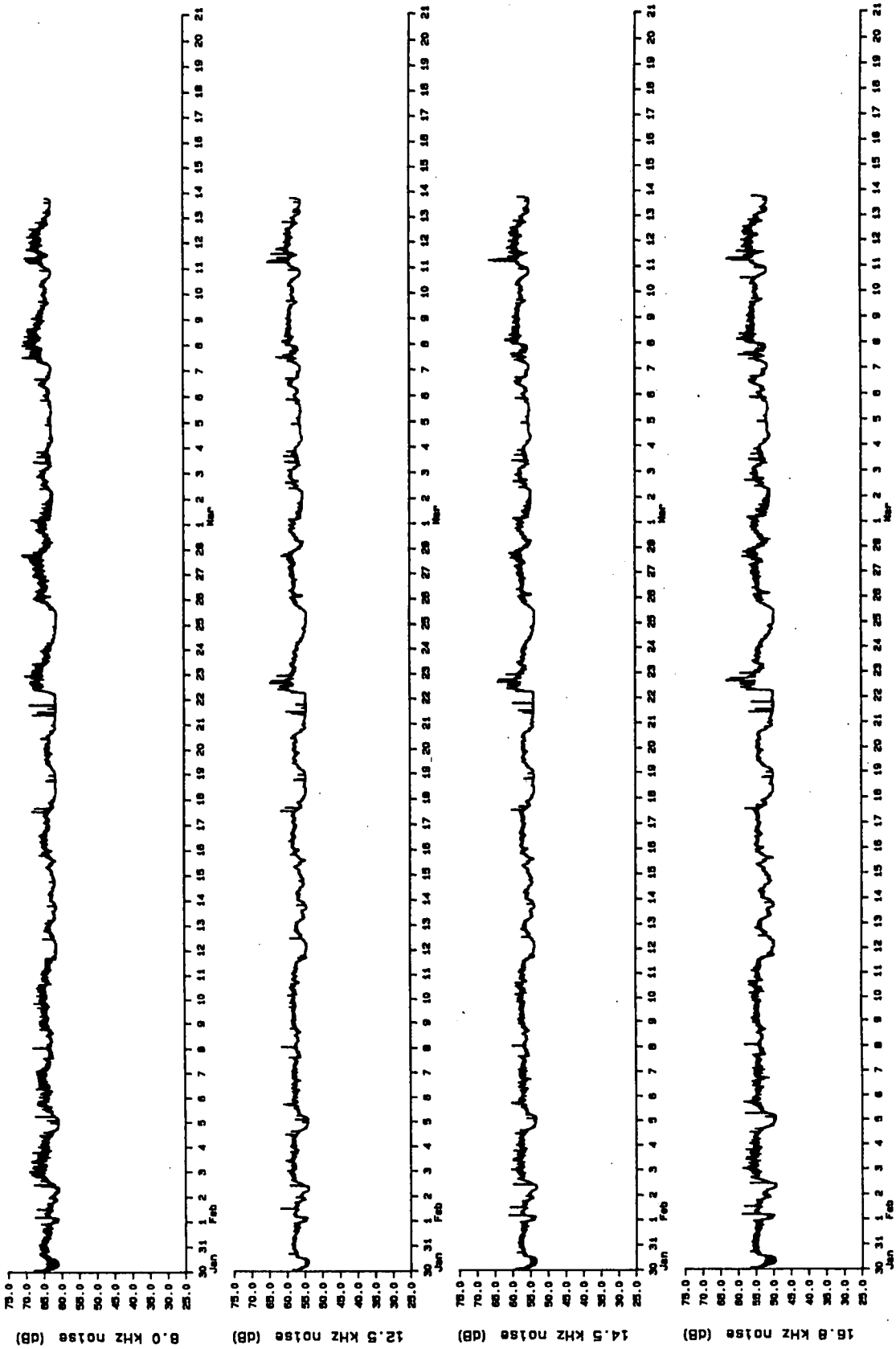

Figure 15 (part 2): Time series of noise spectrum levels at station 2.

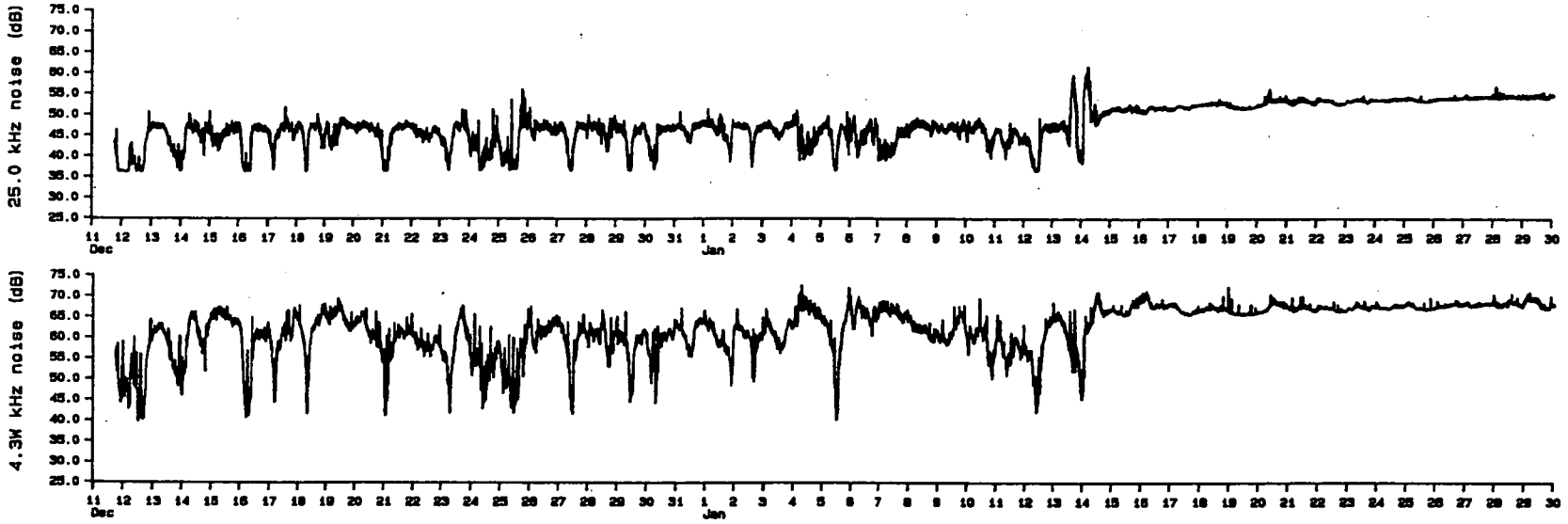

Figure 15 (part 3): Time series of noise spectrum levels at station 2.

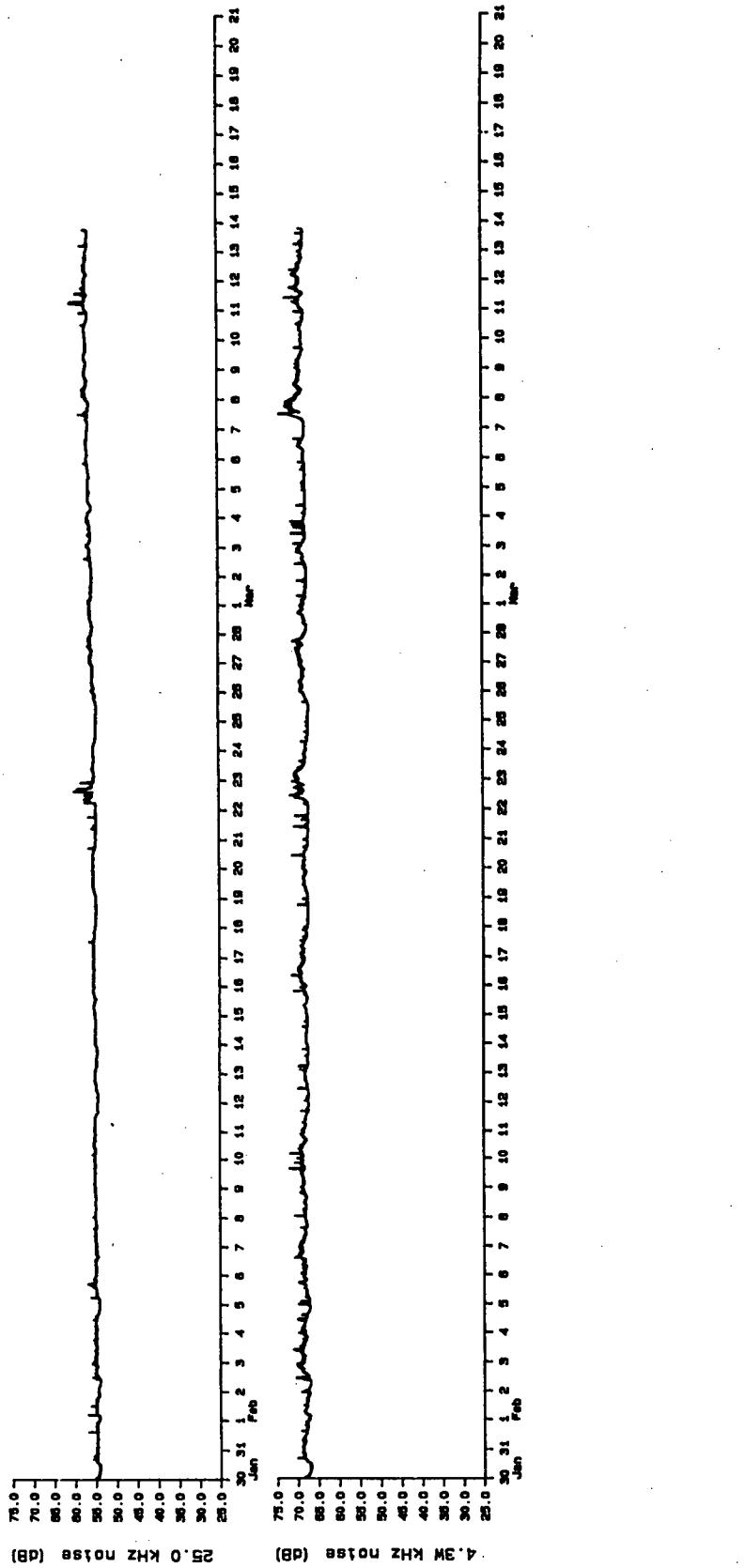

Figure 15 (part 4): Time series of noise spectrum levels at station 2.

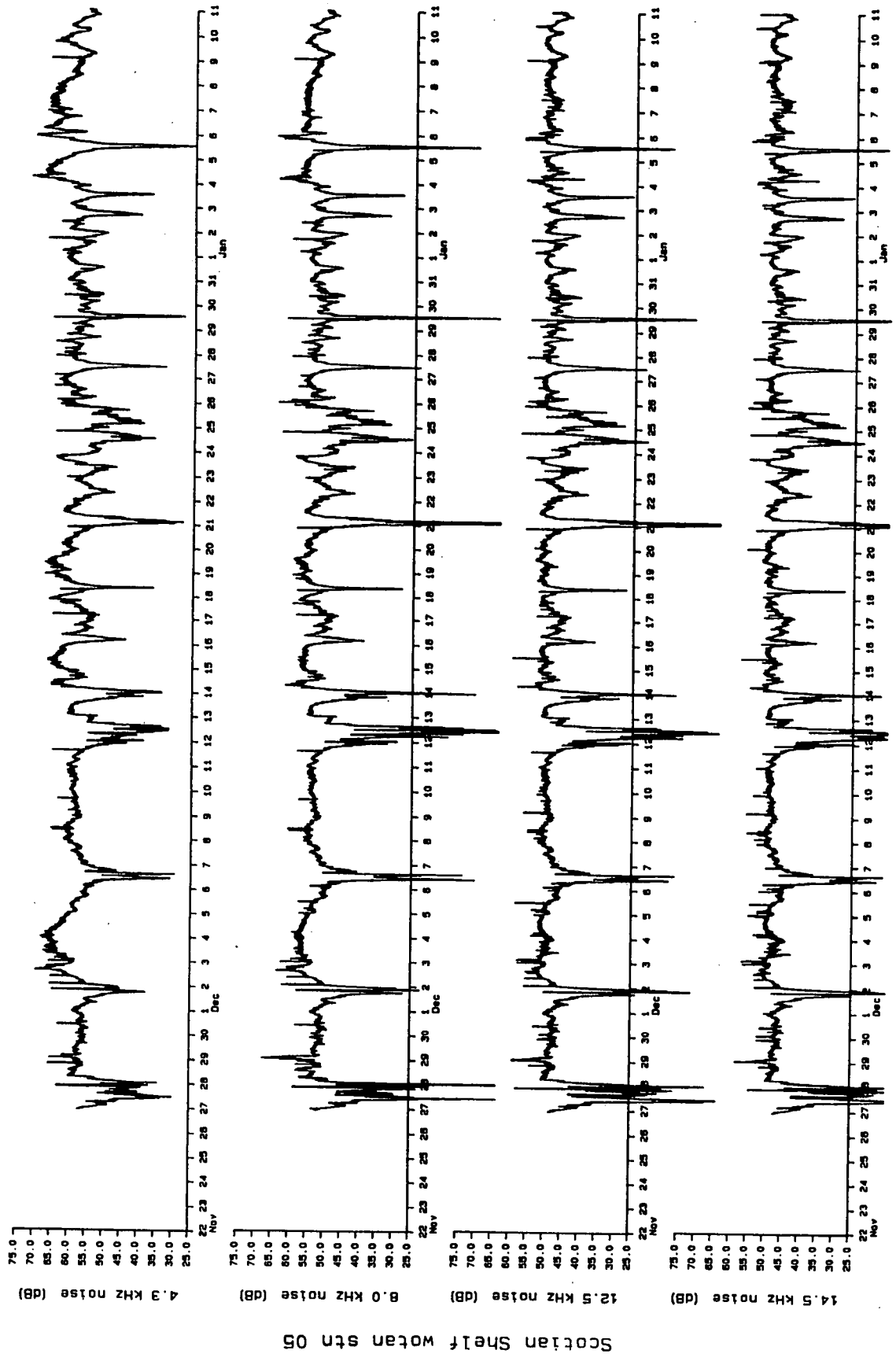

Figure 16 (part 1): Time series of noise spectrum levels at station 5.

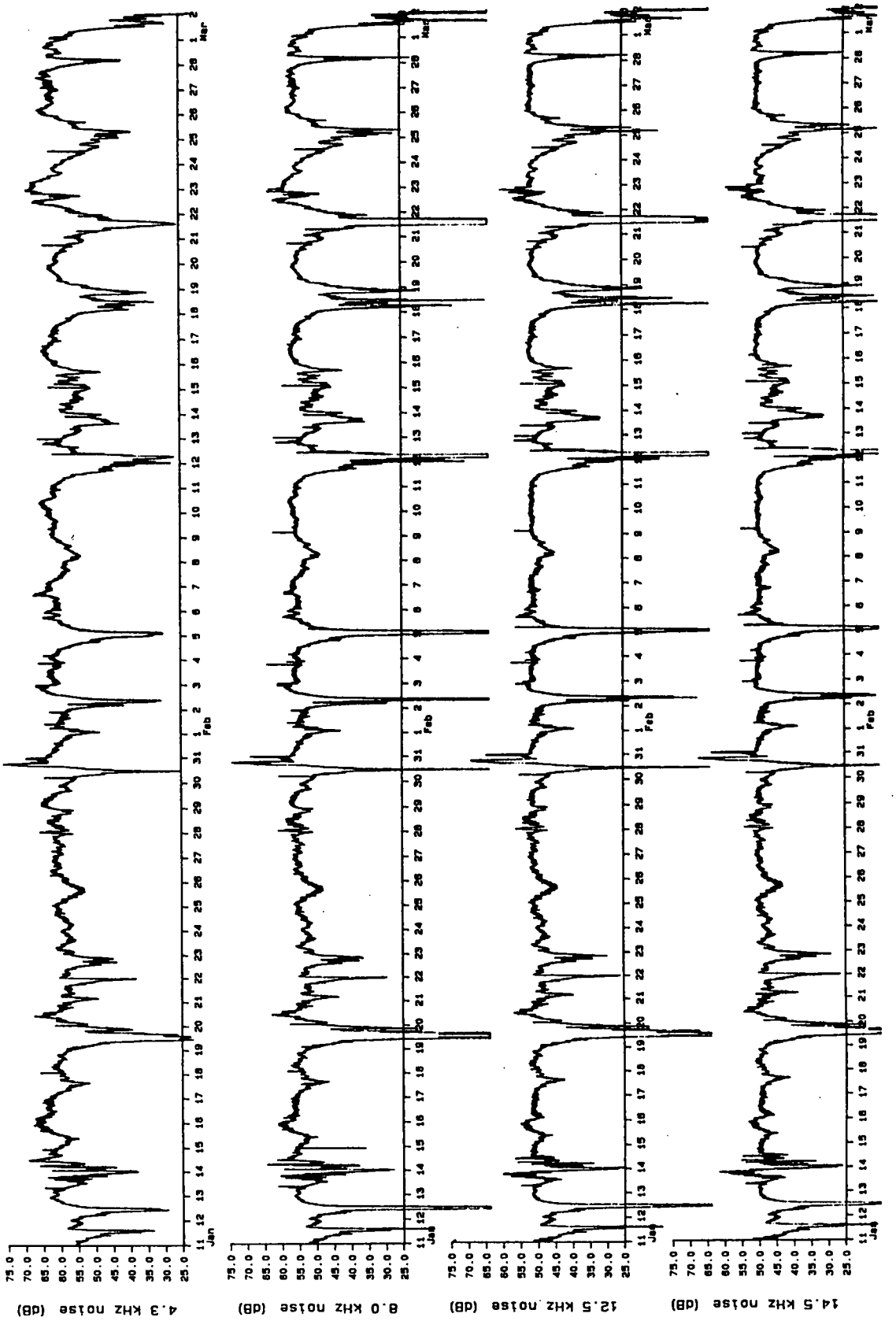

Figure 16 (part 2): Time series of noise spectrum levels at station 5.

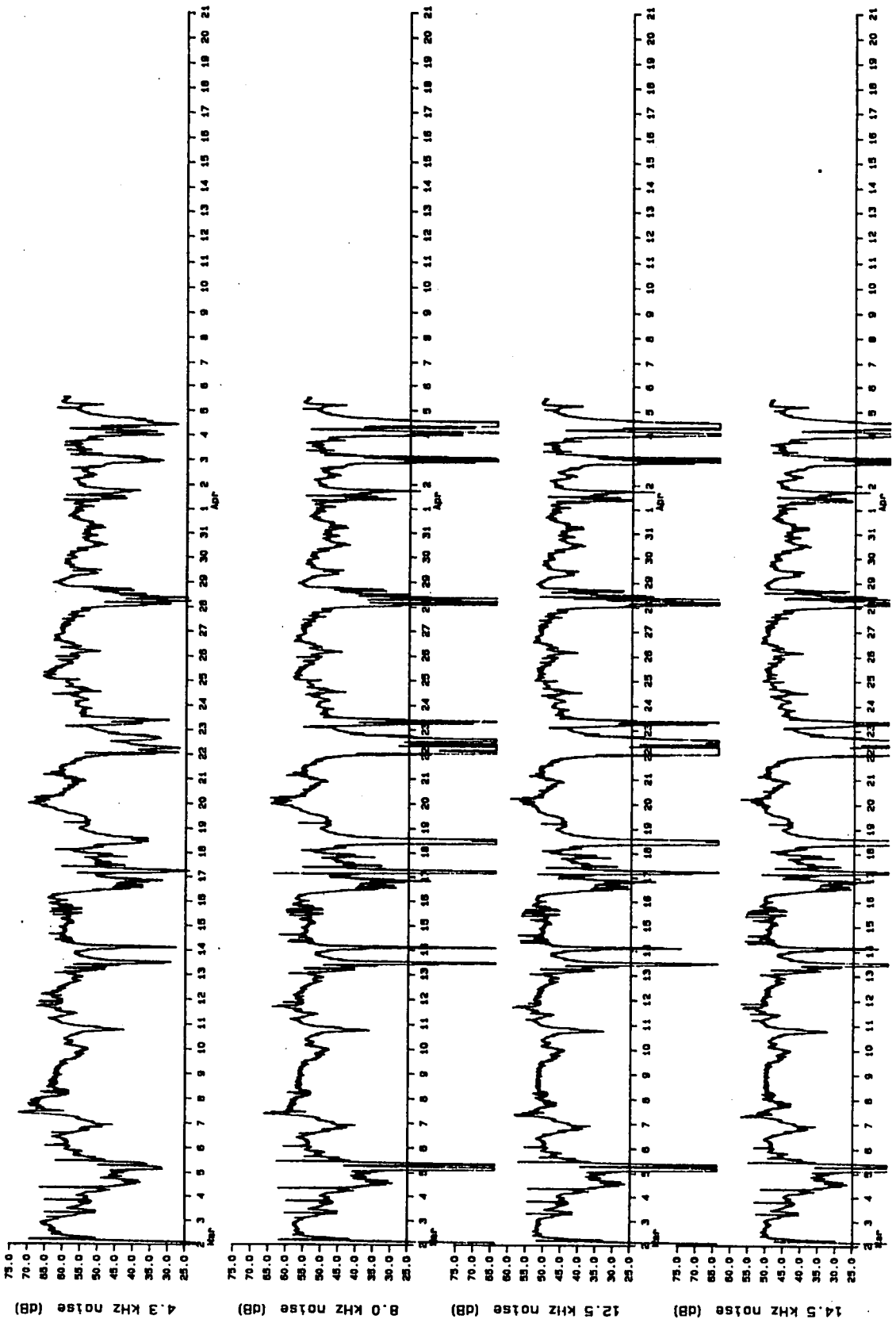

Figure 16 (part 3): Time series of noise spectrum levels at station 5.

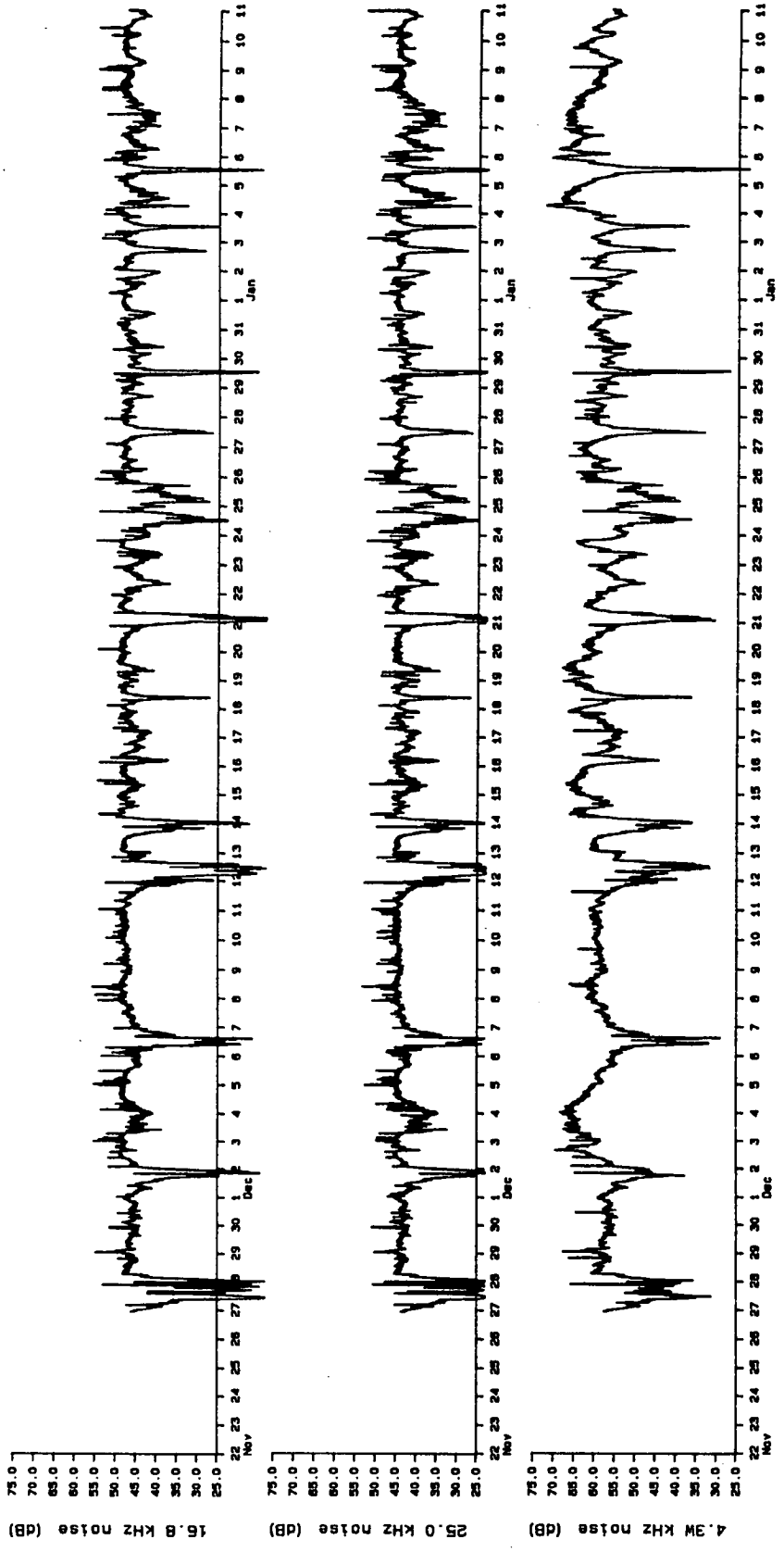

Figure 16 (part 4): Time series of noise spectrum levels at station 5.

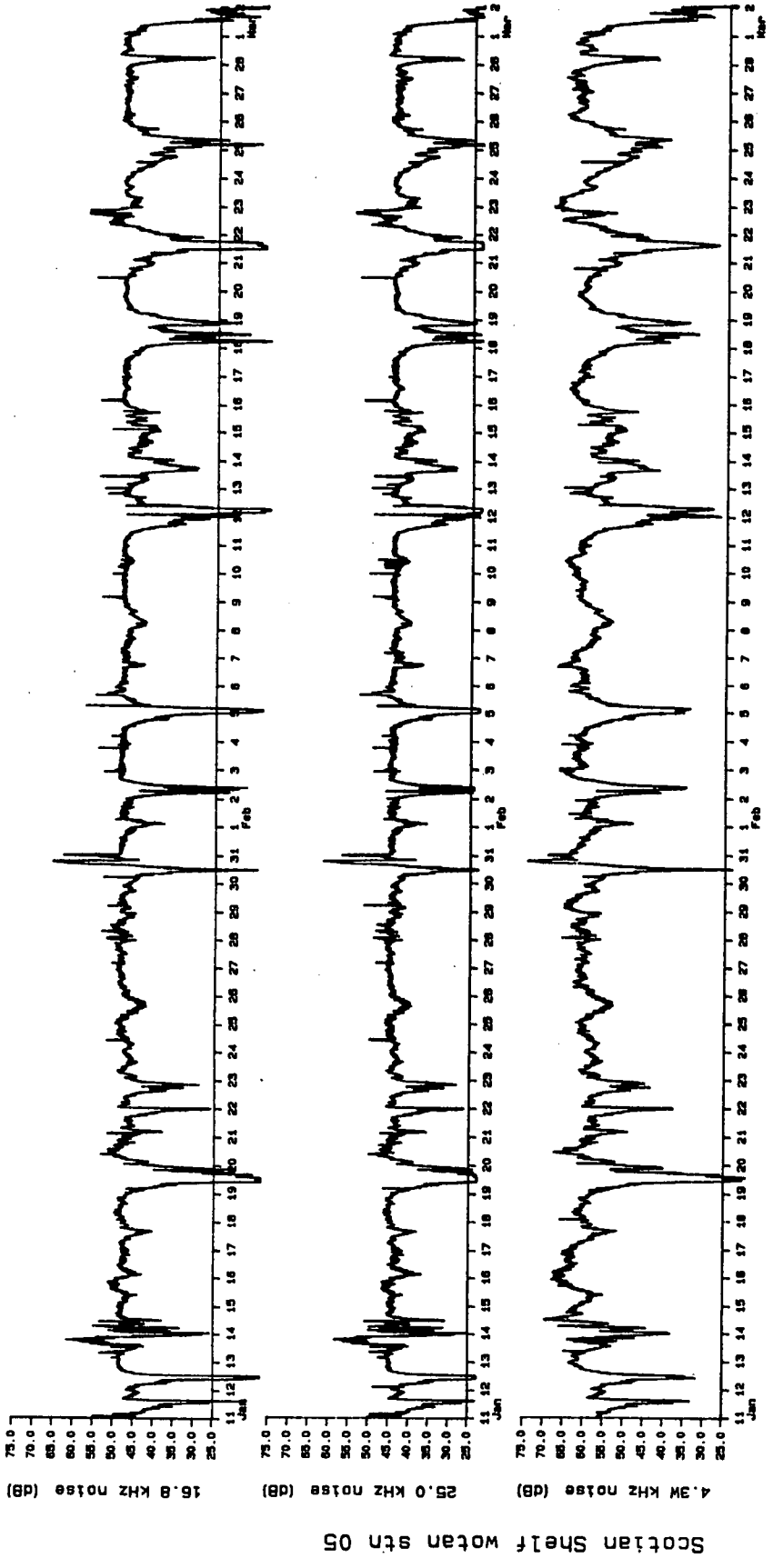

Figure 16 (part 5): Time series of noise spectrum levels at station 5.

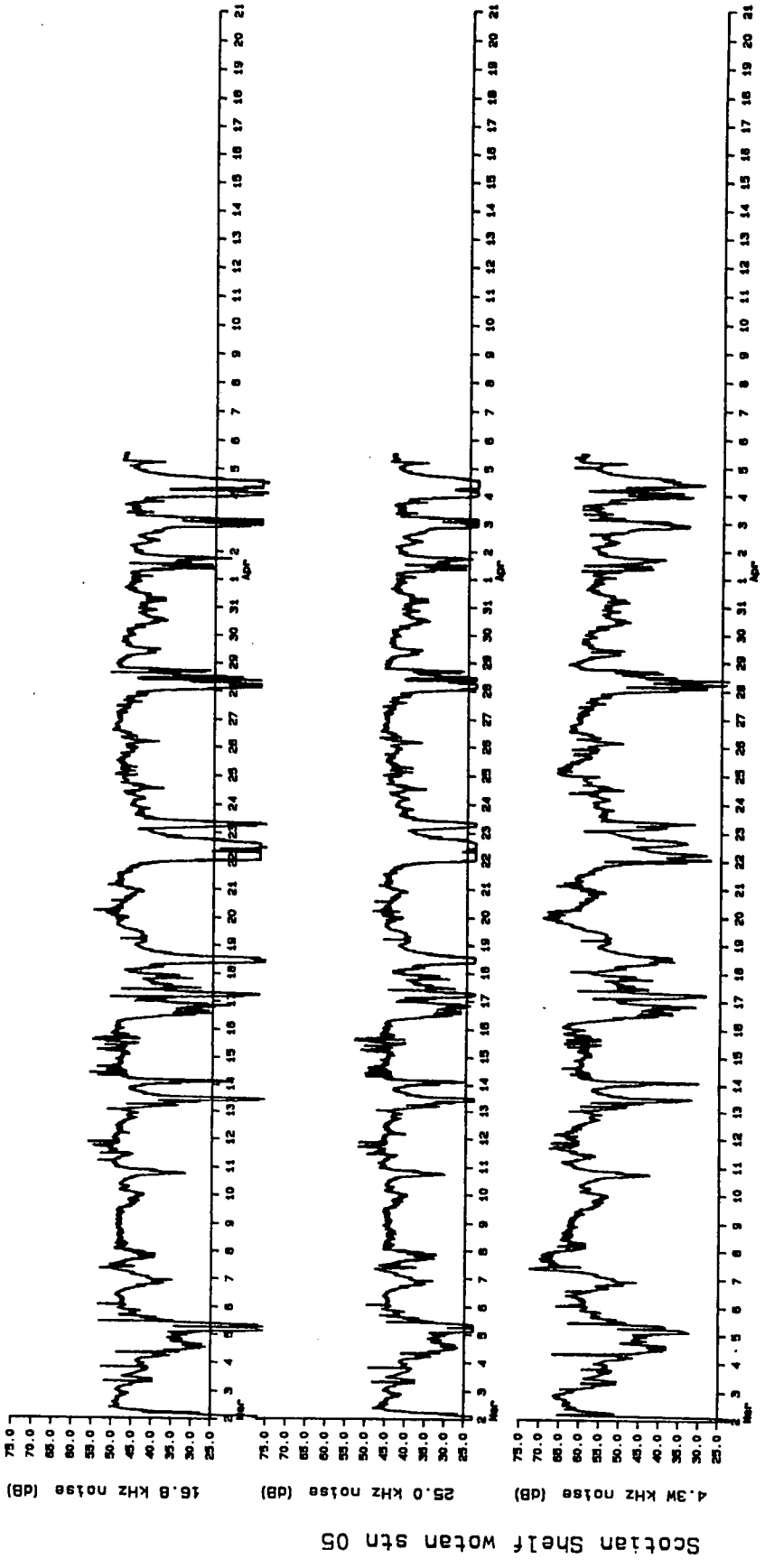

Figure 16 (part 6): Time series of noise spectrum levels at station 5.

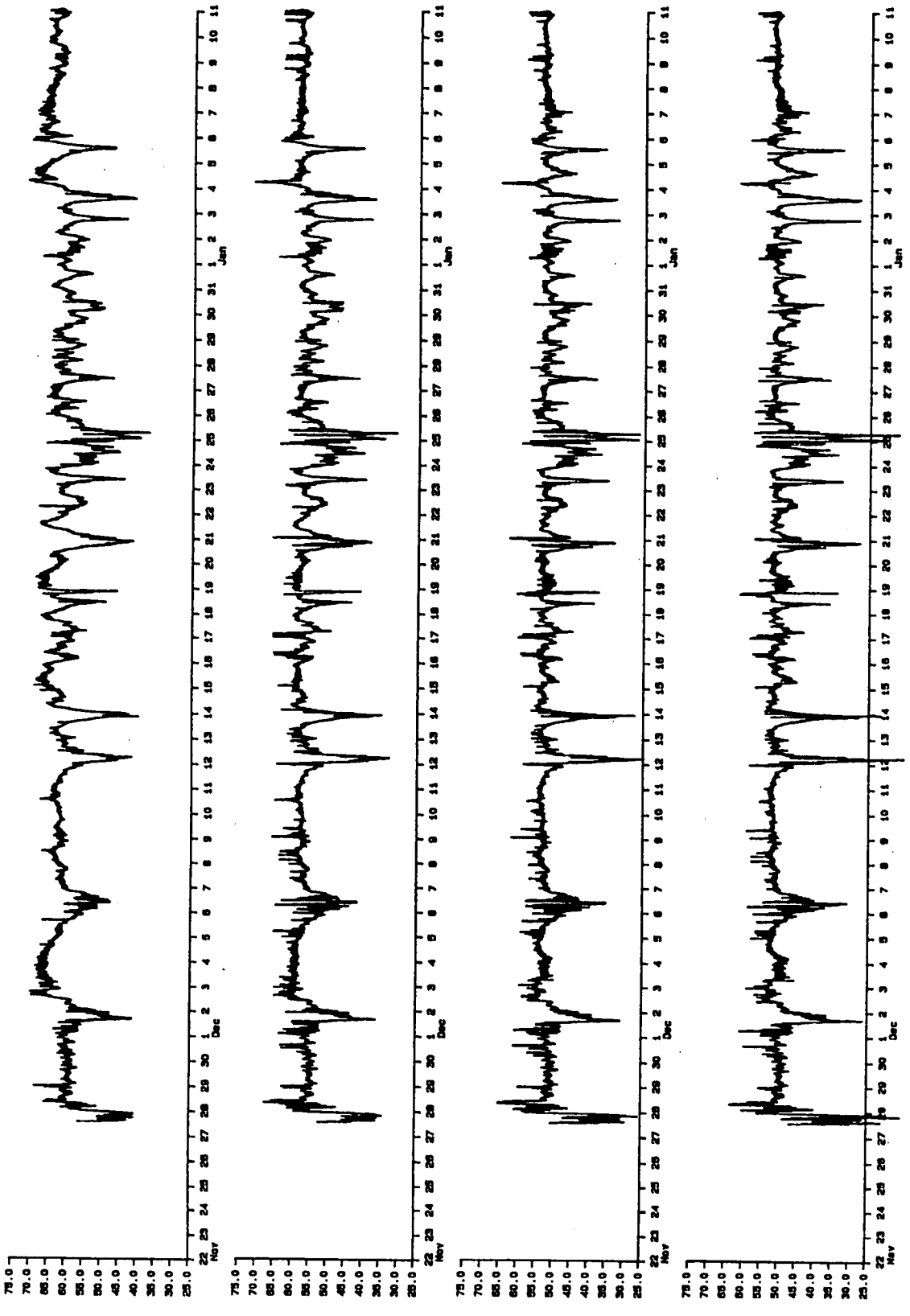

Figure 17 (part 1): Time series of noise spectrum levels at station 12.

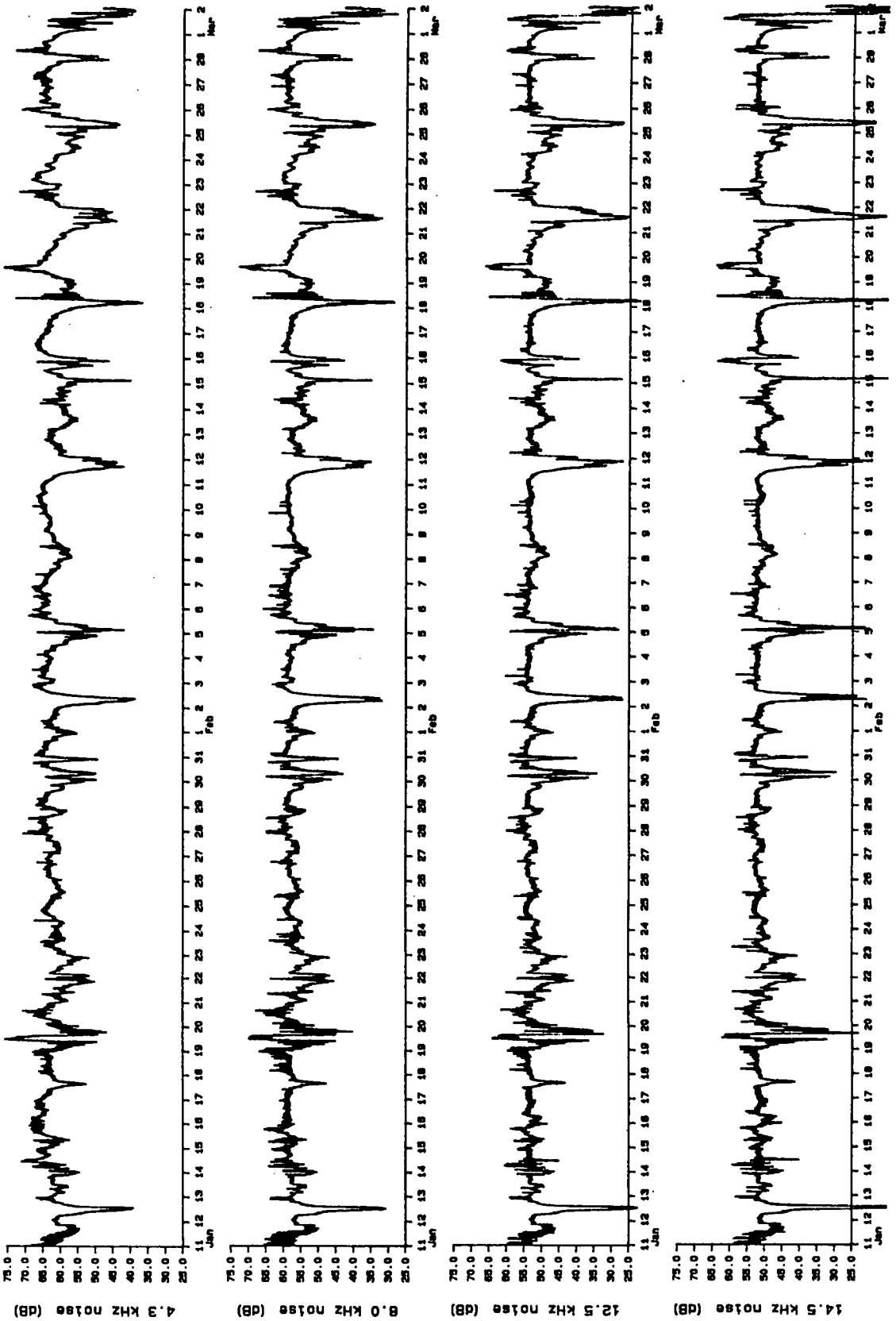

Figure 17 (part 2): Time series of noise spectrum levels at station 12.

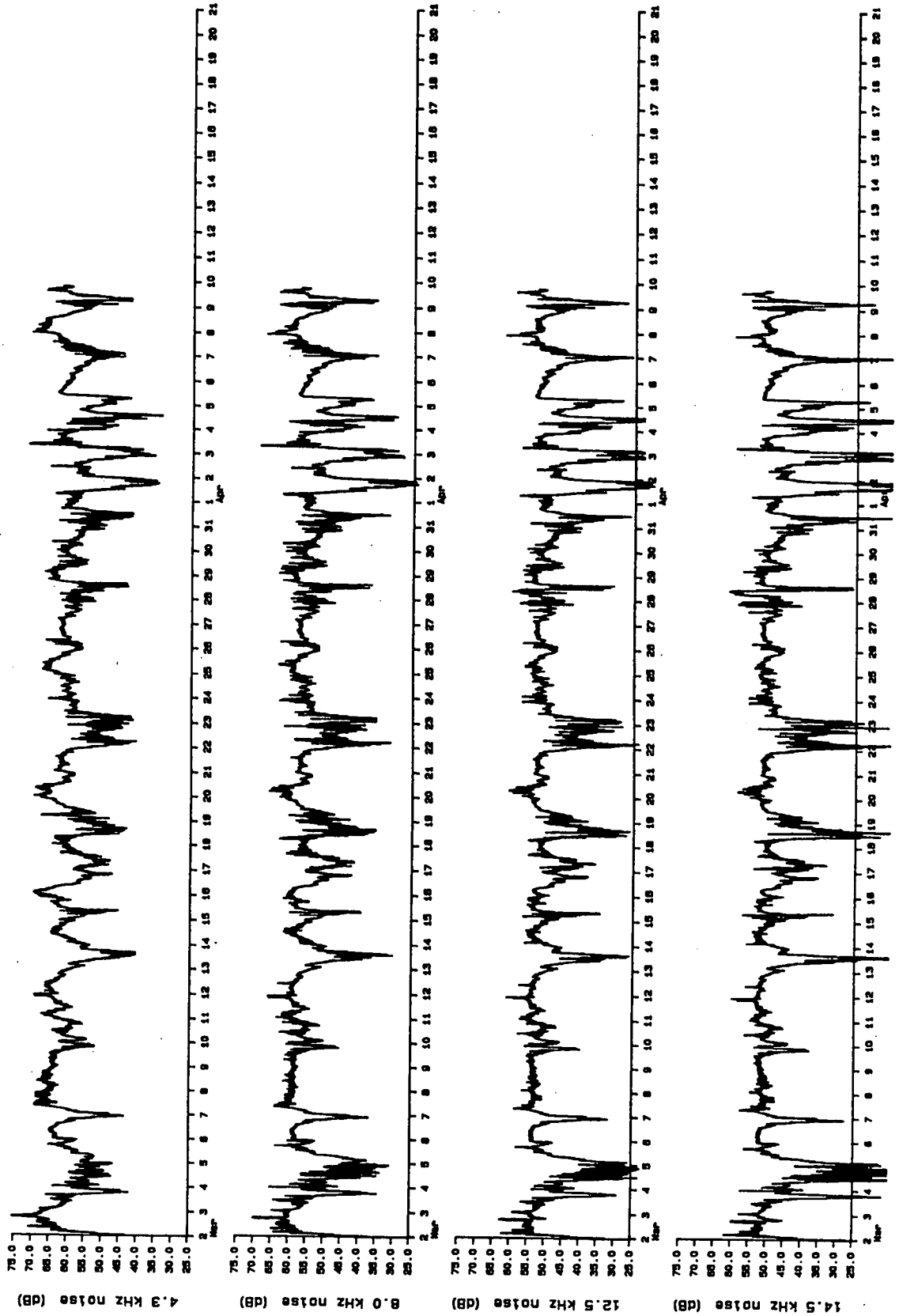

Figure 17 (part 3): Time series of noise spectrum levels at station 12.

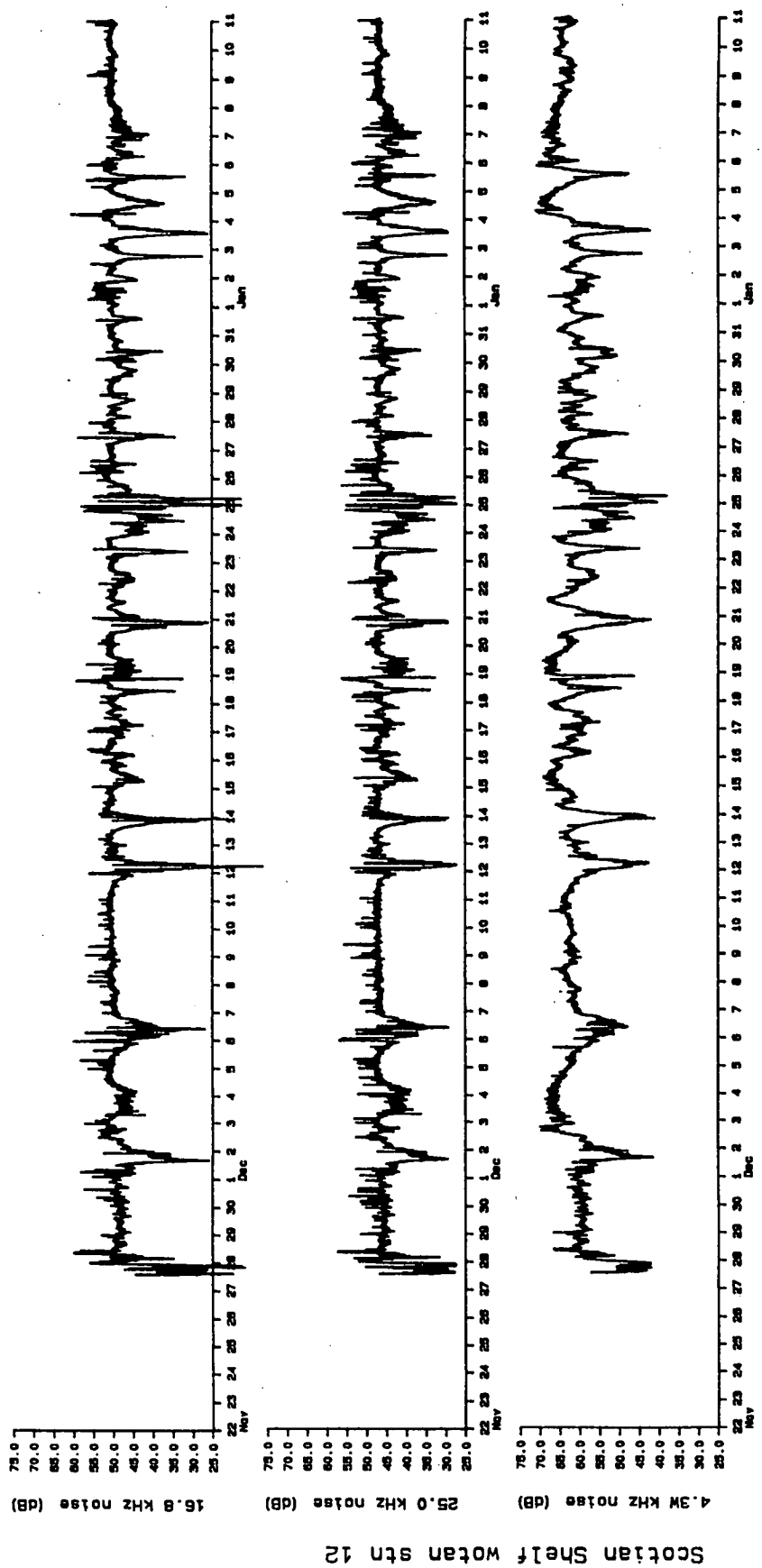

Figure 17 (part 4): Time series of noise spectrum levels at station 12.

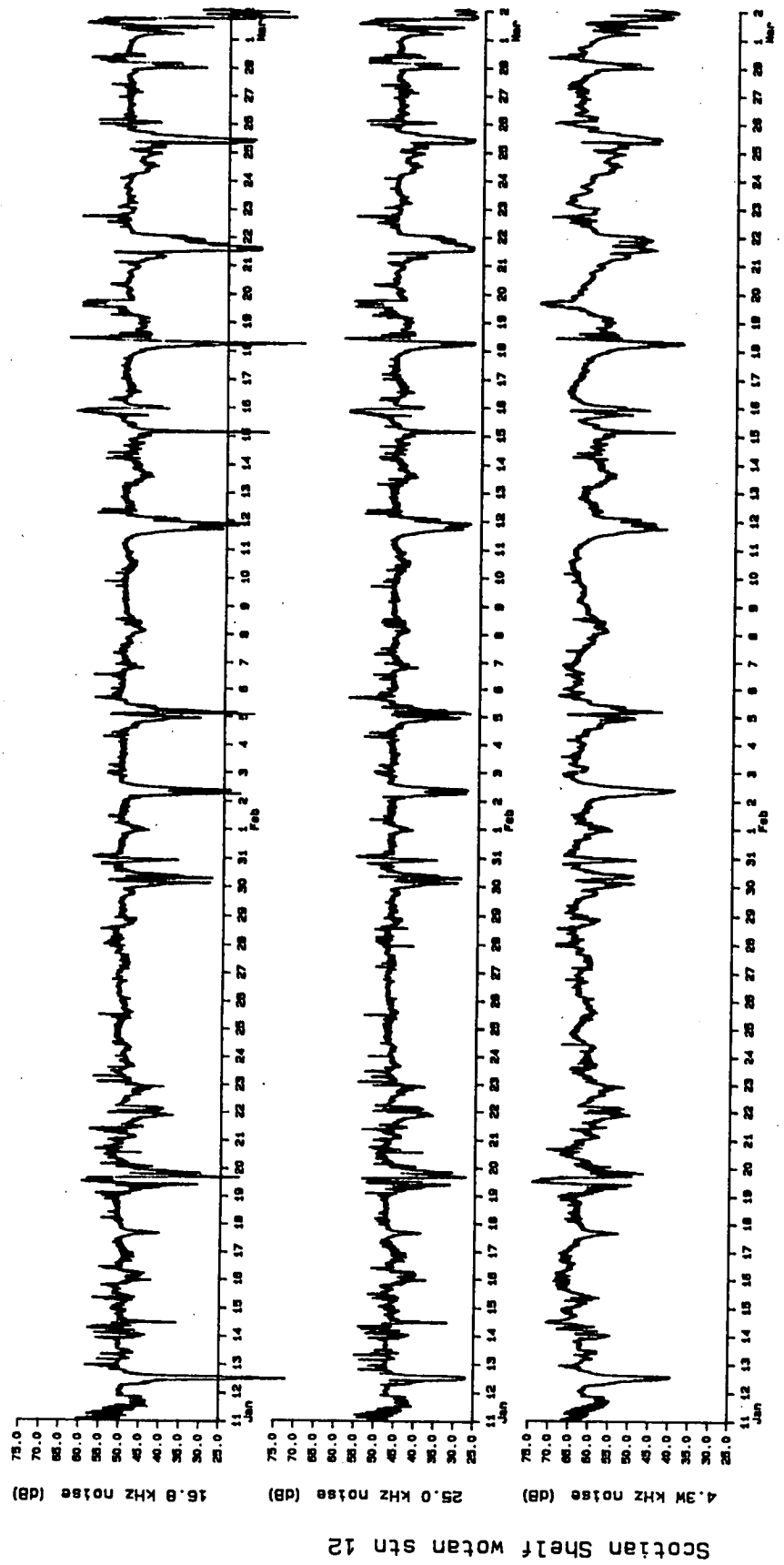

Figure 17 (part 5): Time series of noise spectrum levels at station 12.

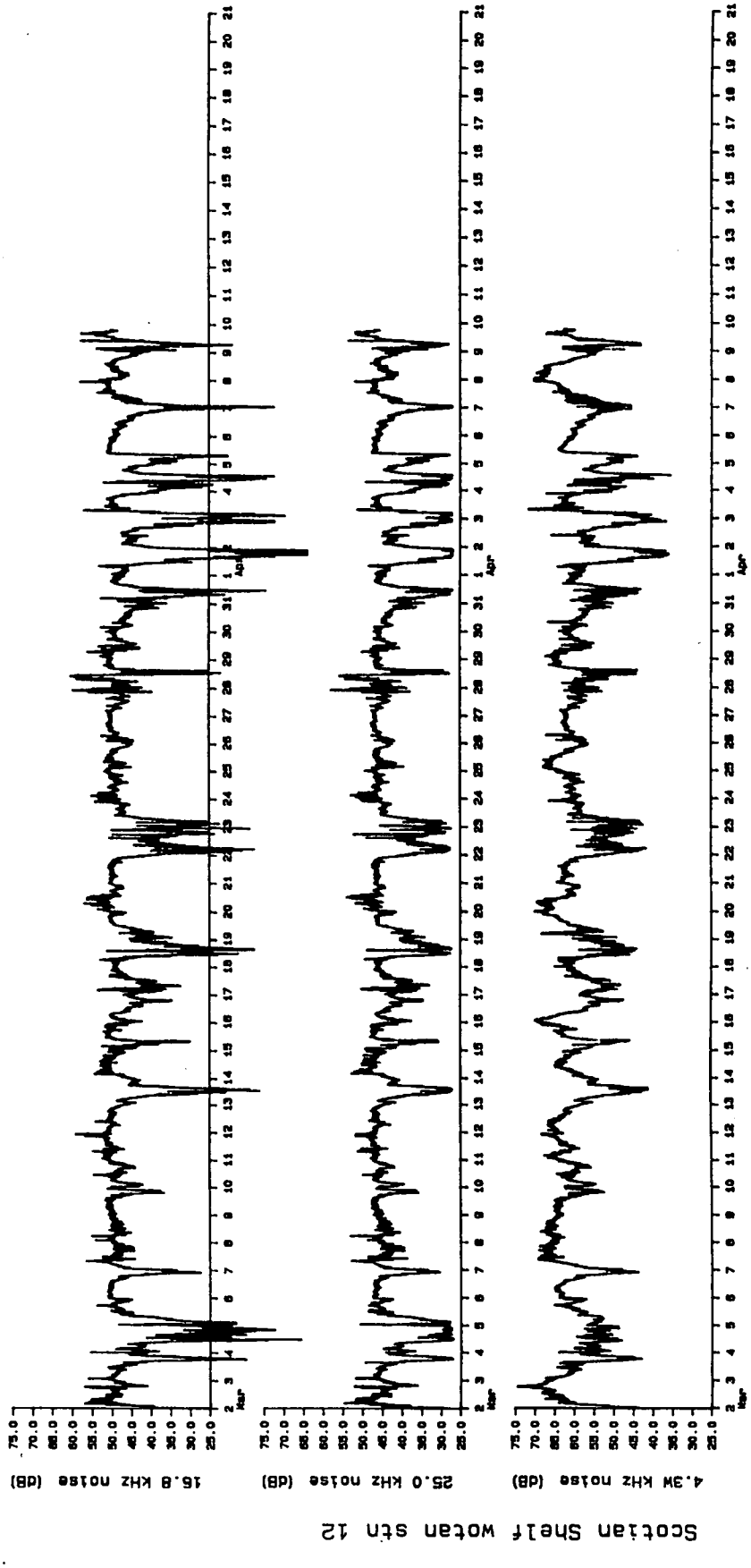

Figure 17 (part 6): Time series of noise spectrum levels at station 12.

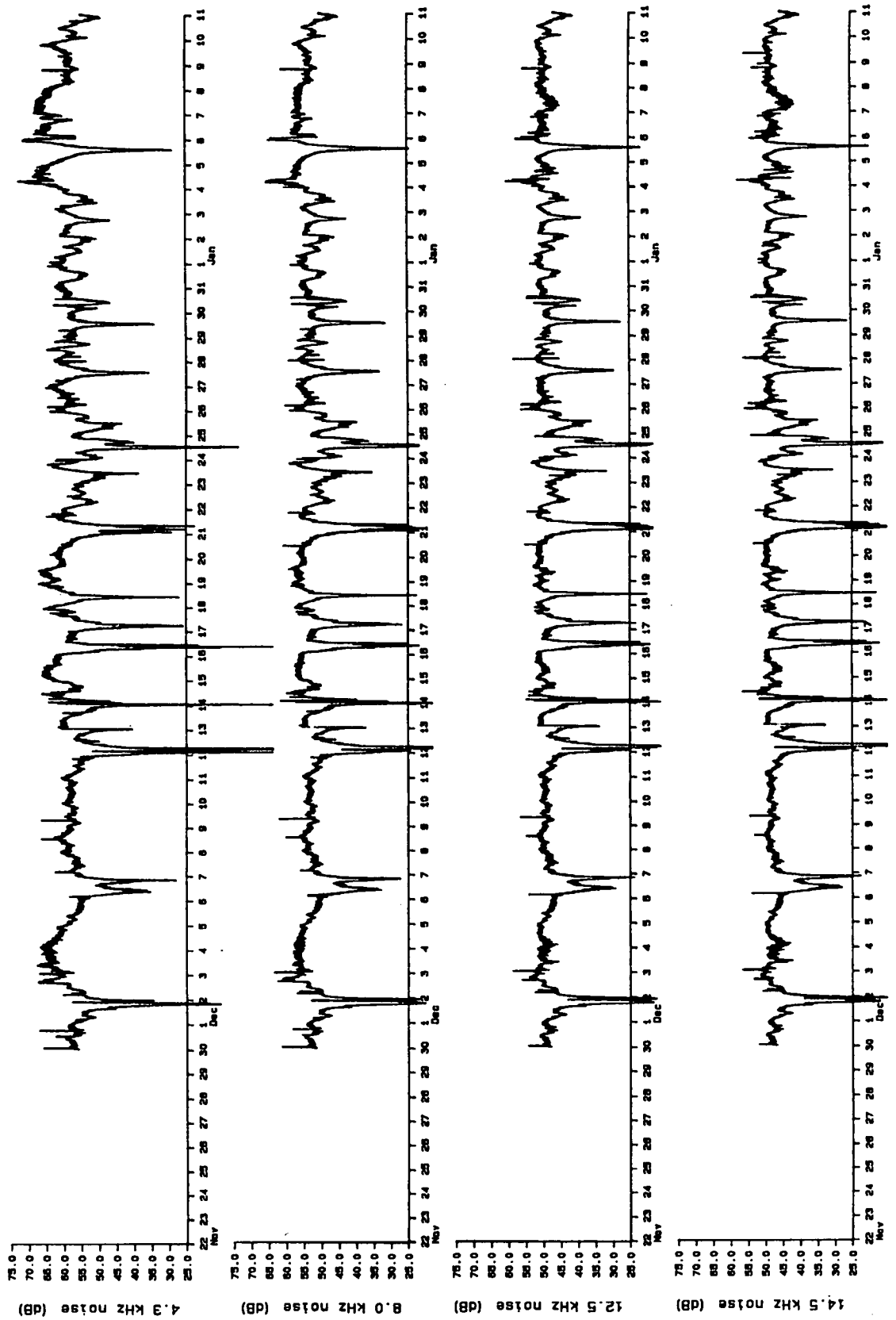

Figure 18 (part 1): Time series of noise spectrum levels at station 13.

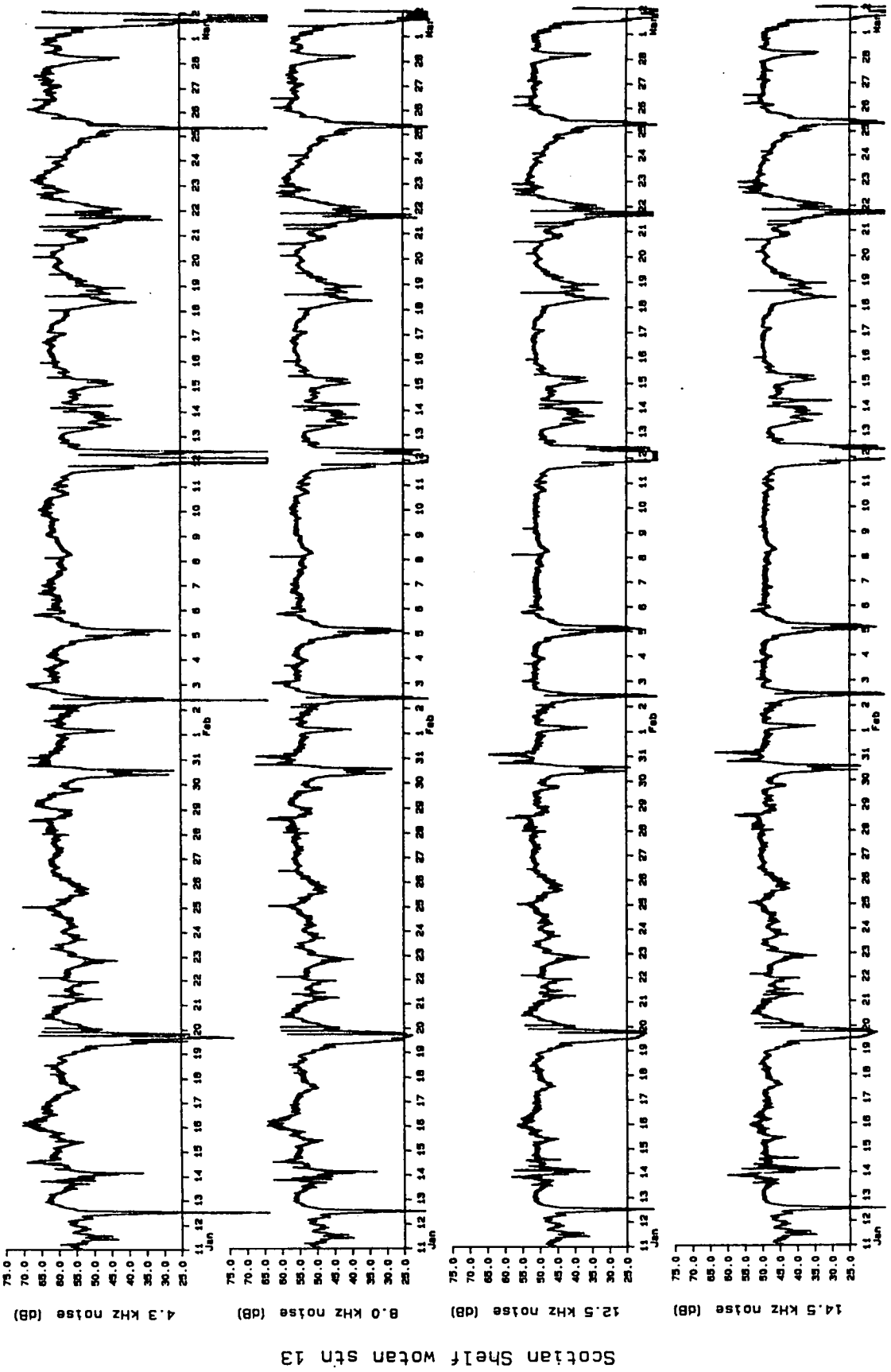

Figure 18 (part 2): Time series of noise spectrum levels at station 13.

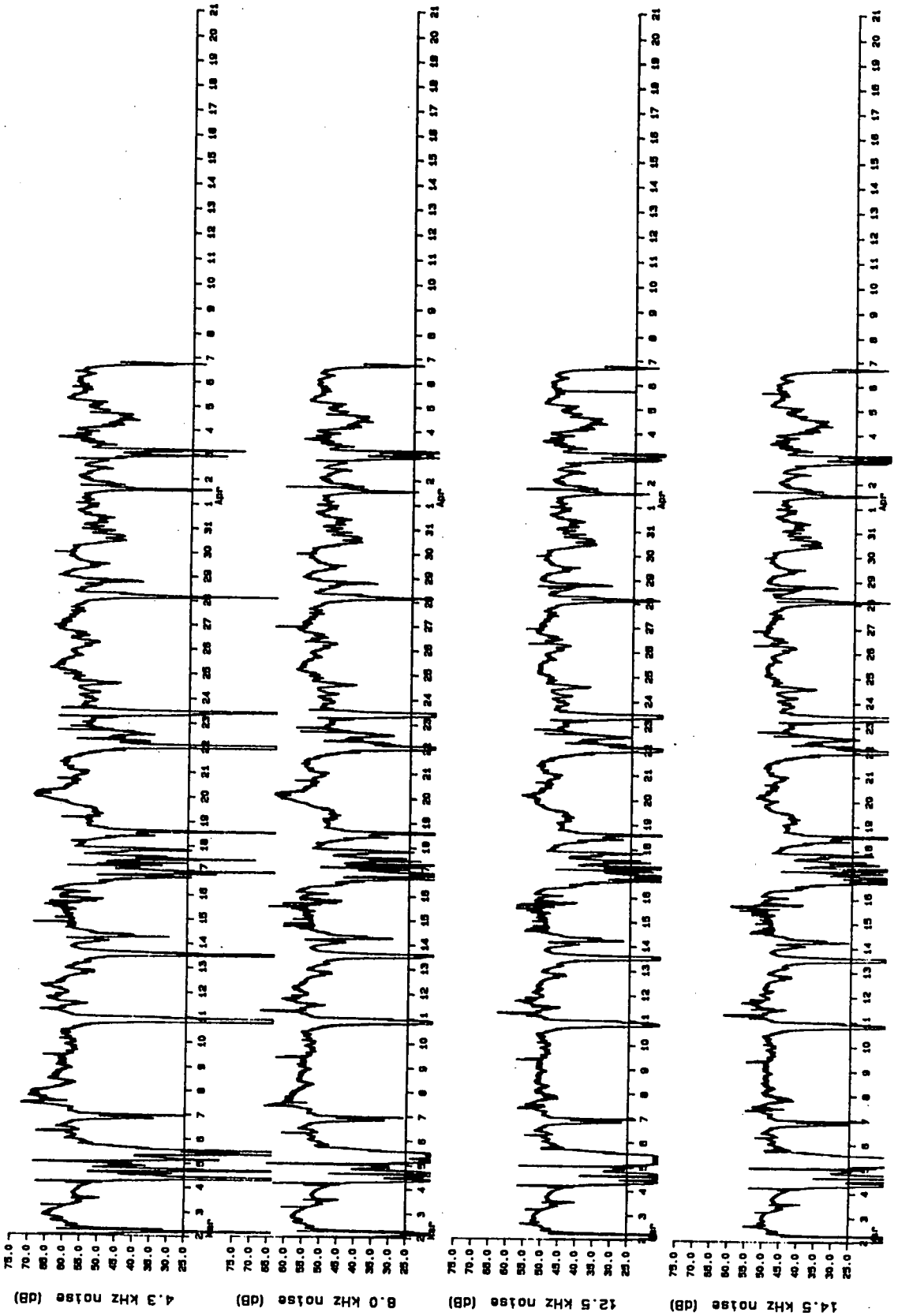

Figure 18 (part 3): Time series of noise spectrum levels at station 13.

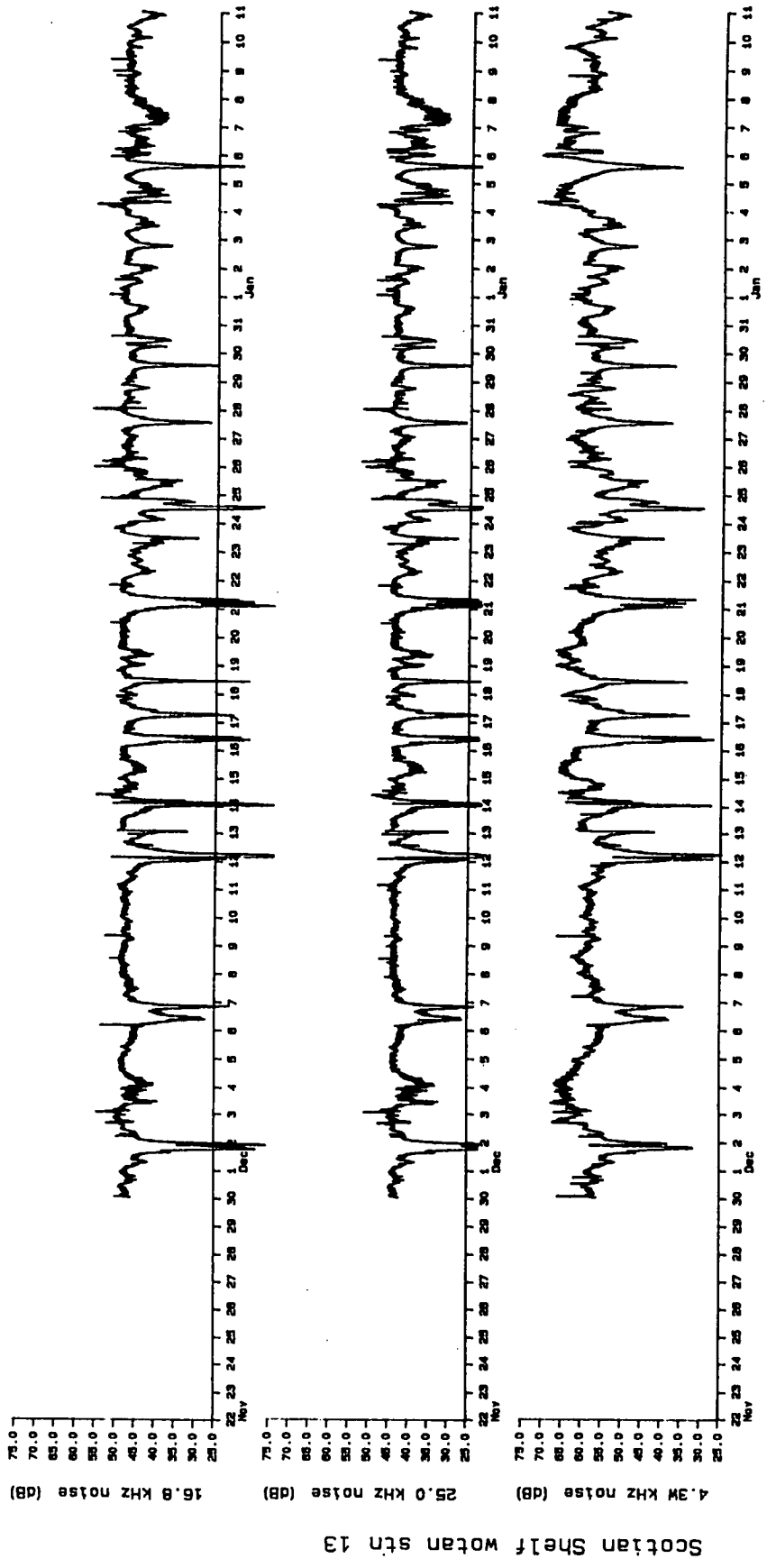

Figure 18 (part 4): Time series of noise spectrum levels at station 13.

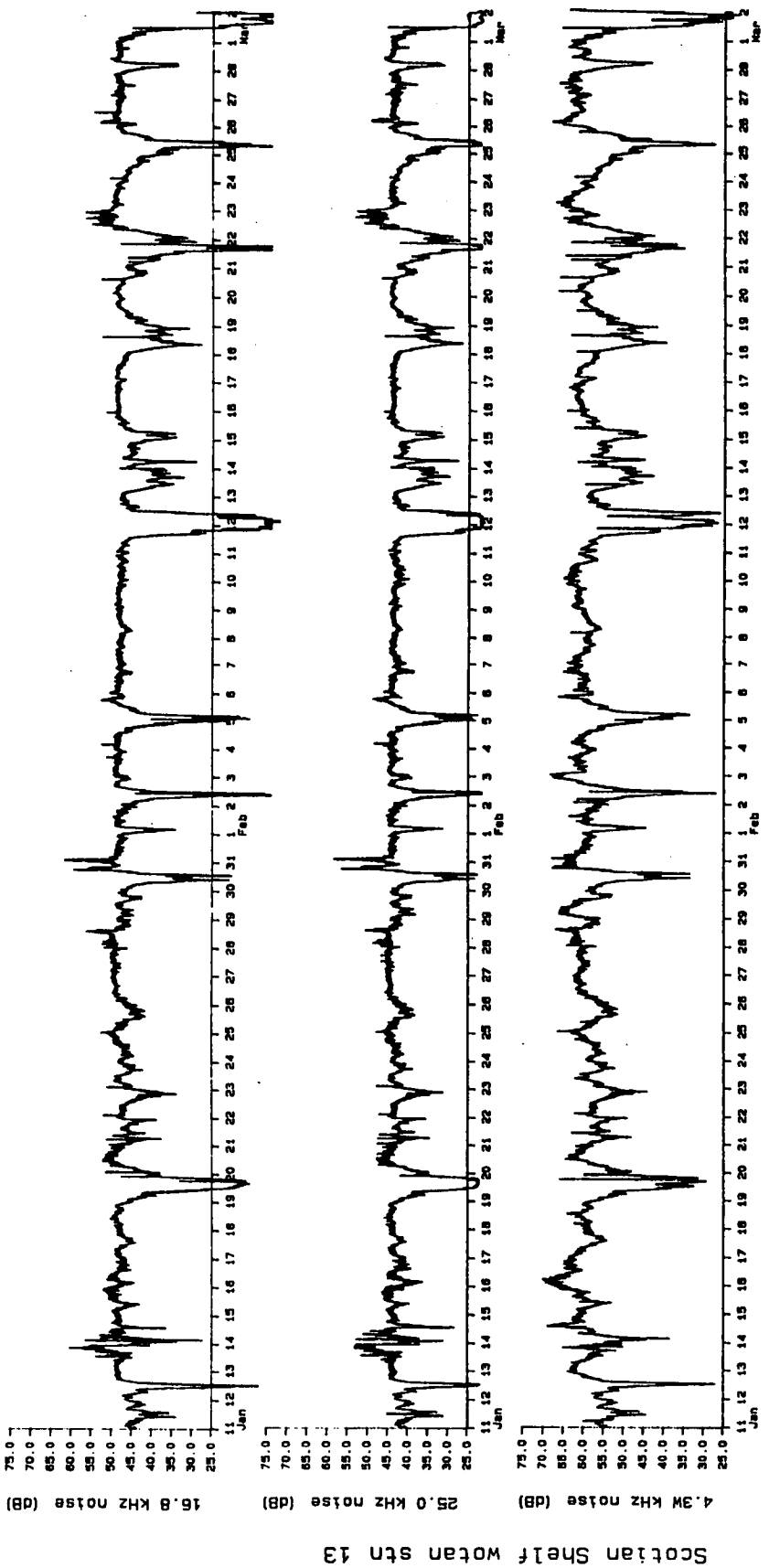

Figure 18 (part 5): Time series of noise spectrum levels at station 13.

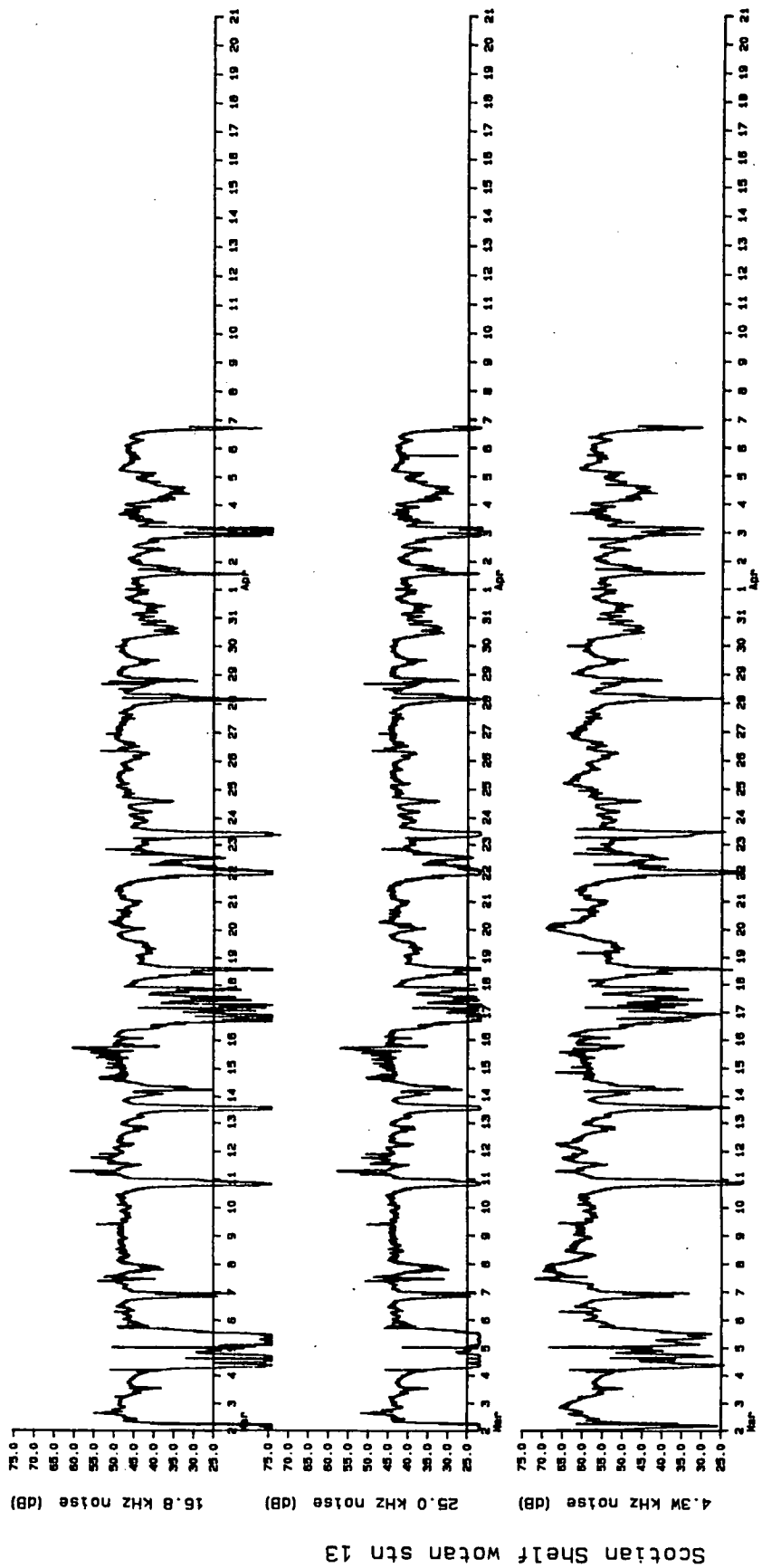

Figure 18 (part 6): Time series of noise spectrum levels at station 13.

speed so that for wind speeds greater than $15 m \cdot s^{-1}$ and frequencies of 8.0 kHz and above, the noise spectrum level actually declines with increasing wind speed. Figure 19 demonstrates the effect.

This effect must be taken into account when calculating wind speed from the acoustic records; once its presence is felt the problem is no longer a simple linear one. Consider the situation where ambient noise is measured at n different frequencies, and suppose that wind is the only contributing source. Then the noise spectrum level at each frequency f_1 is expressed by the equations

$$NSL(f_1)=h_1(\log V);\ NSL(f_2)=h_2(\log V);\ldots;\ NSL(f_n)=h_n(\log V) \qquad (5)$$

where V is the wind speed in $m \cdot s^{-1}$.

Equations (5) are a parametric representation of a curve in a space of n dimensions. If the curve does not cross itself, then any wind speed, V_1, locates a unique point on the curve, and vice versa. If the bubble effects discussed in Farmer and Lemon (1984) did not exist, and, as we have supposed, there were no other noise sources so that the ambient noise was fully described by the original Knudsen curves, then Equations (5) describe a straight line in n-space. In that case, a measurement at any frequency (within the valid frequency band) will produce as good an estimate of wind speed as any other. At every frequency, the logarithm of the wind speed is linearly related to the noise spectrum level. Only one measurement frequency would be necessary, and any one would do.

The bubble effect causes some of the $h_1(\log V)$ to be nonlinear; at sufficiently high frequencies, they are not monotonic. Available evidence suggests, however, that at frequencies below 5 kHz, $h_1(\log V)$ is a linear function. In the absence of other noise sources, then, only a single frequency below 5 kHz is required to estimate wind speed, as the projection of the wind-speed line on that frequency axis is parameterized by a linear function of wind speed, thereby maximizing the accuracy of the inverse relation.

The simplest approach, therefore, is to ignore the contribution from other noise sources and to compute wind speed from the 4.3-kHz channels alone. Such a simplistic scheme can often work quite well, as it is apparent that rainfall-generated noise affects lower frequencies least strongly, and that in areas away from heavy shipping activity, ship noise occurs as isolated, short-lived events.

Figures 20-24 show wind speeds calculated from the 4.3-kHz signals at each of the five CASP WOTAN sites. The wind speeds were computed using the standard empirical relationship (Lemon et al. 1984):

$$20 \log V = a\ NSL - b \qquad (6)$$

where a and b are constants determined from observations.

There is some evidence that the values of the constants a and b depend upon the depth of deployment of the instruments, with the effect that, over most of the normal range of wind speed, constants derived from deeper-water

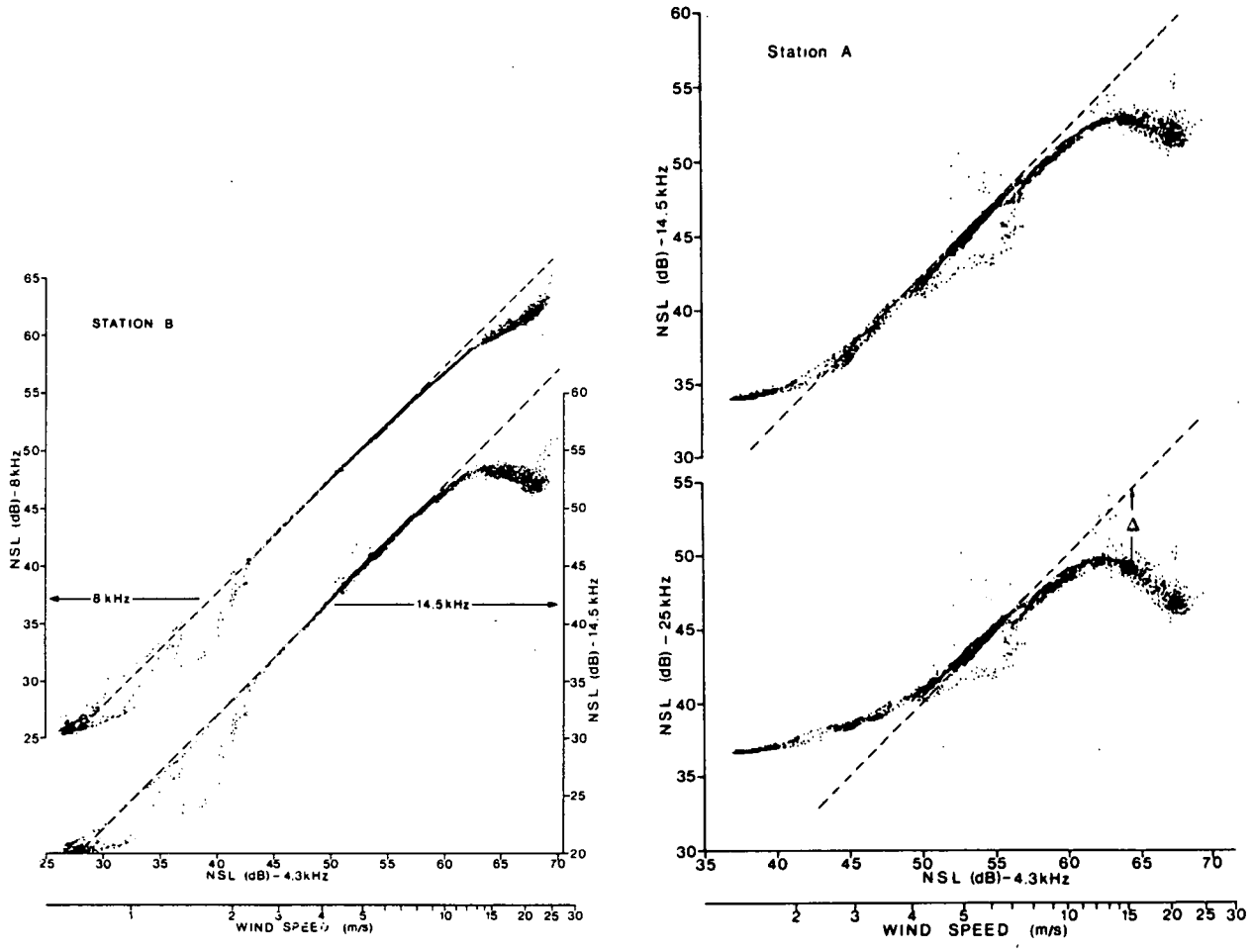

Figure 19: Noise spectrum levels at 8.0, 14.5 and 25.0 kHz plotted against the noise spectrum level at 4.3 kHz for 2 stations in Queen Charlotte Sound (from Farmer and Lemon, 1984).

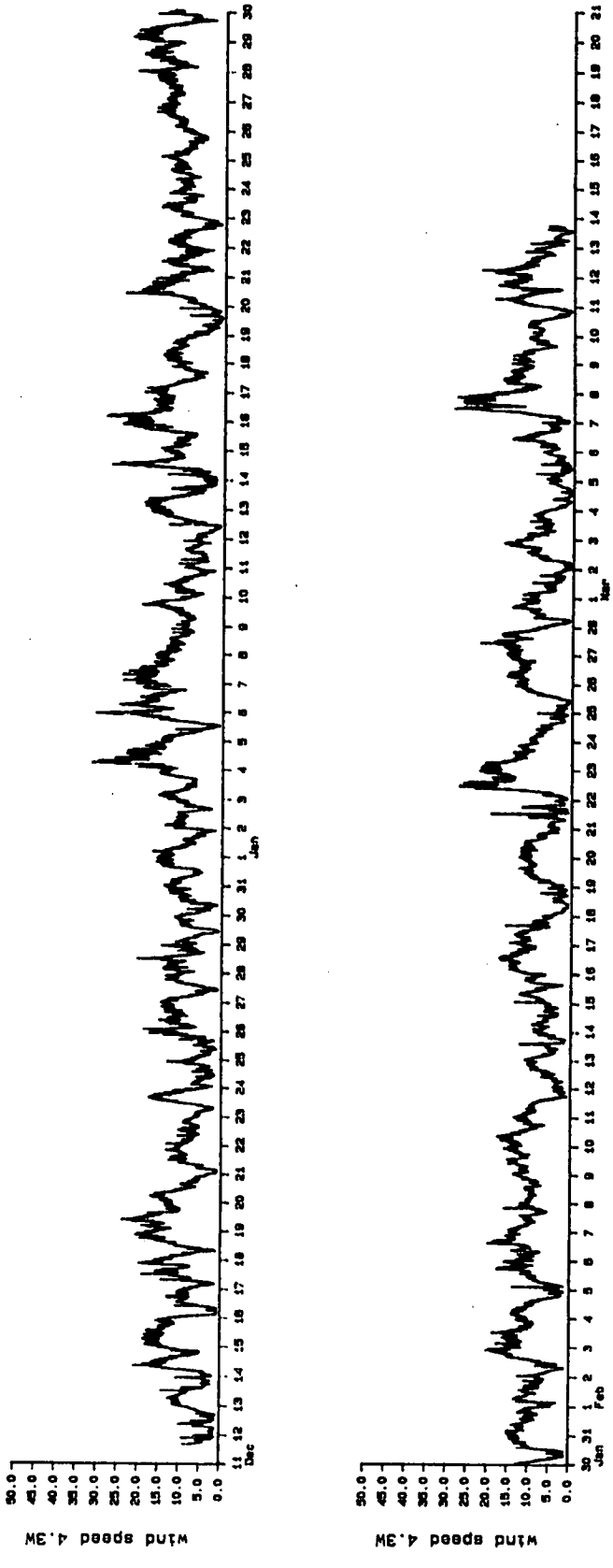

Figure 20: Wind speed at CASP station 1, computed from the 4.3-kHz signal only.

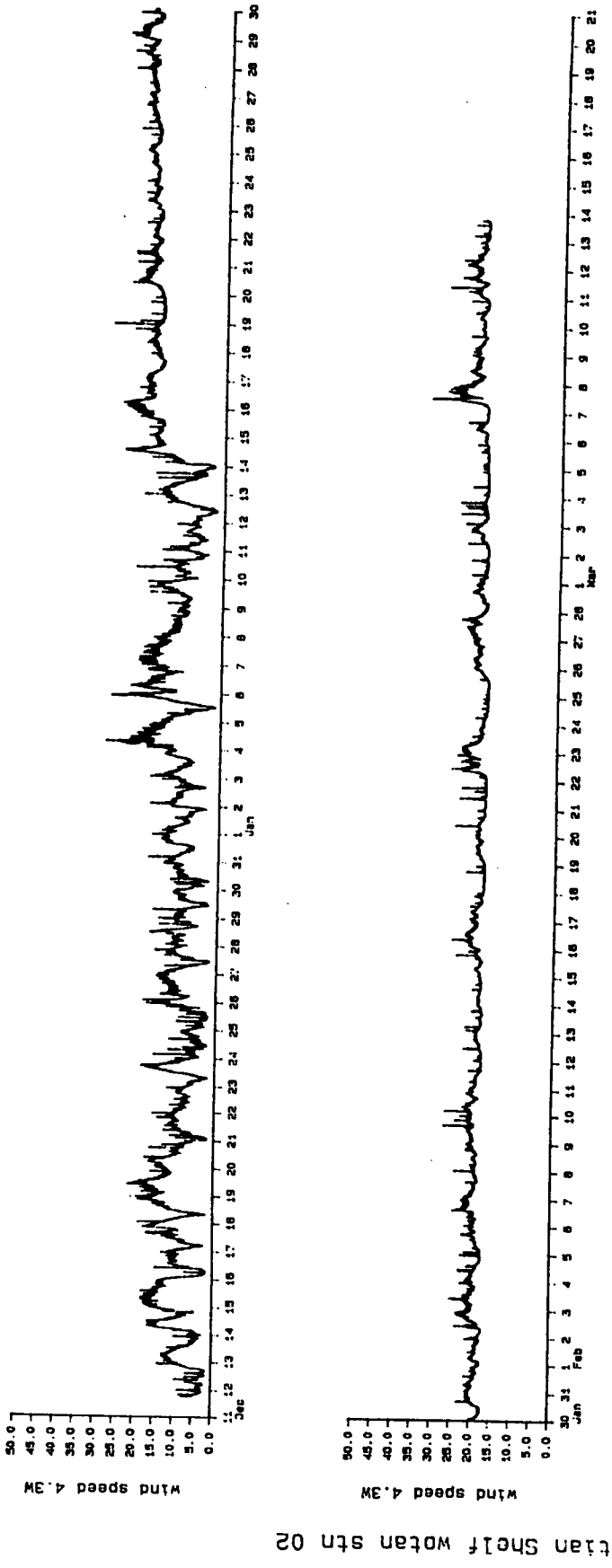

Figure 21: Wind speed at CASP station 2, computed from the 4.3-kHz signal only.

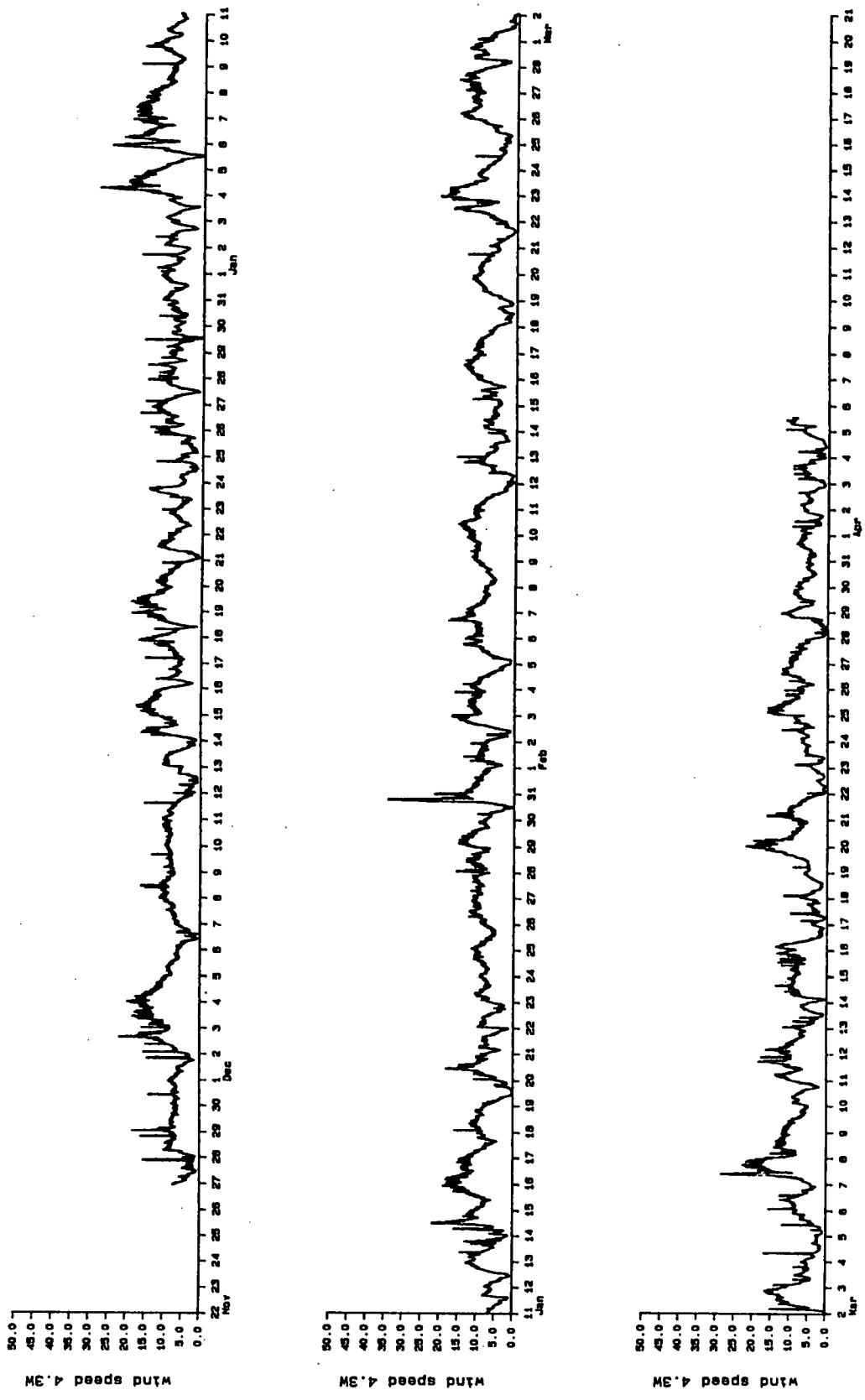

Figure 22a: Wind speed at CASP station 5, computed from the wide-band 4.3-kHz signal only;

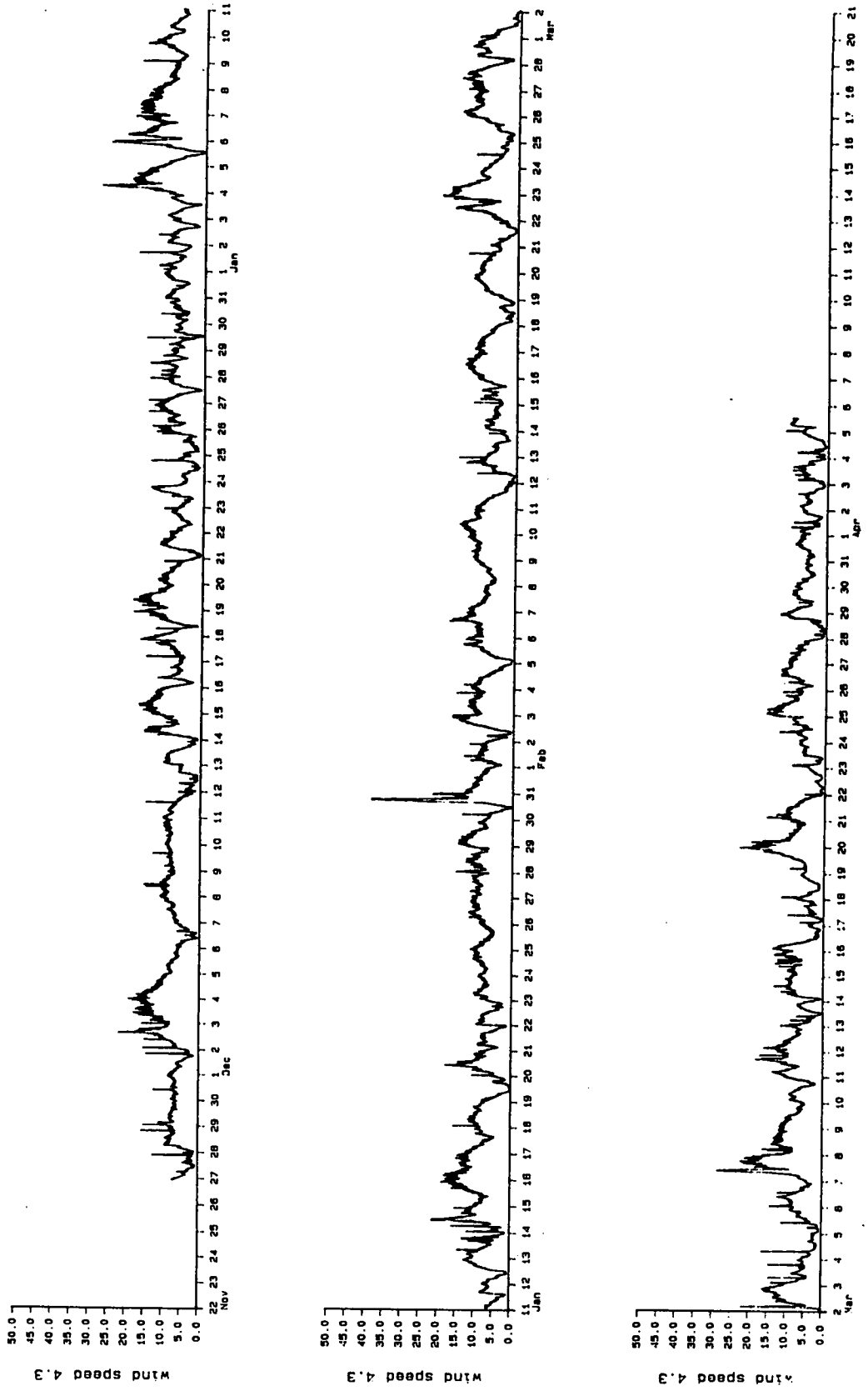

Figure 22b: Wind speed at CASP station 5, computed from the narrow-band 4.3-kHz signal only.

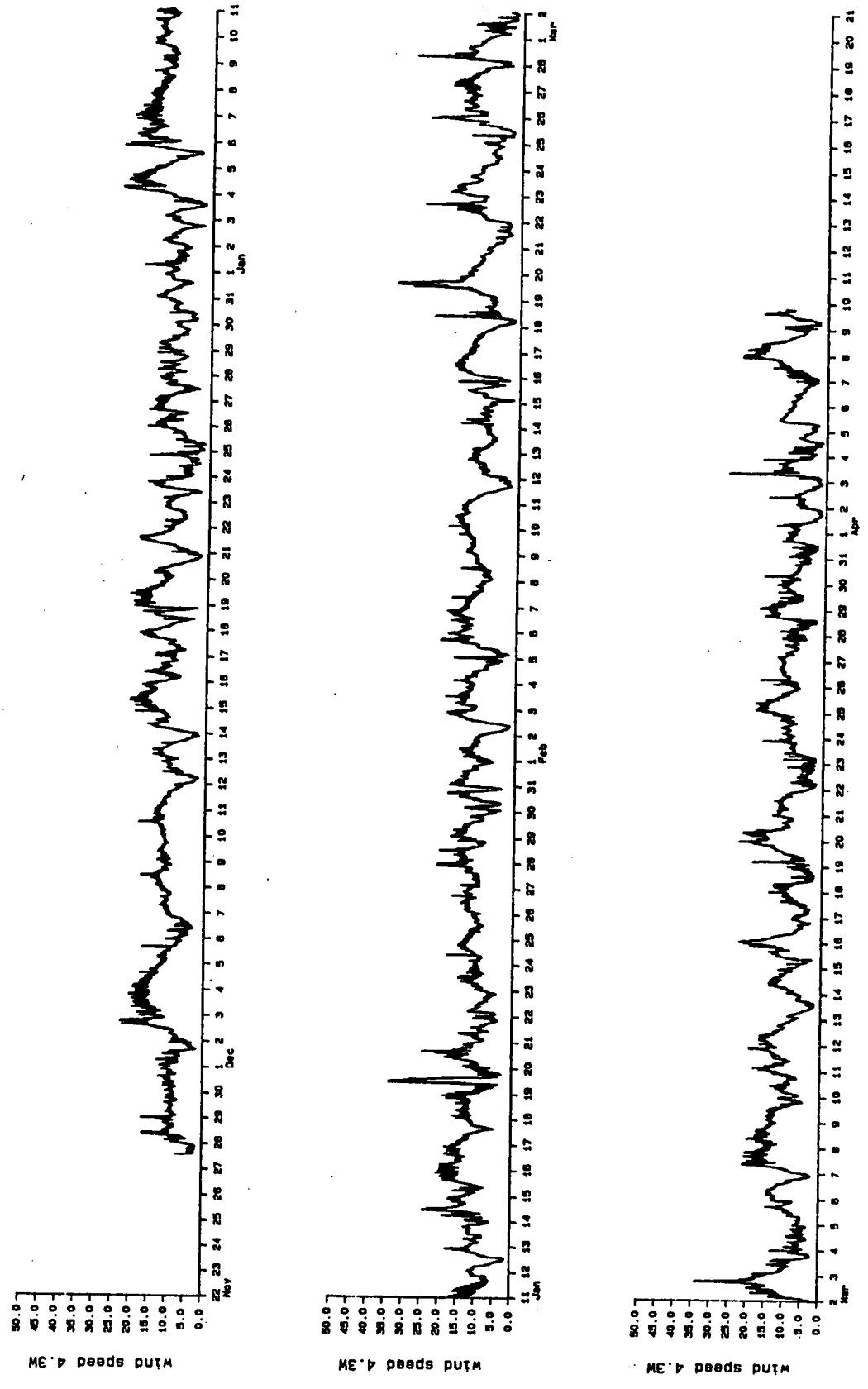

Figure 23a: Wind speed at CASP station 12, computed from the wide-band 4.3-kHz signal only;

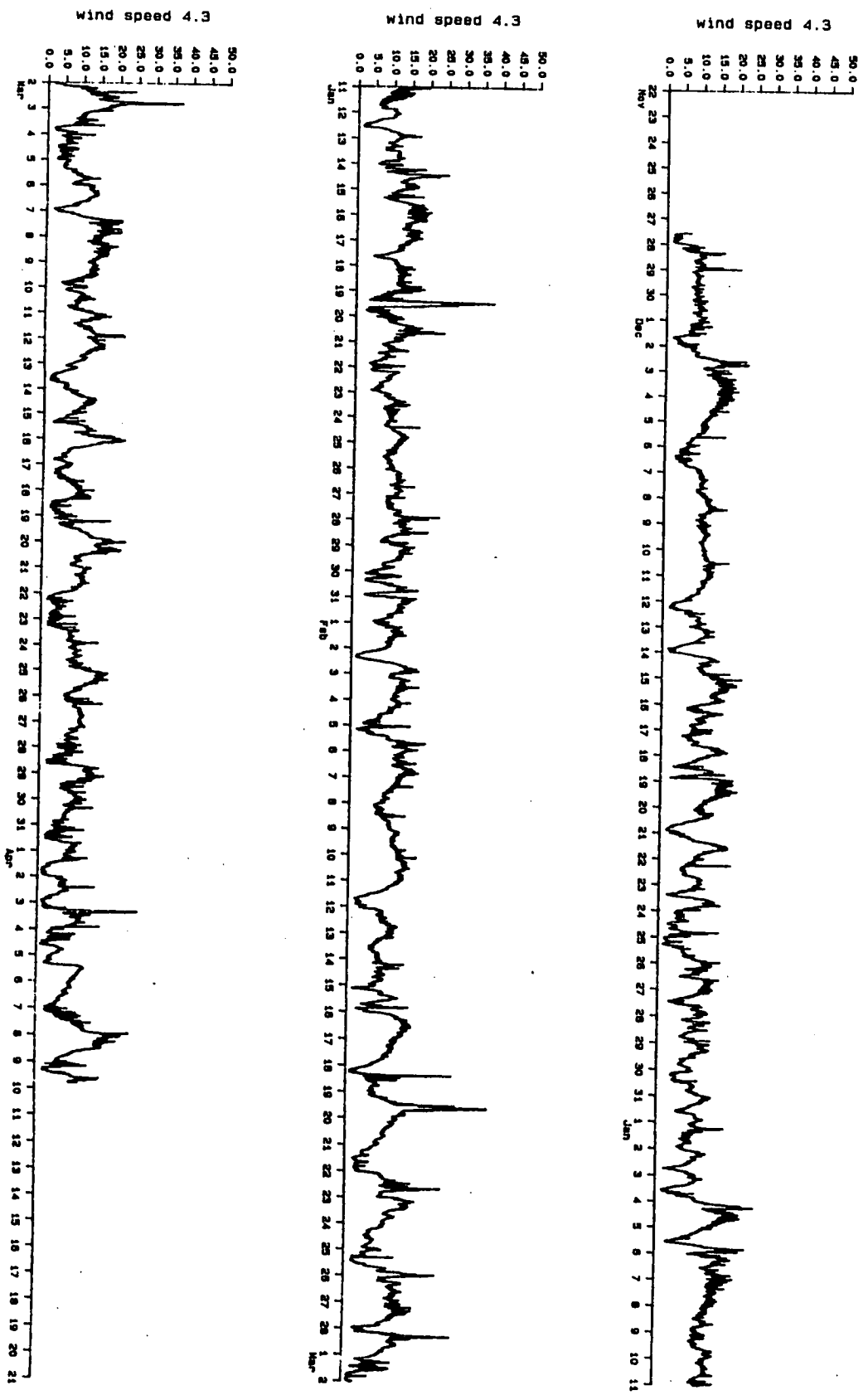

Figure 23b: Wind speed at CASP station 12, computed from the narrow-band 4.3-kHz signal only.

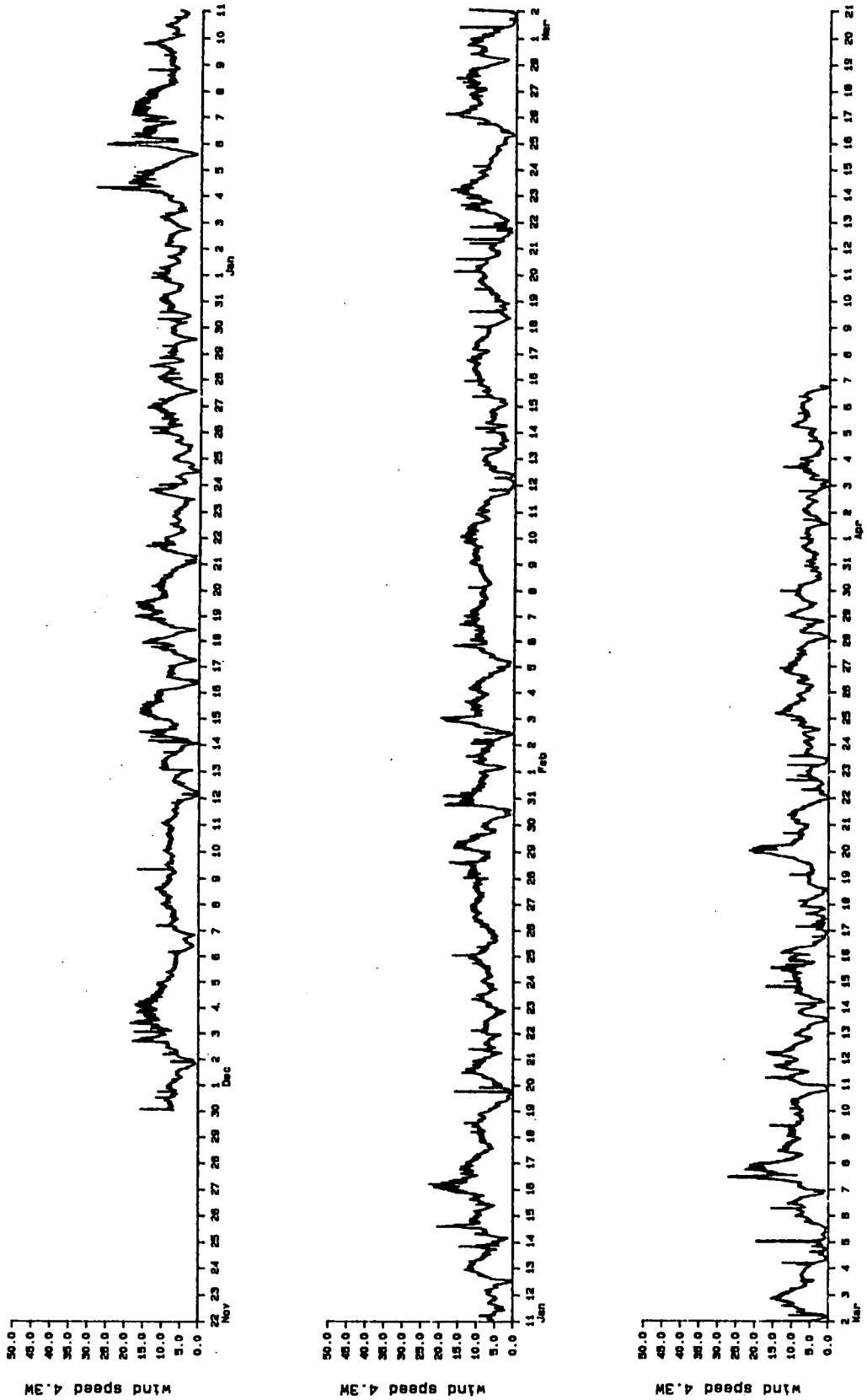

Figure 24a: Wind speed at CASP station 13, computed from the wide-band 4.3-kHz signal only;

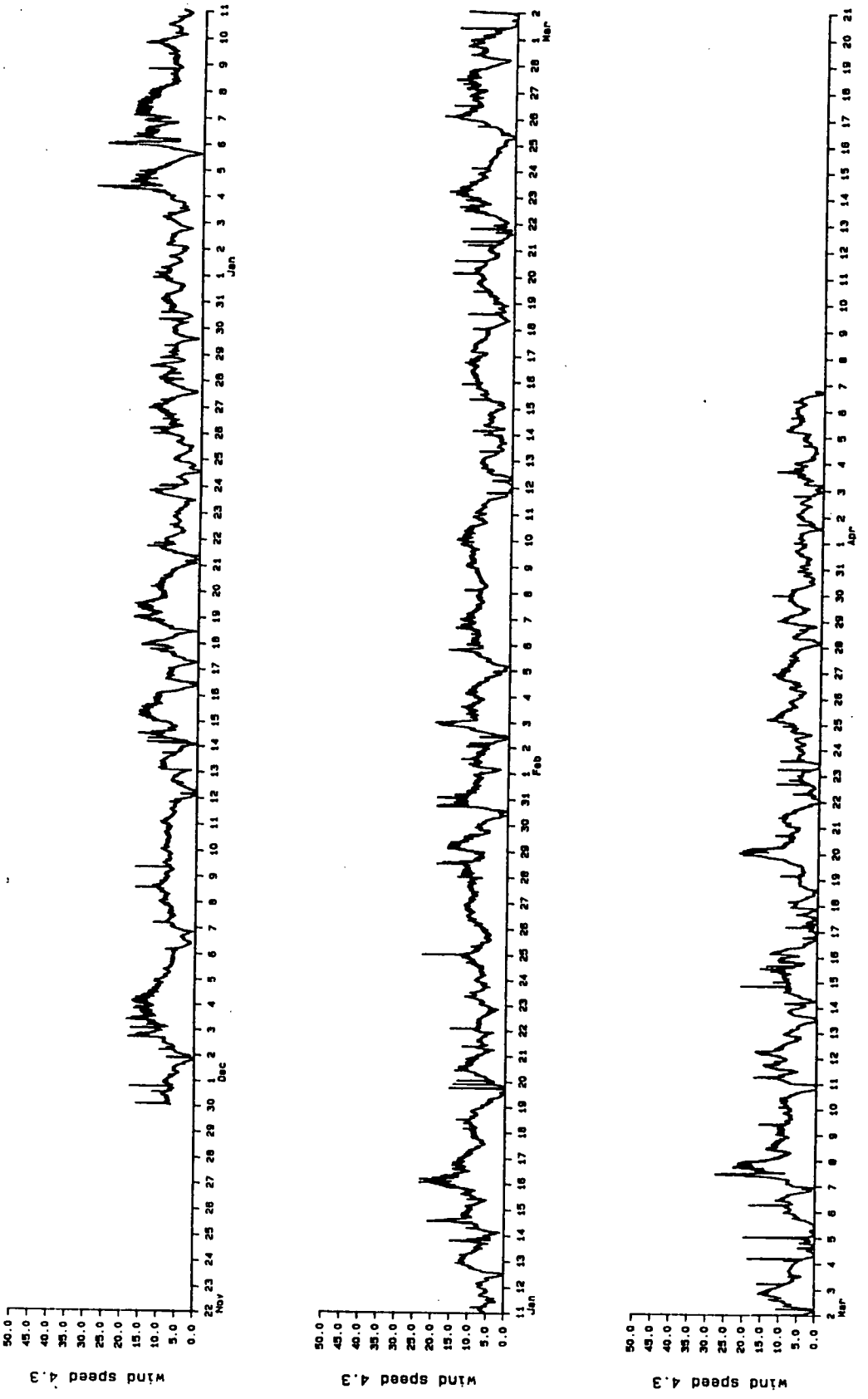

Figure 24b: Wind speed at CASP station 13, computed from the narrow-band 4.3-kHz signal only.

measurements seem to overestimate wind speed when applied to measurements taken in shallow water. Table 6 shows values for a and b at 4.3 kHz from three separate locations at which WOTAN instruments have been moored at diverse depths.

Table 6: Values for the wind speed constants a and b at 4.3-kHz frequency from three locations: (i) deep Pacific (4000 m) (Evans and Watts 1981); (ii) Queen Charlotte Sound (continental shelf, 250 m depth) (Lemon et al. 1984); (iii) Barkley Sound (continental shelf, 15 m depth) (S. Vagle[2])

Location	a	b
i	0.831	29.9
ii	0.783	27.6
iii	0.900	38.0

It is also apparent from data set (iii) that the variance of the wind-generated noise signal increases with decreasing depth.[2] Such an effect is to be expected as the size of the surface-generating area to which the WOTAN is listening, and hence the degree of spatial averaging would also decrease with depth. This effect may be seen in the CASP data as well by comparing, for example, Figures 7 and 10. Given the mooring depths listed in Table 1, it was decided that the most suitable sets of wind-speed coefficients to use would be (iii) for stations 1 and 2, and (ii) for stations 5, 12 and 13. The wind speeds shown in Figures 20 to 24 have been computed on that basis.

When other noise sources are present that contribute at the same frequencies as the wind, then the wind speed calculated from one channel only will be too high. If the interfering noise varies with frequency differently than wind-generated noise (i.e., has a different spectrum), then in principle we should be able to combine noise measurements made at several frequencies to separate the wind-generated noise from the other noise and, thus, recover the true wind speed. Consider a simple example in which wind and only one other noise source, say rainfall, are present. To simplify the problem further, assume that the wind noise falls off linearly with increasing frequency and that at any frequency the noise spectrum level depends linearly on the wind speed (i.e., there are no bubble effects). Assume also that the rain-generated noise spectrum behaves the same way, but with a different spectral slope, and that the two sources are completely independent. If wind only were present, then we would find

---

[2] S. Vagle, 1986, Institute of Ocean Sciences, Sidney, B.C., personal communication

$$NSL_w = \alpha f + \beta V \tag{7}$$

where f is the acoustic frequency, NSL_w is the noise spectrum level in dB and V is the wind speed. Similarly if only rain were present we would find

$$NSL_R = \alpha' f + \beta' R \tag{8}$$

where R is the rate of rainfall. Now pick two frequencies f_1 and f_2 at which measurements are to be made. Data will then consist of the noise at those two frequencies and will depend on the wind speed and rainfall rate.

The noise due to wind only at frequency f_2 can be expressed as

$$10^{NSL_w(f_2)} = 10^{\alpha (f_2-f_1)} \; 10^{NSL_w(f_1)}$$

or

$$M_w(f_2) = K_w M_w(f_1) \tag{9}$$

where M_w is the noise level due to wind expressed in linear units, and K_w is a constant which depends on f_2-f_1. (The spectrum levels have been expressed as exponentials to allow wind and rain noise to be added together below.)

Plotting $M_w(f_2)$ against $M_w(f_1)$ will result in a straight line through the origin with slope K_w. Distance along the line from the origin is parameterized (logarithmically) in terms of the wind speed by Equation (7). (We assume α and β are known.) Similarly, we can express noise due to rainfall only at (f_2) in terms of noise at (f_1) as

$$M_R(f_2) = K_R M_R(f_1) \tag{10}$$

which describes another straight line through the origin, but with slope K_R. Distance along this line is parameterized in terms of rainfall rate R by Equation (8). A measurement taken with both sources of noise present will result in noise levels at (f_1) and (f_2) of

$$M(f_1) = M_w(f_1, V) + M_R(f_1, R)$$

$$M(f_2) = M_w(f_2, V) + M_R(f_2, R) \tag{11}$$

The point $[M(f_1), M(f_2)]$ will lie somewhere between the two lines described by Equations (9) and (10). Both the wind speed and the rainfall rate can be recovered by projecting the vector from the origin to $[M(f_1), M(f_2)]$ onto the wind speed and rainfall lines and using the parameterizations of Equations (7) and (8). Every point between the two lines maps to a unique combination of wind speed and rainfall rate. Under these simple assumptions then, we can recover both quantities by measuring at two frequencies only.

If a third noise source with the same type of frequency dependence and parameterization by a source quantity (e.g., shipping noise) were present, then there would be three lines on the plot (one for each source) and all measured points would lie between the lines with maximum and minimum slope. Each point would not determine a unique combination of the three sources however, so that a third measurement frequency channel would be required to determine the contribution from each source. Then there would be a three-dimensional co-ordinate system [$M(f_1)$, $M(f_2)$, $M(f_3)$] and each noise source would describe a line radiating from the origin. Measured points would be within the volume enclosed by the planes described by each pair of lines, and the contribution from each source would be measured by the projection of the measured noise vector on each of the three lines.

In fact, none of the actual noise relationships are simple linear functions as described above, so that the straight lines in the example above would become curves (see, for example, Figure 19) which complicates the process of mapping noise levels to combinations such as wind speed and rainfall rate. At present, the shape of the rainfall spectrum is not well enough known to allow the equivalent of Equation (8) to be written. It should be possible, however, to use the known frequency dependence of wind-generated noise to improve wind speed estimates beyond those possible using only one channel. Even with the presence of bubbles, pure wind-generated noise at one frequency plotted against a second will produce a well-defined curve (e.g., Figure 19), which we may then use to optimize wind-speed estimation for any data set. As stated previously, rain-generated noise favours higher frequencies, whereas industrial noise favours lower frequencies. Noise measurement points contaminated with rain noise will, therefore, deviate to the higher-frequency side of the curve, whereas those contaminated with industrial noise will deviate to the lower-frequency side of the curve. In each case, we can then use the frequency least likely to be affected to compute the wind speed, and should achieve an overall improvement in the wind-speed estimates.

We will use the 4.3-kHz and 8.0-kHz channels as an example. The data from Queen Charlotte Sound, shown in Figure 19, were used to generate the curve defining wind-generated noise. The curve is shown in Figure 25 and is labelled as line W. (The noise levels are plotted in decibel units, rather than the linear units used in the example above.) To allow for small random measurement errors, the line was expanded to a band 1 dB wide, labelled zone A in Figure 25. Any point lying within A was taken to be purely wind-generated. Within A, wind speed was computed by returning to W along a perpendicular from the measured point and computing the wind speed from the average 4.3-kHz relation for Queen Charlotte Sound given in Lemon et al. (1984):

$$20 \log V = (0.783 \pm 0.016)\ NSL - (27.6 \pm 0.9) \qquad (12)$$

where V is the wind speed in $m \cdot s^{-1}$ and NSL is the 4.3-kHz noise level in dB re 1 μ Pa/Hz. (The additive constant has been corrected to allow for the bandwidth difference between the noise generator and voltmeter used in deriving the instrument calibrations for Queen Charlotte Sound. The difference amounts to 0.7 dB.) Points falling below zone A were taken to be contaminated with shipping or industrial noise; wind speed was computed by returning to line W along the horizontal (constant 8.0-kHz noise level) and

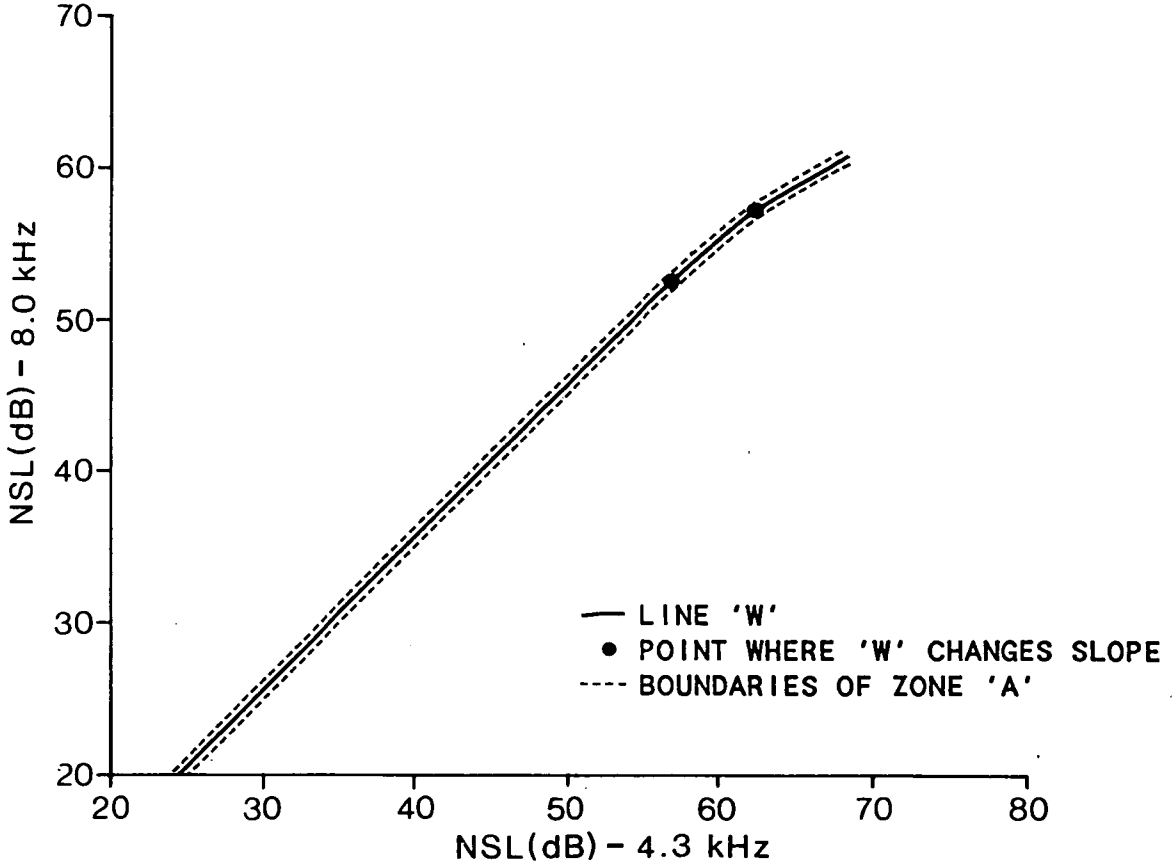

Figure 25: Definition of line W and zone A used in computing wind speed. The slopes of the various portions of line W have been taken from Farmer and Lemon (1984). The intercept was computed from data collected at station 13.

applying Equation (12). Points lying above zone A were assumed to contain precipitation noise and, in this case, wind speed was computed by returning to line W vertically (constant 4.3-kHz noise level) and applying Equation (12). In fact both of these (or other) extraneous noise sources could be present on either side of A. However, without full knowledge of the rainfall spectrum at least, a better separation cannot be achieved at present. Current knowledge strongly suggests that the two sources would dominate as described. Figures 26 to 30 show the wind speed calculated at each site as described.

Inspection of Figures 26 to 30 clearly shows that the procedure described does not produce realistic wind-speed time series, particularly in the case of station 13 (Figure 30). The step-like nature of the time series is unrealistic. Figures 31 to 34 show scatterplots of the 8.0-kHz noise spectrum level versus the 4.3-kHz noise spectrum level at CASP stations 1, 5, 12 and 13, respectively. The data have been selected from the period February 8-28 1986, during which the Martinique Beach meteorological station showed minimal precipitation.[3] Line W has been plotted with the data from station 13 (Figure 34) and clearly does not match it. It does not match any of the curves from the other stations very well either, which accounts for the poor appearance of the wind-speed plots in Figures 26 to 30. In fact, the curves in Figures 31 to 34 are all different, so that no single line W could be used for all four sites (station 2 has been excluded because of the noise problems from January 14 1986 on).

Zone A was, therefore, defined separately for each station as follows [$N_{4.3}$ is the 4.3-kHz noise signal (narrow-band for stations 5, 12 and 13) and N_8 is the 8.0-kHz noise signal, both in dB re 1 μ Pa/Hz]:

Station 1:

$N_{4.3} \leq 60.3$ dB: $\quad -7.53 \text{ dB} \leq N_8 - 1.02\, N_{4.3} \leq -6.53 \text{ dB}$

$N_{4.3} > 60.3$ dB: $\quad 6.72 \text{ dB} \leq N_8 - 0.784\, N_{4.3} \leq 7.72 \text{ dB}$

Station 5:

$N_{4.3} \leq 56.7$ dB: $\quad -7.74 \text{ dB} \leq N_8 - 1.04\, N_{4.3} \leq -6.74 \text{ dB}$

$56.7 \text{ dB} < N_{4.3} \leq 60.3$ dB: $\quad 2.28 \text{ dB} \leq N_8 - 0.861\, N_{4.3} \leq 3.28 \text{ dB}$

$N_{4.3} > 60.3$ dB: $\quad -23.6 \text{ dB} \leq N_8 - 0.507\, N_{4.3} \leq 24.6 \text{ dB}$

Station 12:

$N_{4.3} \leq 60.6$ dB: $\quad -5.0 \text{ dB} \leq N_8 - N_{4.3} \leq -4.0 \text{ dB}$

$60.6 \text{ dB} < N_{4.3} \leq 63.2$ dB: $\quad 9.0 \text{ dB} \leq N_8 - 0.769\, N_{4.3} \leq 10.0 \text{ dB}$

$N_{4.3} > 63.2$ dB: $\quad -23.0 \text{ dB} \leq N_8 - 0.469\, N_{4.3} \leq 29.0 \text{ dB}$

Station 13:

$N_{4.3} \leq 59.4$ dB: $\quad -0.98 \text{ dB} \leq N_8 - 0.92\, N_{4.3} \leq 0.02 \text{ dB}$

$N_{4.3} > 59.4$ dB: $\quad -20.0 \text{ dB} \leq N_8 - 0.57\, N_{4.3} \leq 21.0 \text{ dB}$

---

[3] Data supplied by Dr. F. Dobson, Bedford Institute of Oceanography, personal communication, 1986.

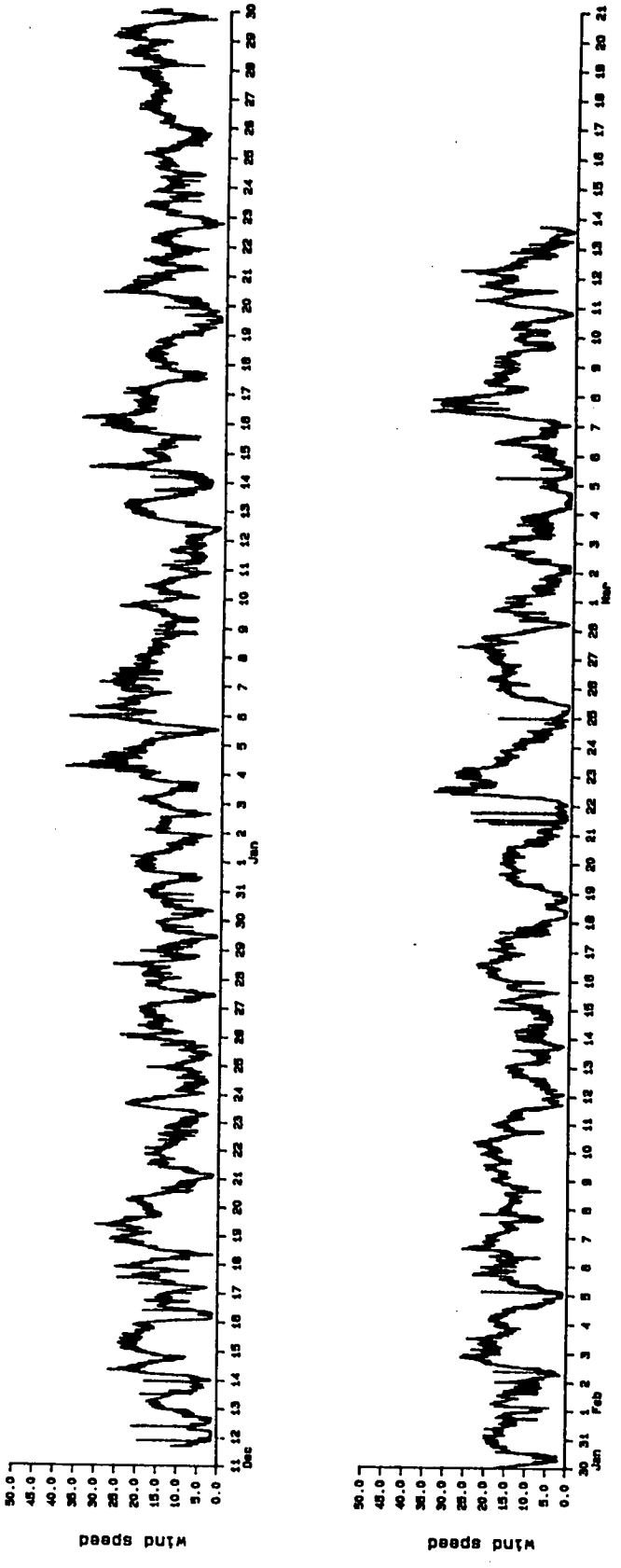

Figure 26: Wind speed ($m \cdot s^{-1}$) at station 1 computed from the 4.3-kHz and 8.0-kHz signals, using the relationship derived from the Queen Charlotte Sound measurements.

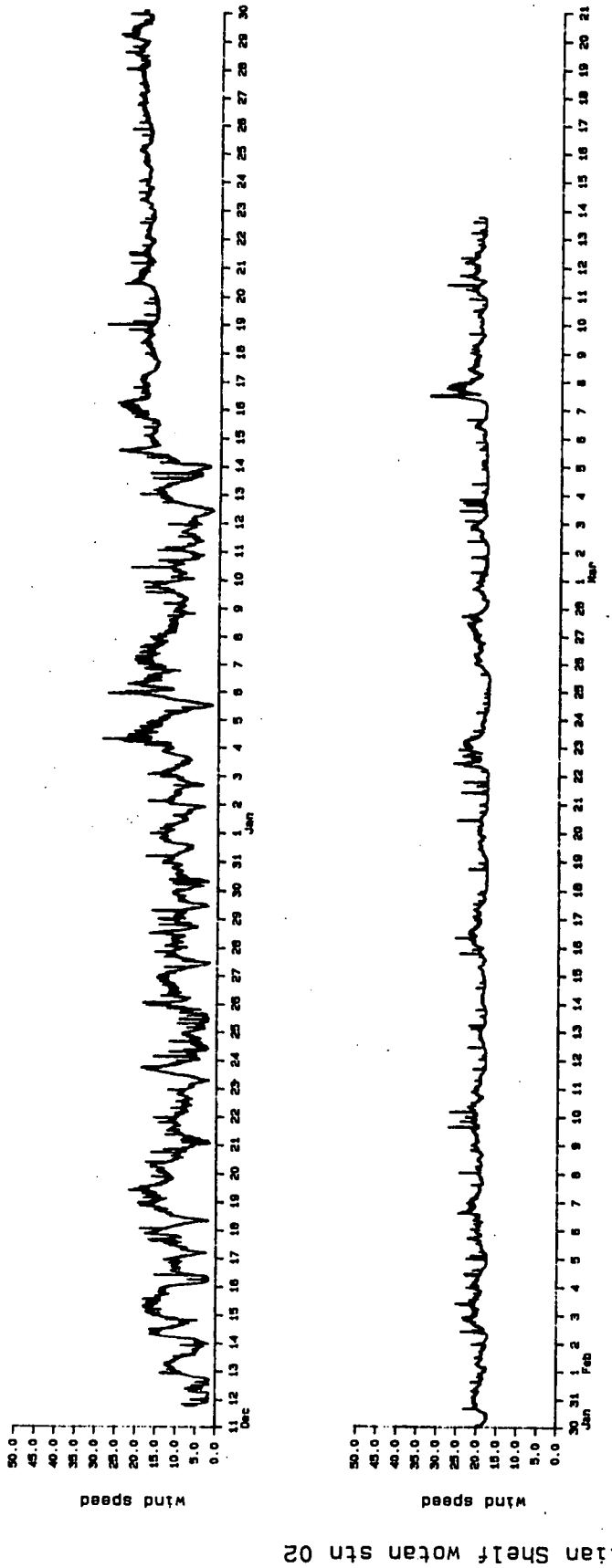

Figure 27: Wind speed ($m \cdot s^{-1}$) at station 2 computed from the 4.3-kHz and 8.0-kHz signals, using the relationship derived from the Queen Charlotte Sound measurements.

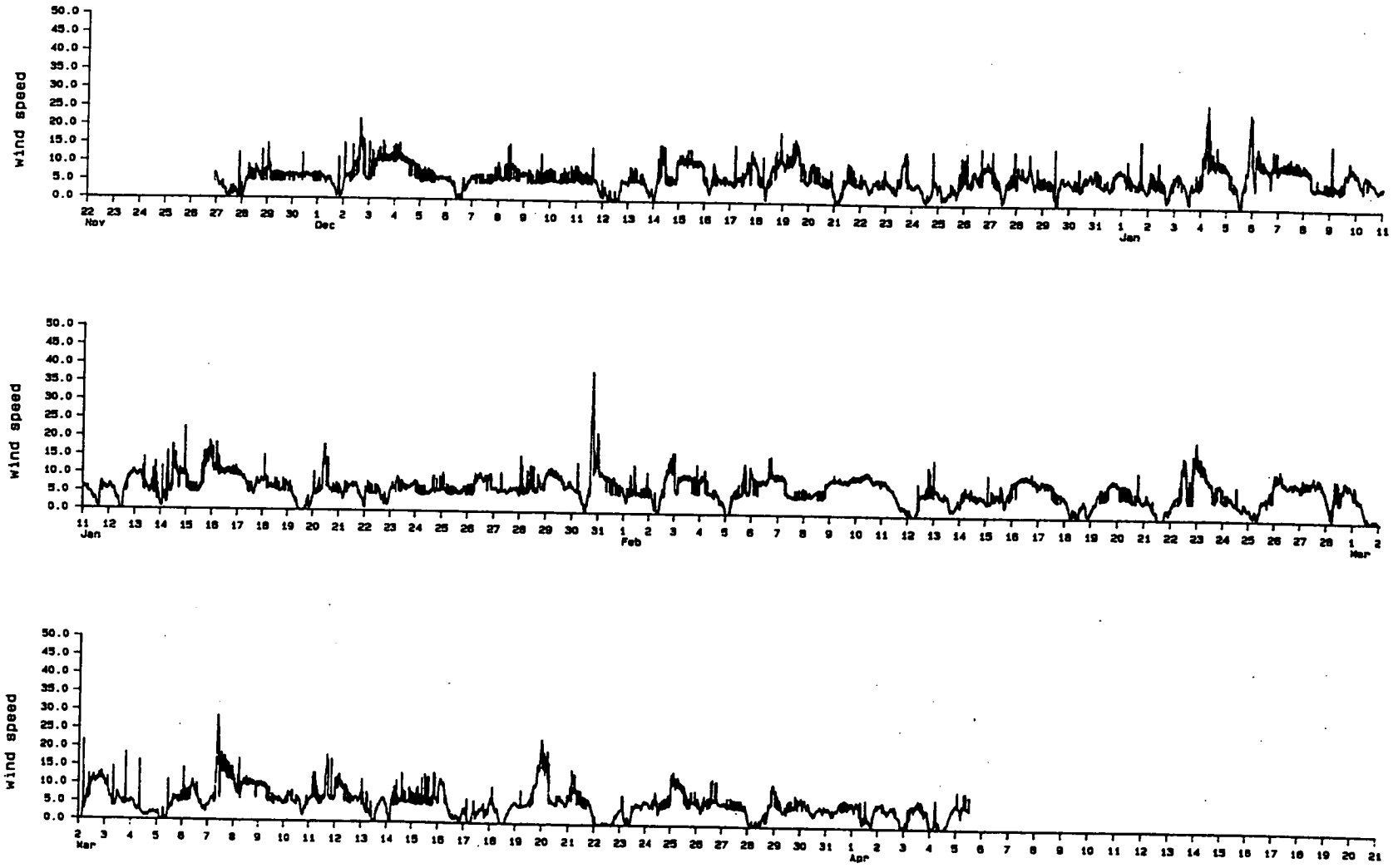

Figure 28: Wind speed ($m \cdot s^{-1}$) at station 5 computed from the narrow-band 4.3-kHz and 8.0-kHz signals, using the relationship derived from the Queen Charlotte Sound measurements.

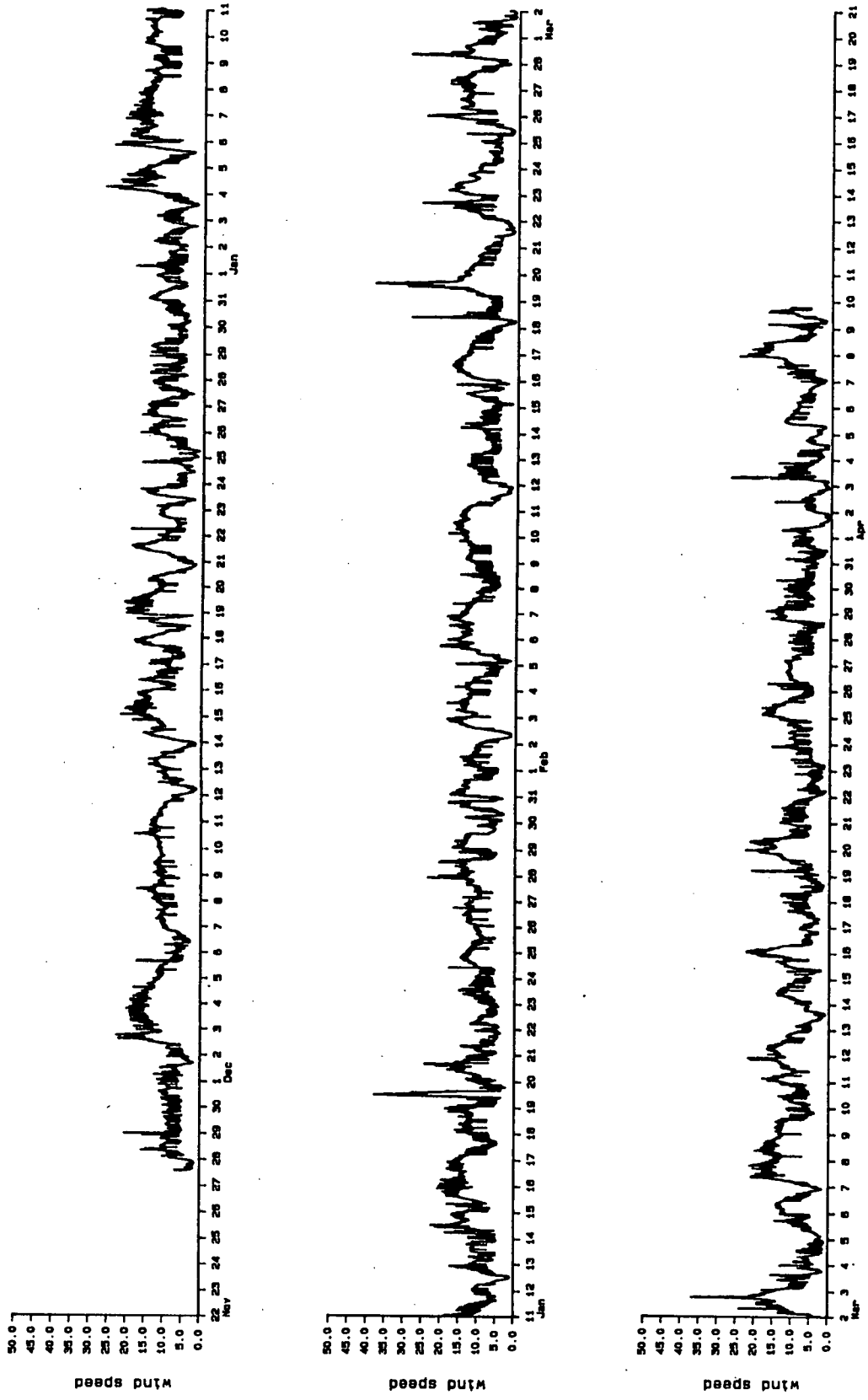

Figure 29: Wind speed ($m.s^{-1}$) at station 12 computed from the narrow-band 4.3-kHz and 8.0-kHz signals, using the relationship derived from the Queen Charlotte Sound measurements.

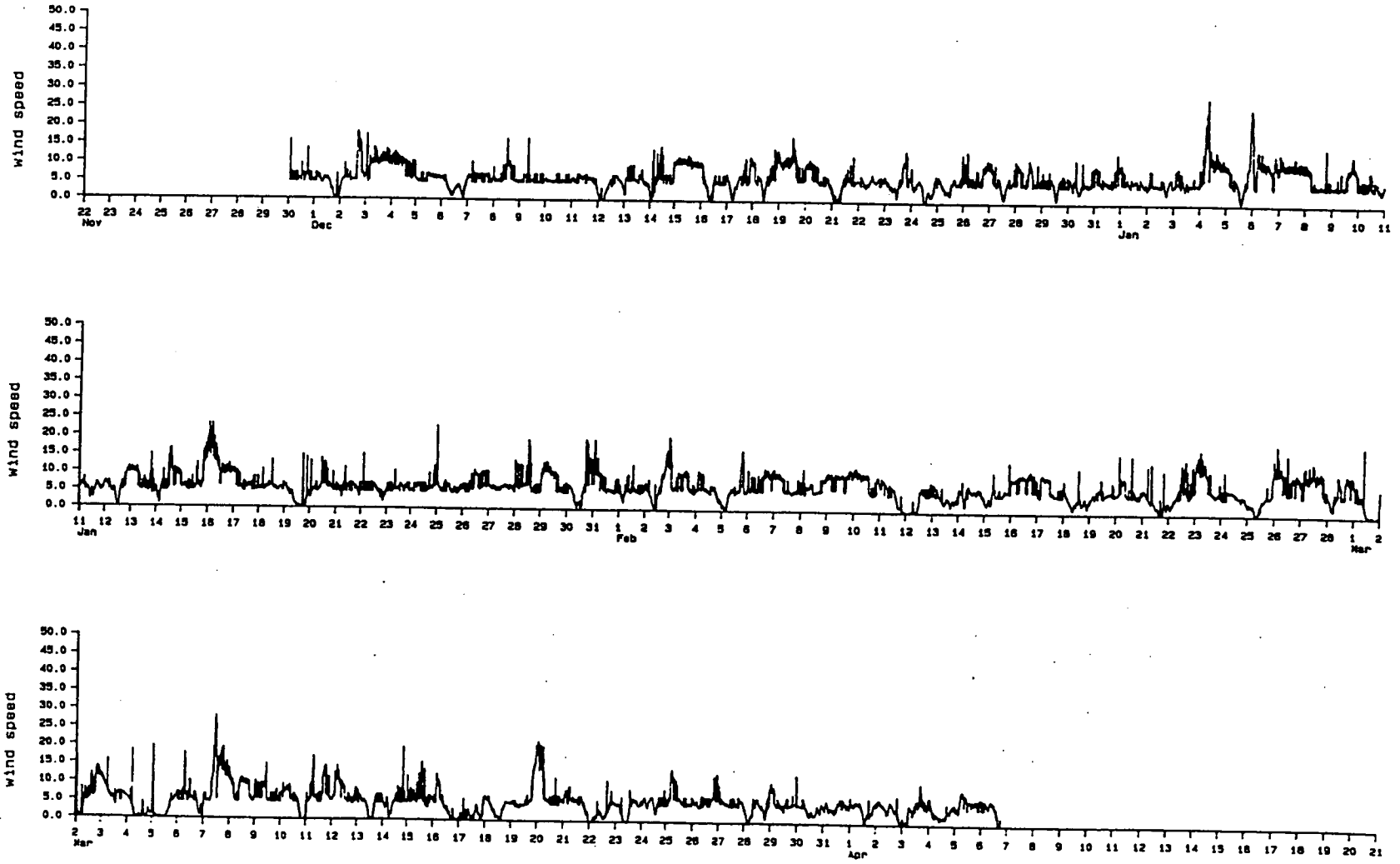

Figure 30: Wind speed ($m \cdot s^{-1}$) at station 13 computed from the narrow-band 4.3-kHz and 8.0-kHz signals, using the relationship derived from the Queen Charlotte Sound measurements.

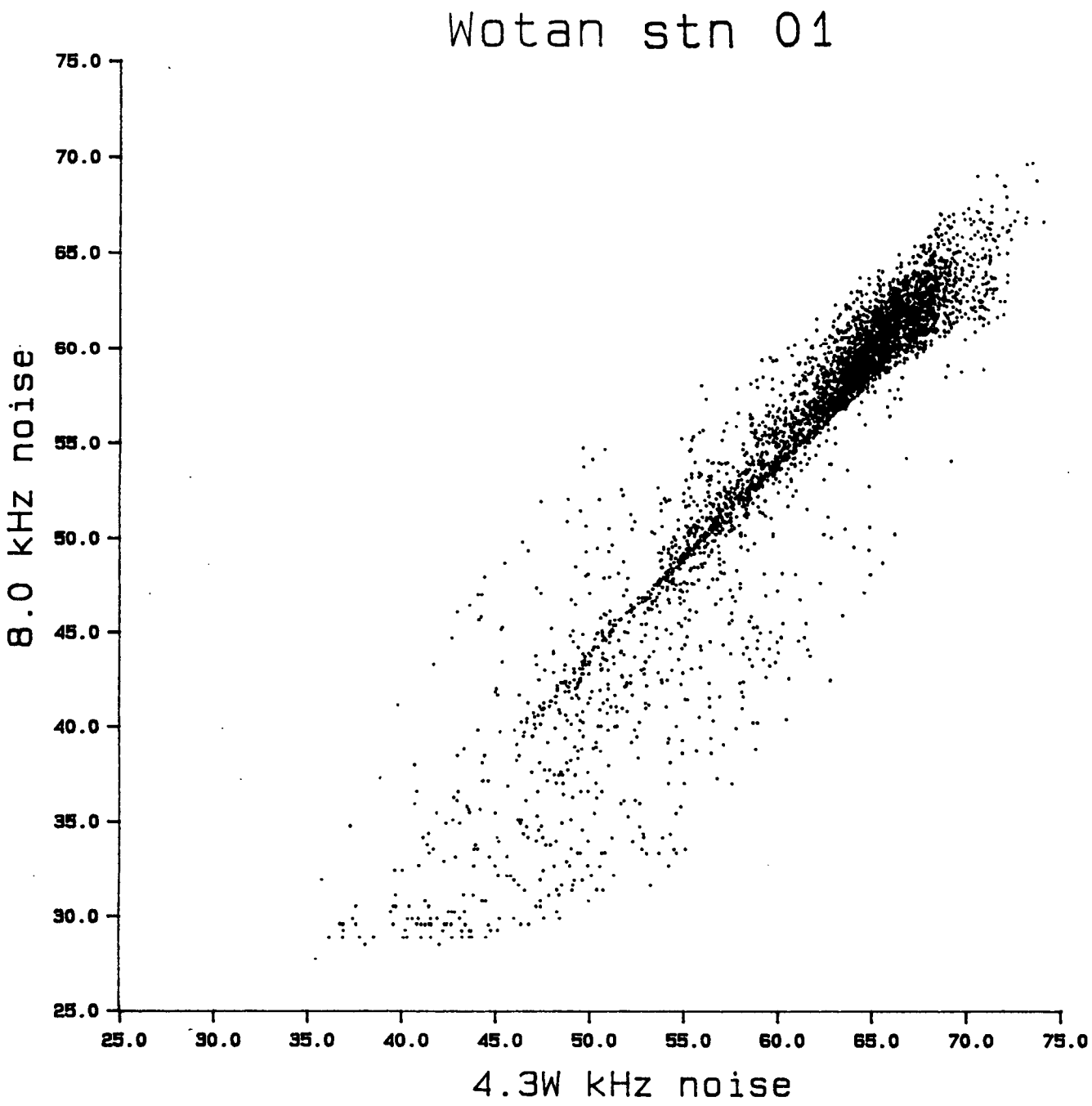

Figure 31: Noise spectrum level at 8.0 kHz vs noise spectrum level at 4.3 kHz at station 1 for the period February 8-28, 1986.

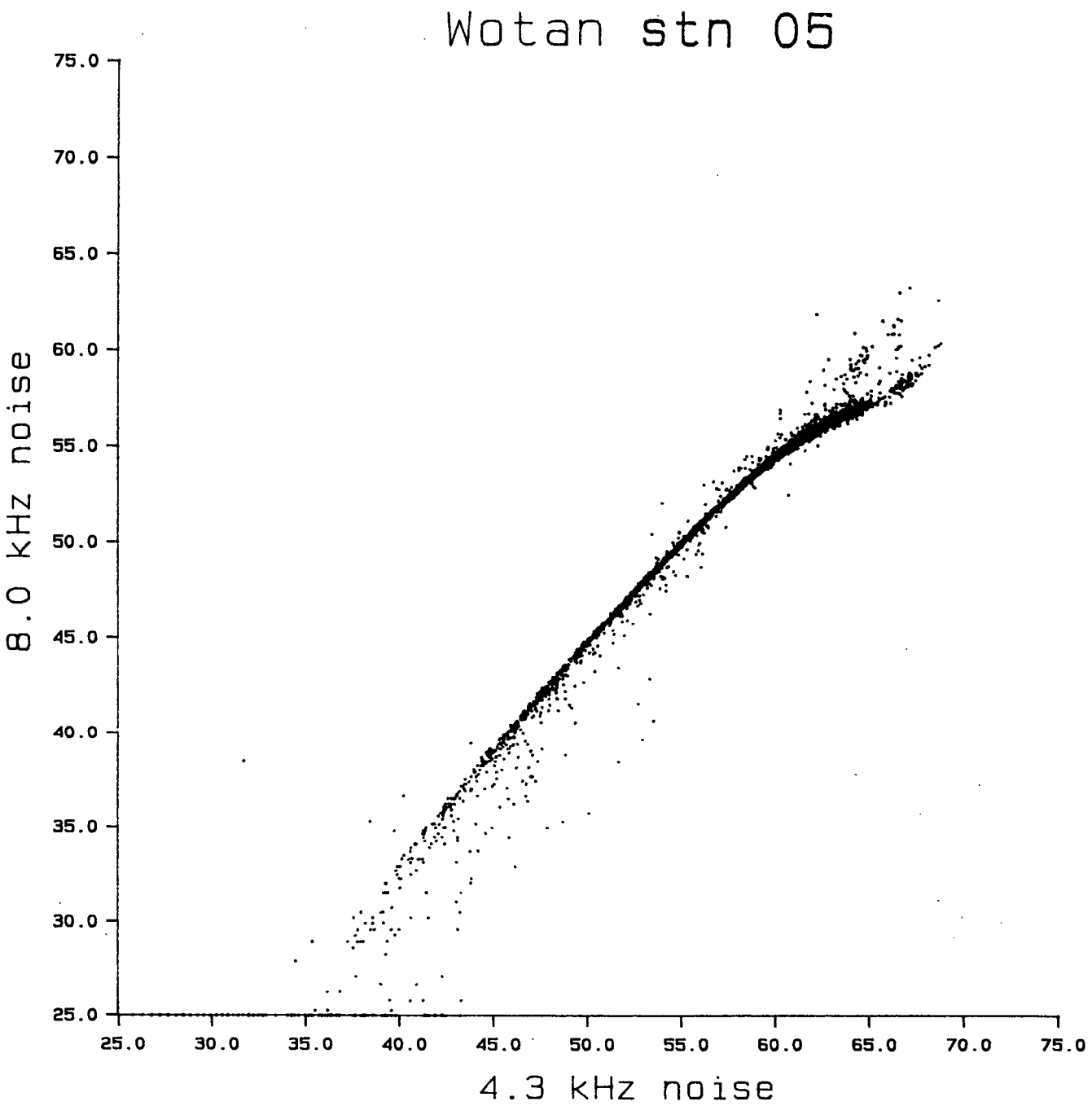

Figure 32: Noise spectrum level at 8.0 kHz vs noise spectrum level at 4.3 kHz at station 5 for the period February 8-28, 1986.

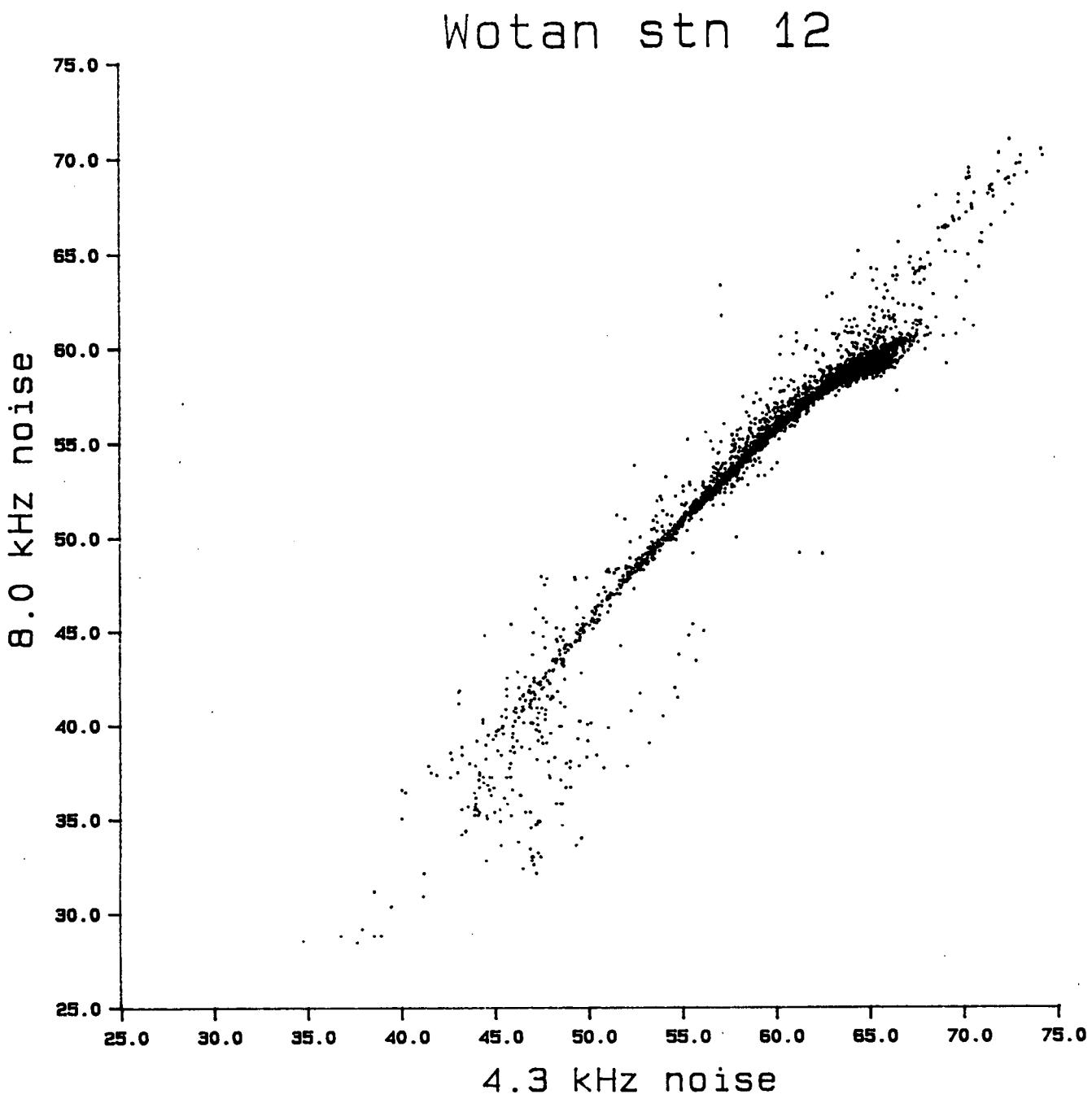

Figure 33: Noise spectrum level at 8.0 kHz vs noise spectrum level at 4.3 kHz at station 12 for the period February 8-28, 1986.

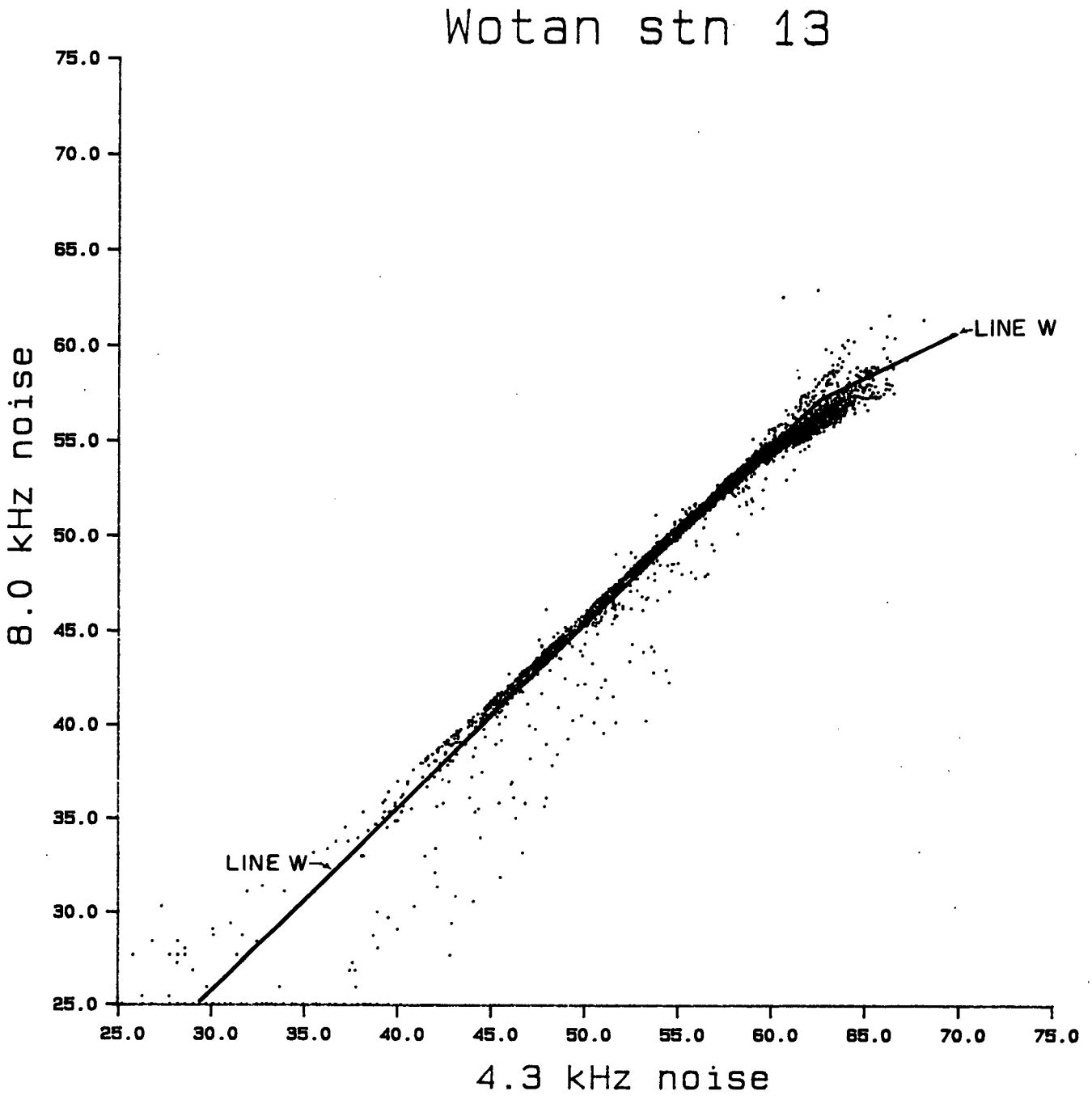

Figure 34: Noise spectrum level at 8.0 kHz vs noise spectrum level at 4.3 kHz at station 13 for the period February 8-28, 1986.

A corrected time series for noise spectrum level was calculated for each station, combining the 4.3-kHz and 8.0-kHz signals in the algorithm, but with zone A defined individually for each station as above. Wind speeds were computed using the constants in Table 6; set (iii) for station 1, set (ii) for stations 5, 12 and 13. The resulting wind-speed time series are shown in Figures 35 to 38. The unrealistic step-like nature of the time series is no longer present.

3.3 COMPARISON WITH SURFACE BUOY WIND SPEEDS

Figure 39 is a time-series plot of wind speed measured by the surface buoy at station 2.[4] Comparison with the WOTAN record at station 2 is not possible as the uncontaminated portion of the WOTAN record does not overlap the surface buoy record supplied to us. However, the WOTAN at station 1 was only 12 km distant, so a comparison can be made between the WOTAN wind speeds from station 1 and with the surface buoy measurements at station 2.

Inspection of the time series in Figures 35 and 39 shows a high degree of visual correlation between them. Linear regressions on the surface-buoy data (over their common measurement period) of the WOTAN wind speed computed from the 4.3-kHz signal only (Figure 20) and the combined 4.3-kHz and 8.0-kHz signals (Figure 35) were calculated with the following results: (V_w is the WOTAN wind speed, V_s is the surface-buoy wind speed).

(a) 4.3 kHz only on surface-buoy winds:

$$V_w = 1.40\ V_s + 1.859\ ms^{-1}$$ Correlation coefficient R=0.892

(b) 4.3 kHz and 8.0 kHz on surface-buoy winds:

$$V_w = 1.16\ V_s + 0.01\ ms^{-1}$$ Correlation coefficient R=0.900

Although the combined calculation produced a slightly better fit, the correlation coefficients show that in both cases, the fit was by no means perfect. Station 1 is close to the main shipping route to Halifax harbour, which suggests that there is probably a large amount of ship noise in the record. Ships passing close overhead are likely to be heard on the 8.0-kHz as well as on the 4.3-kHz channel. Development of an algorithm for identifying ship signals (perhaps exploiting the characteristic structure noted in Lemon et al. 1984) would be a very useful step.

---

[4] Data supplied by Dr. F. Dobson, Bedford Institute of Oceanography, personal communication, 1986.

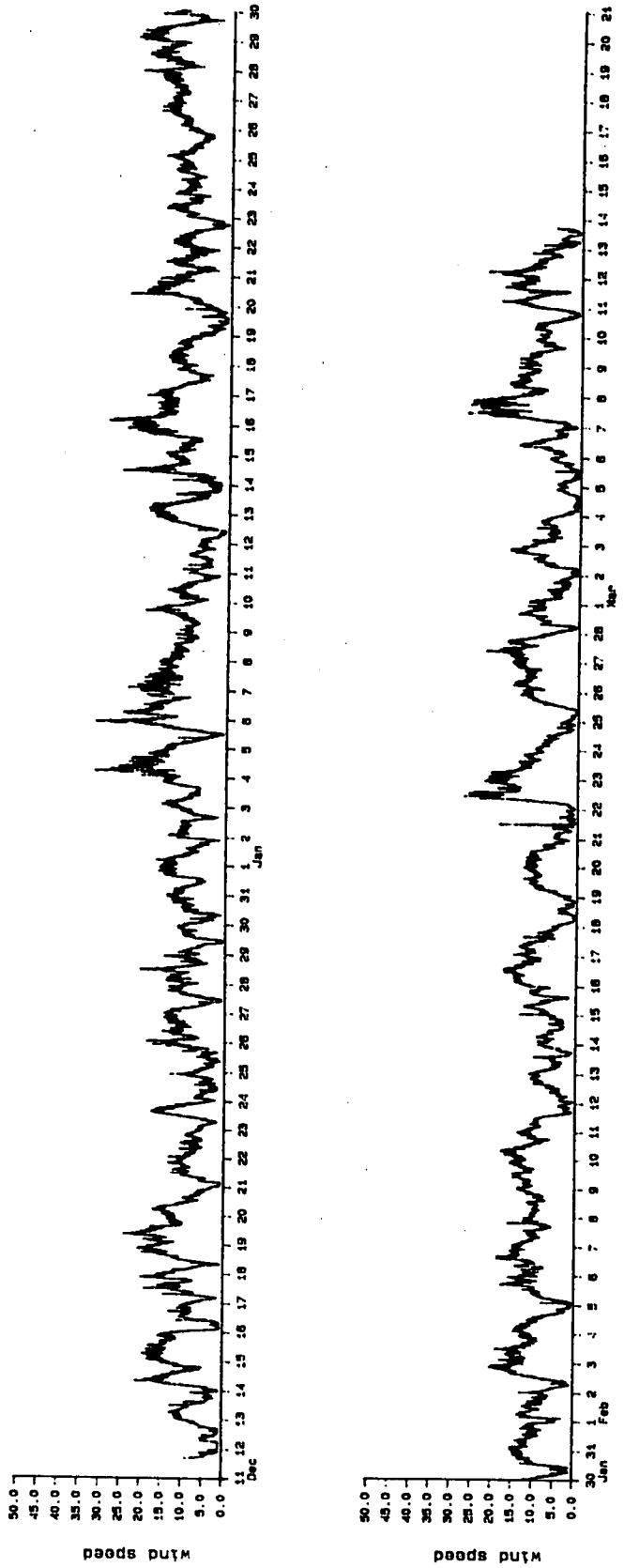

Figure 35: Wind speed ($m \cdot s^{-1}$) at station 1 computed from the 4.3-kHz and 8.0-kHz signals, using the relationship defined specifically for this station.

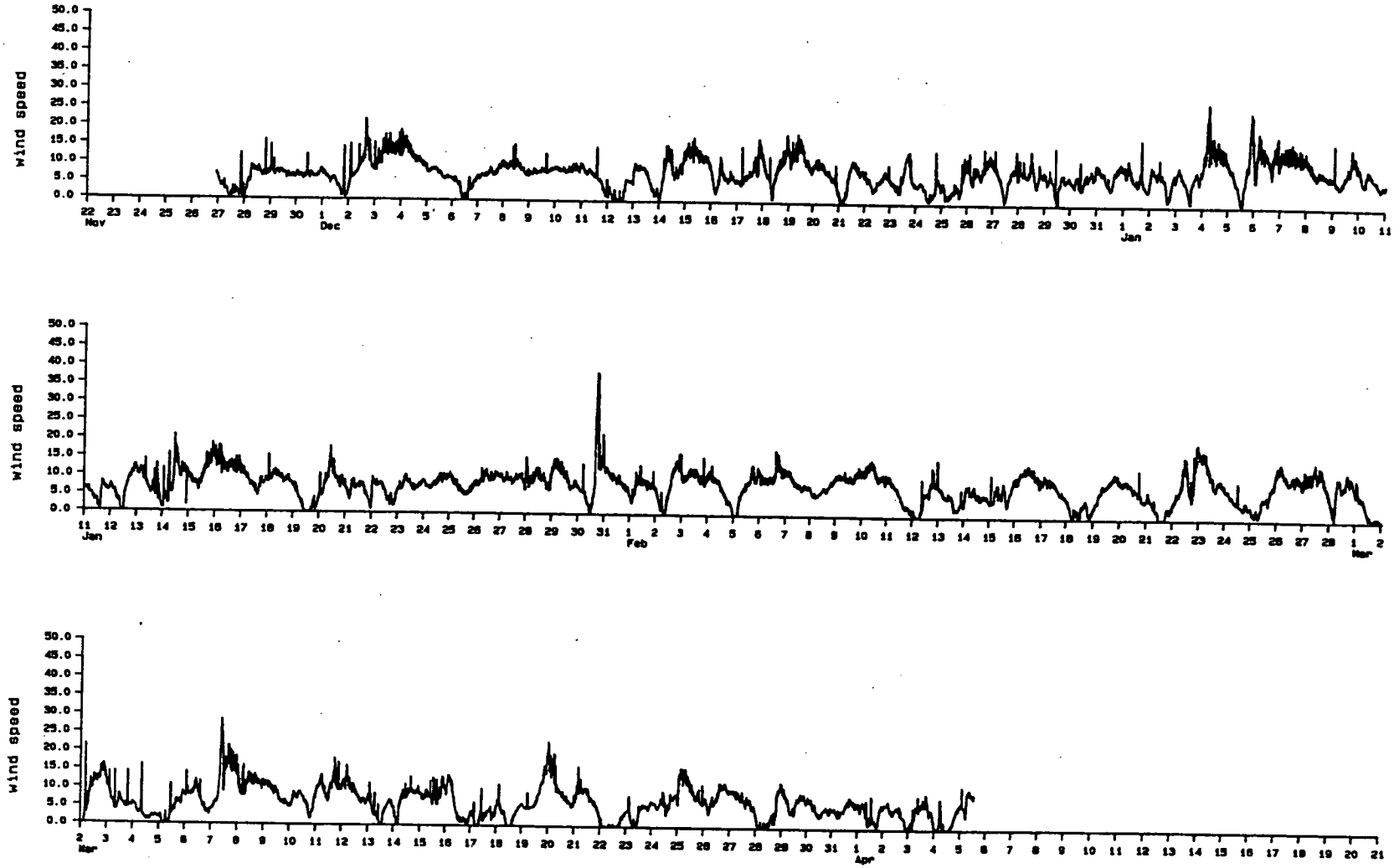

Figure 36: Wind speed ($m \cdot s^{-1}$) at station 5 computed from the narrow-band 4.3-kHz and 8.0-kHz signals, using the relationship defined specifically for this station.

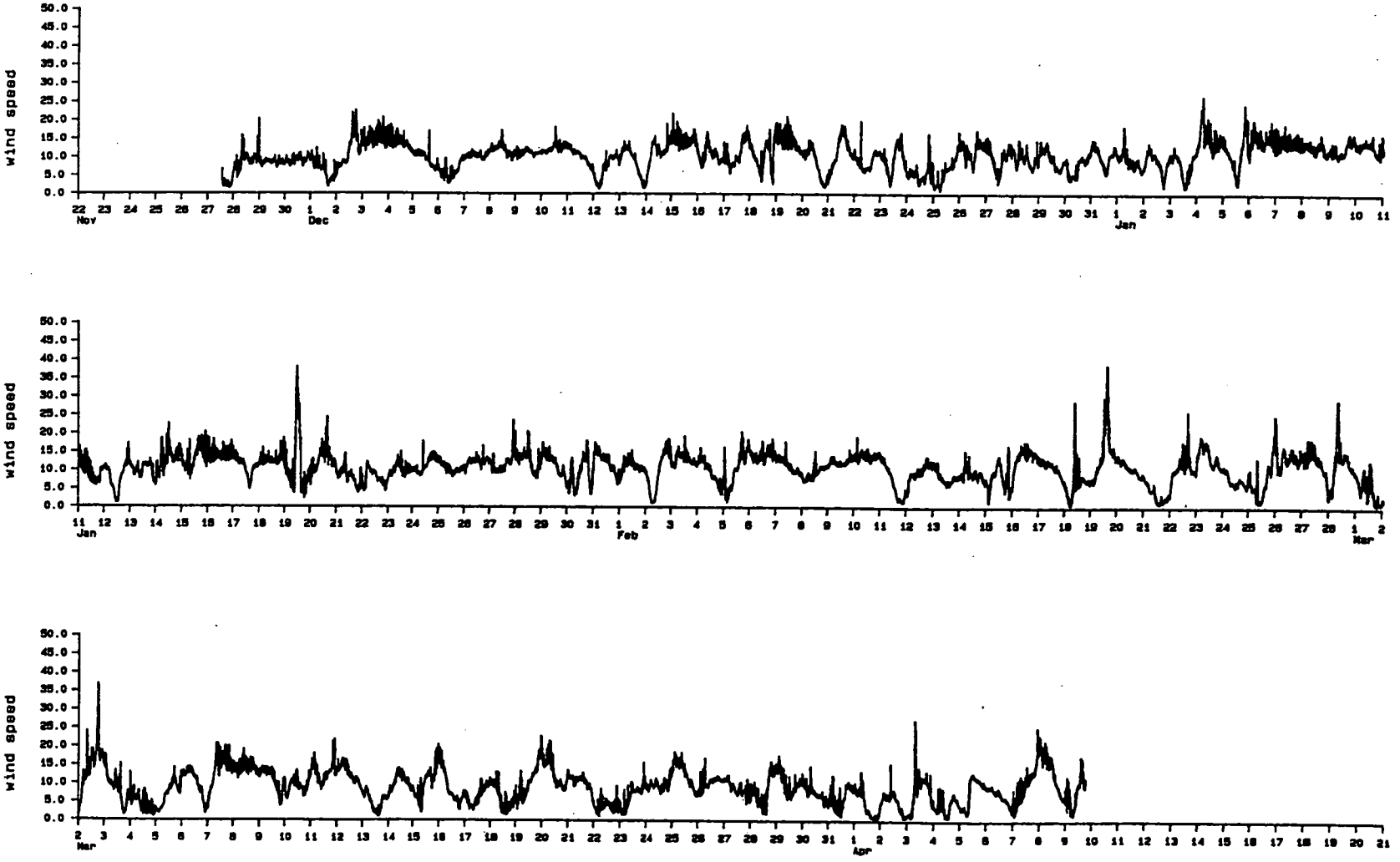

Figure 37: Wind speed ($m \cdot s^{-1}$) at station 12 computed from the narrow-band 4.3-kHz and 8.0-kHz signals, using the relationship defined specifically for this station.

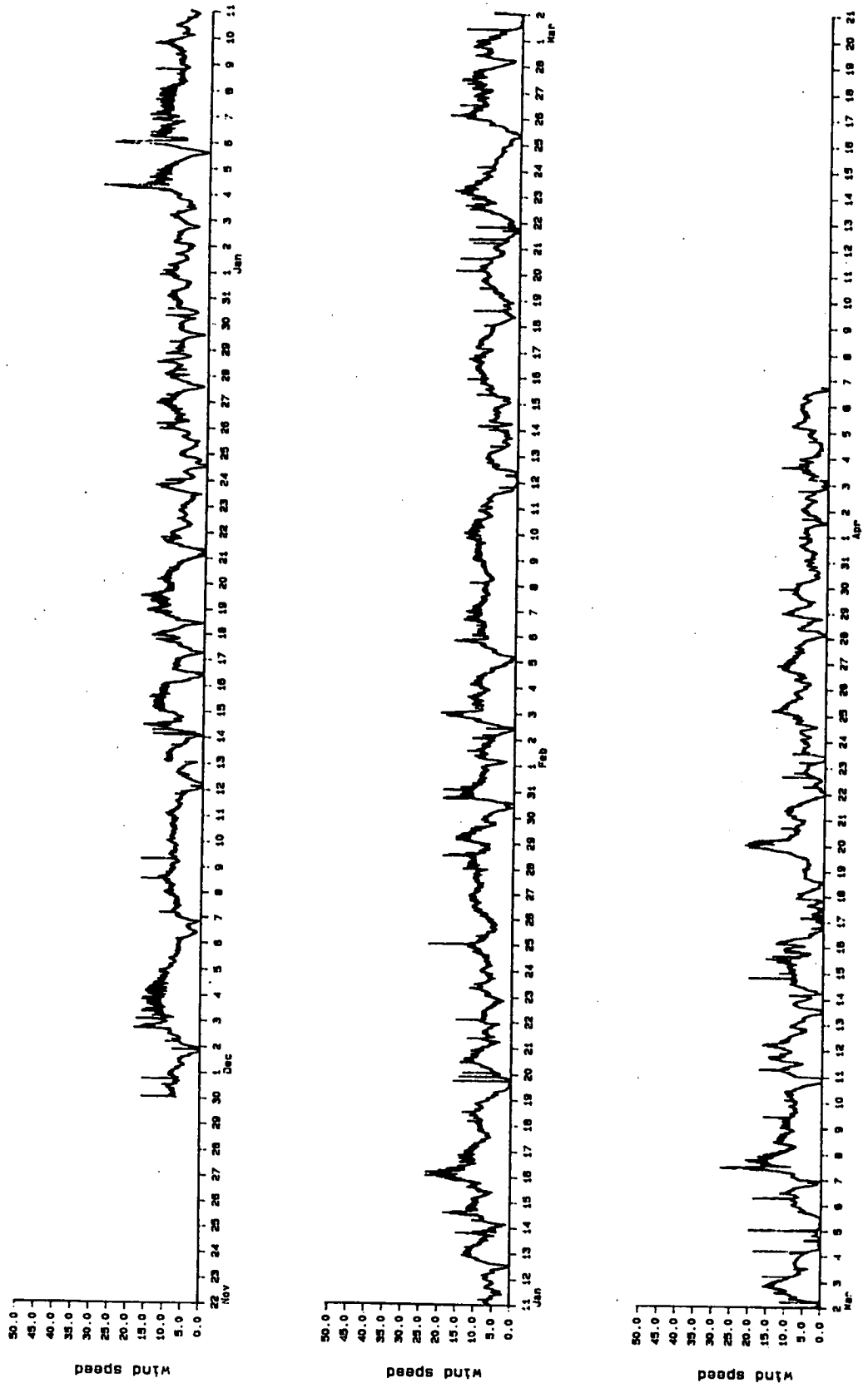

Figure 38: Wind speed ($m \cdot s^{-1}$) at station 13 computed from the narrow-band 4.3-kHz and 8.0-kHz signals, using the relationship defined specifically for this station.

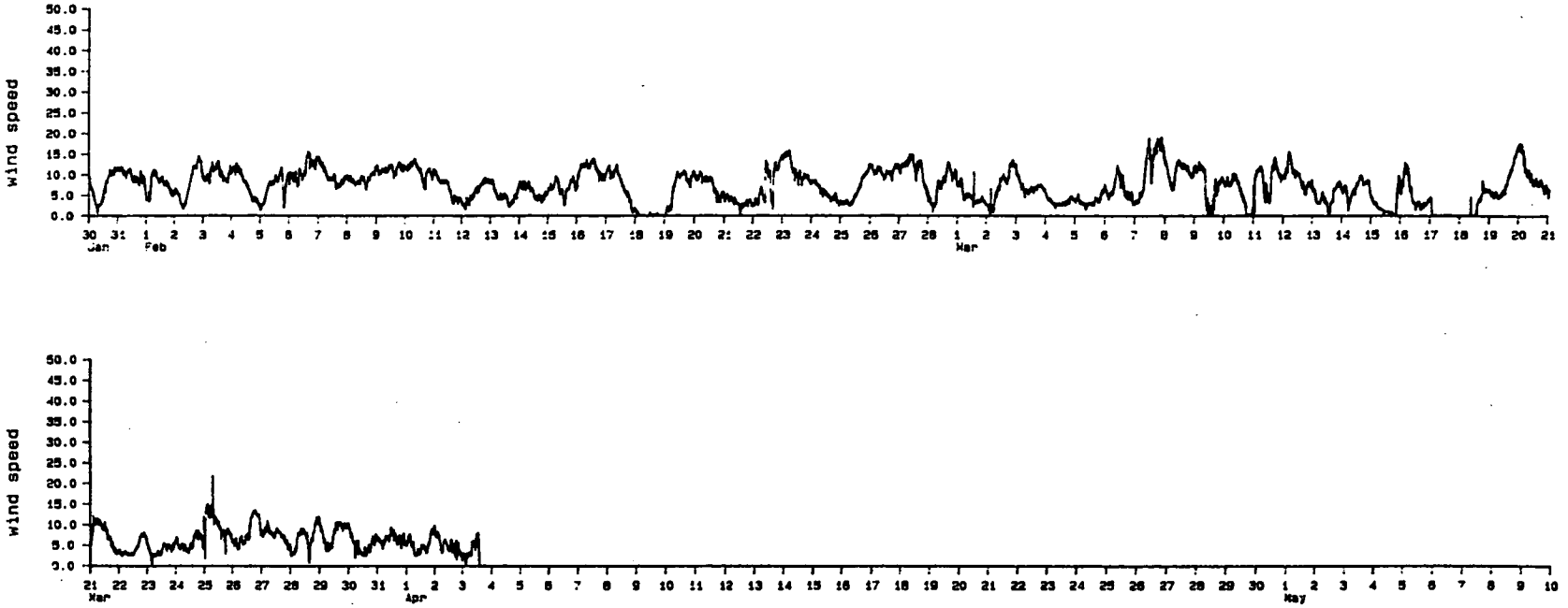

Figure 39: Wind speed ($m \cdot s^{-1}$) from surface buoy at CASP station 2. (Data supplied by Dr. F. Dobson, Bedford Institute.)

4.0 CONCLUSIONS

Five WOTAN instruments were deployed as part of the CASP experiment, from December 1985 to April 1986. Data recovery was very successful, with over 90% of the total records possible being immediately usable. Four of the instruments produced complete noise records on all channels, while the fifth (station 2) was contaminated by noise from an as yet unknown source from January 15 1986 until it was recovered on March 13 1986.

Time series of wind speeds calculated from WOTAN measurements at CASP stations 1, 5, 12 and 13 have been presented using two algorithms to compute wind speed. Comparison with the wind speeds measured by the surface buoy showed marginally better performance by the algorithm combining the noise signals from the 4.3-kHz and 8.0-kHz channels. In both cases, a good fit with a high degree of correlation (R=0.9) was found. It was not possible, however, to derive an algorithm for the dual-channel calculation which would work at all the stations. Significant differences were observed in the relationship of the 8.0-kHz signal to the 4.3-kHz signal among the various stations. It is not clear why that is the case. It may be related to reasons for the apparent variation of the wind-speed calibration constants with instrument depth. Further investigation of that phenomenon and the effects of rainfall using the data from the higher-frequency channels may result in further improvements to the wind-speed measurements and the possibility of making accurate rainfall measurements at sea. Such an investigation is, however, beyond the scope of this report.

5.0 REFERENCES

Evans, D.L. and D.R. Watts, 1982. Wind speed and stress at the sea surface from ambient noise measurements. Proc. Int. Symp. Acoustic Remote Sensing Atmos. and Oceans; Dept. Physics, University of Calgary, Calgary, Canada, pp. III 69-III 78.

Farmer, D.M. and D.D. Lemon, 1984. The influence of bubbles on ambient noise in the ocean at high wind speeds. J. Phys. Ocgy., 14(11), pp. 1762-1778.

Franz, G.J., 1959. Splashes as sources of sound in liquids. J. Acoust. Soc. Am., 45, pp. 1080-1096.

Hill, W., 1984. A generation of WOTAN underwater wind-recording instruments. Proc. IEEE, Oceans'84, pp. 31-36.

Jasco Research Ltd., 1985. Development of an undersea acoustic technique to determine rainfall. Report to Institute of Ocean Sciences, Sidney, B.C. by Jasco Research Ltd., Sidney, B.C. (unpubl. man.).

Kerman, B.R., D.L. Evans, D.R. Watts and D. Halpern, 1983. Wind dependence of underwater ambient noise. Bound. Layer Meteor., 26, pp. 105-113.

Knudsen, V.O., R.S. Alford and J.W. Emling, 1948. Underwater ambient noise. J. Mar. Res., 7, pp. 410-429.

Lemon, D.D., D.M. Farmer and D.R. Watts, 1984. Acoustic measurements of wind speed and precipitation over a continental shelf. J. Geophys. Res., 89, pp. 3462-3472.

Motchenbacher, C.D. and F.C. Fitchen, 1973. Low-noise Electronic Design. Wiley-Interscience (John Wiley & Sons), New York.

Nystuen, J.A., 1986. Rainfall measurements using underwater ambient noise. J. Acoust. Soc. Am., 79(4), pp. 972-982.

Shaw, P.T., D.R. Watts and H.T. Rossby, 1978. On the estimation of oceanic wind speed and stress from ambient noise measurements. Deep-Sea Res., 25, pp. 1225-1233.

Wenz, G.M., 1962. Acoustic ambient noise in the ocean: spectra and sources. J. Acoust. Soc. Am., 34, pp. 1936-1956.